

Summer 7-2017

STUDIES IN DIRECTED CATALYTIC ASYMMETRIC HYDROBORATION OF 1,2-DISUBSTITUTED UNSATURATED AMIDE

Shuyang Zhang

University of Nebraska - Lincoln, shuyang.zhang@huskers.unl.edu

Follow this and additional works at: <http://digitalcommons.unl.edu/chemistrydiss>



Part of the [Organic Chemistry Commons](#)

Zhang, Shuyang, "STUDIES IN DIRECTED CATALYTIC ASYMMETRIC HYDROBORATION OF 1,2-DISUBSTITUTED UNSATURATED AMIDE" (2017). *Student Research Projects, Dissertations, and Theses - Chemistry Department*. 85.
<http://digitalcommons.unl.edu/chemistrydiss/85>

This Article is brought to you for free and open access by the Chemistry, Department of at DigitalCommons@University of Nebraska - Lincoln. It has been accepted for inclusion in Student Research Projects, Dissertations, and Theses - Chemistry Department by an authorized administrator of DigitalCommons@University of Nebraska - Lincoln.

STUDIES IN DIRECTED CATALYTIC ASYMMETRIC HYDROBORATION OF 1,2-

DISUBSTITUTED UNSATURATED AMIDE

by

Shuyang Zhang

A THESIS

Presented to the Faculty of

The Graduate College at the University of Nebraska

In Partial Fulfillment of Requirements

For the Degree of Master of Science

Major: Chemistry

Under the Supervision of Professor James M. Takacs

Lincoln, Nebraska

July 2017

DIRECTED CATALYTIC ASYMMETRIC HYDROBORATION OF 1,2-
DISUBSTITUTED ALKENES

Shuyang Zhang, M.S.

University of Nebraska 2017

Advisor: Professor James M. Takacs

The Rh-catalyzed, substrate directed catalytic asymmetric hydroboration of γ,δ -unsaturated amides provides a direct route to enantioenriched acyclic secondary γ -borylated carbonyl derivatives with high regio- and enantioselectivity. The catalytic condition optimization and substrate scope study is discussed, including the effects in catalytic asymmetric hydroboration on pre-installed chiral γ,δ -unsaturated amides. A mechanistic study from kinetic approach by graphical manipulation (reaction progress kinetic analysis for substrate orders and normalized time analysis for catalyst order.) was discussed in this thesis.

Table of Contents

| | |
|---|------|
| Acknowledgement | VI |
| Table of figures | VII |
| Index of tables..... | XII |
| List of Abbreviations..... | XIII |
| Chapter 1- introduction | XV |
| 1.1 Chiral compounds and why it's important? | 1 |
| 1.2 Catalytic asymmetric hydroboration..... | 6 |
| 1.3 Rhodium-catalyzed hydroboration..... | 6 |
| 1.4 Rh-catalyzed enantioselective alkene hydroboration..... | 8 |
| 1.5 Enantioselective hydroboration catalyzed by transition metal other than Rh | 10 |
| 1.6 Substrates directed Rh-catalyzed enantioselective alkene hydroboration. | 12 |
| 1.7 Recent development on amide directed CAHB..... | 13 |
| 1.8 Mechanistic insights into the CAHB | 14 |
| 1.9 Summary | 17 |
| Chapter 2: Carbonyl-directed catalytic asymmetric hydroboration (CAHB) of 1,2- disubstituted γ,δ -unsaturated amide..... | 19 |

| | |
|--|----|
| 2.1 Background: amide directing asymmetric hydroboration of γ,δ -unsaturated 1,2 disubstituted alkene..... | 19 |
| 2.2 Motivation on study of directed CAHB of γ,δ -unsaturated amide. | 24 |
| 2.3 Rh-catalyzed asymmetric hydroboration of two-point binding substrates: condition optimization | 25 |
| 2.4 Optimization studies on CAHB of substrate..... | 27 |
| 2.5 The substrate scope of CAHB on γ,δ -unsaturated amide | 29 |
| 2.5.1 General information on preparation of γ,δ -unsaturated amide substrate | 30 |
| 2.5.2 Substrate scope study with different substituents | 33 |
| 2.6 CAHB on morpholine amide | 35 |
| 2.7 The effect of an existing chiral center on CAHB..... | 37 |
| 2.7.1 Motivation on study of pre-installed chiral substrate CAHB: A mechanistic investigation..... | 38 |
| 2.7.2 Preparation of α -Me chiral substrate..... | 38 |
| 2.7.3 The results of CAHB on preinstalled chiral substrates..... | 40 |
| 2.7.4 Preliminary results for future directions on chiral substrate CAHB... | 42 |
| 2.8 Employing the Tropos ligand into the CAHB study. | 46 |

| | |
|--|----|
| 2.9 Conclusion: | 48 |
| Chapter 3: Investigations of Rh-catalyzed asymmetric hydroboration on a 1,2-disubstituted γ , δ -unsaturated amide informed by reaction progress kinetic analysis. | 50 |
| 3.1 The introduction on Reaction Progress Kinetic Analysis (RPKA):..... | 50 |
| 3.1.1 The definition of RPKA..... | 50 |
| 3.1.2 What can RPKA provide? | 51 |
| 3.1.3 The key parameter in PRKA: “excess” | 51 |
| 3.1.4 The in-situ tools for the RPKA: | 52 |
| 3.1.5 How to determine the orders of reactants by PRKA..... | 54 |
| 3.2 PRKA on CAHB of 1,2-disubstituted γ , δ -unsaturated amide..... | 57 |
| 3.2.1 The experimental design: | 57 |
| 3.3 The general procedures of data processing. | 59 |
| 3.3.1 Peaks integration. | 59 |
| 3.3.2 Transform the raw data to concentrations. | 60 |
| 3.3.3 Curve fitting of the concentration data. | 61 |
| 3.3.4. Transform the rate equation to normalized rate functions. | 62 |
| 3.3.5. Prepare the plot of the normalized rate equation. | 63 |

| | |
|---|----|
| 3.3.6. Summarize the data from different reaction conditions in one plot... | 64 |
| 3.4 The detailed reaction conditions and results of the kinetic study: | 66 |
| 3.4.1 The same excess experiment: the stability of the catalyst | 66 |
| 3.4.2 The order of PinBH..... | 68 |
| 3.4.3 The Alkene substrate order: | 73 |
| 3.5 The Order of catalyst determined by “normalized time” graphical analysis. | 77 |
| 3.5.1 Introduction:..... | 77 |
| 3.5.2 Experimental conditions: | 80 |
| 3.6 The mechanistic implications derived from the kinetic results. | 82 |
| 3.7 The Hydrogenation process : | 84 |
| 3.8 Discussion..... | 87 |
| 3.9 Conclusion | 87 |
| Chapter 4: Experimental procedures..... | 88 |
| General procedures. | 88 |
| 4.1 Reaction progress kinetic analysis experiments setup and data processing. . | 89 |
| 4.1.1 Setting up reactions:..... | 89 |
| 4.1.2 Integration on raw data | 90 |

| | |
|--|-----|
| 4.2 Procedures:..... | 91 |
| 4.2.1 Set up the template:..... | 91 |
| 4.2.2 Automatic integration: | 91 |
| 4.2.3 Import the data into Excel..... | 91 |
| 4.3 Data analysis | 92 |
| Chapter 5: Representative procedure for the preparation of substrates | 94 |
| 5.1 procedures for preparing the γ,δ -unsaturated amide..... | 94 |
| 5.2 Procedures for preparing pre-chiral installed γ,δ -unsaturated amide | 110 |
| Chapter 6: Reference..... | 136 |

Acknowledgement

First, I would like to thank my research advisor, Prof. James Takacs for his guidance, kindness and exceptional tolerance on me throughout the past four years. I really appreciate the directions that he gave in term of designing the experiments as well as editing the thesis with extreme patience.

I would like to thank my committee members: Prof. Zhang and Prof. Stains. I also would like to thank my undergraduate research advisor, Prof. Ying-Chun Chen who help me build up an understanding on experimental organic chemistry and encourage me to continue my study in science.

I also would like to thank my colleagues in the Takacs group. Dr. Gia Hoang guide me when I first joined the group and collaborate with me in the past four years. He gave me many useful advices not only in research but also about the life. I would like to thank Shoba Veronika and Suman Chakrabarty. It's always joyful to work and study with them. Best wishes for them and all other group members Ryan Carr and Andrew Bochat.

Special thanks to my parents who always trust on my potentials and my wife Ou Wang who is using her optimistic emotions as well as outstanding achievement in the graduate study to motivate me to challenge myself. Last but not least, I would like to thank myself for not giving up even in those hardest days. I was capable but not willing to finish a work, but this time, the work is done! Thank you!

Table of figures

| | |
|---|----|
| Figure 1 the enantiomers of thalidomide | 1 |
| Figure 2 the functional groups transformation of organoboronates..... | 3 |
| Figure 3 chiral borane reagents in stoichiometric asymmetric hydroboration | 5 |
| Figure 4. A comparison between catalyzed and uncatalyzed hydroboration reactions | 8 |
| Figure 5 The early Rh-catalyzed enantioselective hydroboration reaction..... | 8 |
| Figure 6. Examples of Enantioselective catalytical hydroboration | 9 |
| Figure 7. Catalytical asymmetric hydroboration catalyzed by other transitional metals | 11 |
| Figure 8. Highly regio- and enantioselective amide directed Rh catalyzed CAHB on β,γ -unsaturated amides..... | 14 |
| Figure 9 proposed catalytic cycle of the Rh-catalyzed hydroboration | 15 |
| Figure 10 Mechanistic investigation by deuterium labeling..... | 16 |
| Figure 11 The competition reaction of γ,δ unsaturated amide substrates..... | 20 |
| Figure 12 The directed CAHB reaction of acyclic γ,δ -unsaturated amide and cyclic unsaturated ester substrates..... | 20 |
| Figure 13. Examples of amide directed β,γ -unsaturated amide CAHB..... | 22 |

| | |
|--|----|
| Figure 14 Computational study experimental results. | 23 |
| Figure 15. Mechanistic interpretation of CAHB on cyclic γ,δ - amide | 24 |
| Figure 16 Examples on amide functionalization from the organoboronates. | 25 |
| Figure 17 comparison between previous CAHB results and the topic in this thesis. | 26 |
| Figure 18 The ligand optimization of amide directed CAHB on γ,δ -unsaturated amides | 27 |
| Figure 19. The preparation of γ,δ -unsaturated amide by Pd catalyze allylic substitution..... | 31 |
| Figure 20. The preparation of γ,δ -unsaturated amide by Claisen-Johnson rearrangement. | 32 |
| Figure 21 The preparation of γ,δ -unsaturated amide by Wittig reaction. | 32 |
| Figure 22 substrate scope study and the possible products..... | 33 |
| Figure 23 CAHB on morpholine amide..... | 36 |
| Figure 24. The two possible geometry models of intermediate after alkene association with Rh complex. | 37 |
| Figure 25. Preparation of an α -Me chiral substrate by using Evans chiral auxiliary group method. | 40 |

| | |
|--|----|
| Figure 26 The preparation of α -Me, β -OH, γ,δ unsaturated amide chiral substrate. | 43 |
| Figure 27. The preparation of β -OH, γ,δ unsaturated amide chiral substrate. | 44 |
| Figure 28 Three different chiral silyl ether substrates for CAHB..... | 45 |
| Figure 29 the CAHB on α -Me chiral substrate with tropos ligand catalyst..... | 48 |
| Figure 30 Examples of “different excess” overlay in the RPKA..... | 55 |
| Figure 31 Examples of “same excess” overlay in the RPKA | 57 |
| Figure 32 The standard condition used in the PRKA study. | 57 |
| Figure 33 The multiple displays of ^{19}F NMR spectra..... | 58 |
| Figure 34 The integrals from NMR spectra. | 60 |
| Figure 35. The transformation of raw data to the concentration..... | 61 |
| Figure 36 Curve fitting of the raw data..... | 62 |
| Figure 37 The normalized rate data. | 63 |
| Figure 38 The plot of normalized rate vs. [Alkene] from 1 reaction. | 64 |
| Figure 39 The plot of normalized rate vs. [Alkene] from 2 different reactions... | 65 |
| Figure 40 Data from "same excess" experiments, rate vs time in two experiments. | 67 |
| Figure 41 The "different excess" experiments, rate vs time under three reaction | |

| | |
|--|----|
| conditions..... | 69 |
| Figure 42 The "different excess" experiments, normalized rate vs. [alkene] substrate | 70 |
| Figure 43 The adjusting on "n" | 71 |
| Figure 44 A published example of RPKA on Pd catalyzed Sonogashira reactions | 72 |
| Figure 45 Substrate order by the "different excess" experiments: rate vs. time .. | 74 |
| Figure 46 Substrate order by "different excess" experiments: normalized rate vs. [PinBH]..... | 75 |
| Figure 47 A published example of RPKA on the oxidative coupling reactions ^[65] | 76 |
| Figure 48 The adjusting on "m" in our RPKA on CAHB..... | 77 |
| Figure 49 A published example of normalized time analysis from the Ref 66.... | 79 |
| Figure 50 The adjusting of "n" in the normalized time graphical analysis..... | 80 |
| Figure 51 The mechanistic insights based on the kinetic studies | 82 |
| Figure 52 The assumption for a competing hydrogenation process in the CAHB condition illustrated for a simple, hypothetical alkyl-rhodium intermediate | 84 |

Figure 53 The "different excess" analysis on reduction pathway. The normalized rate versus $[\text{Alkene}]^1$ 85

Index of tables

| | |
|--|----|
| Table 1 ligand optimization of amide directed CAHB on γ,δ -unsaturated amide | 28 |
| Table 2. Results of substrate scope study with different substituents | 33 |
| Table 3 CAHB on morpholine amide with BINOL series ligands | 36 |
| Table 4. Results of CAHB on phenyl substituted γ,δ -unsaturated chiral substrate, and comparison with the achiral substrate. | 41 |
| Table 5 Results of CAHB on phenethyl substituted γ,δ -unsaturated chiral substrate and comparison with the achiral substrate. | 41 |
| Table 6 experimental design for the "same excess" experiment | 66 |
| Table 7 The experimental design for the "different excess" experiment with 1mol% Rh catalyst loading | 68 |
| Table 8 Reaction conditions of the "different excess" experiments to investigate the order of alkene substrate | 73 |
| Table 9 The reaction conditions in the "different excess" experiment to study the hydrogenation process. | 84 |

List of Abbreviations

| | |
|--------------------|---|
| CAHB | Catalytic Asymmetric Hydroboration |
| 9-BBN | 9-Borabicyclo(3.3.1)nonane |
| TMDB | 4,4,6-Trimethyl-1,3,2-dioxaborinane |
| BINAP | 2,2'-Bis(diphenylphosphino)-1,1'-binaphthyl |
| Bn | Benzyl |
| Bu | Butyl |
| CDI | Carbonyldiimidazole |
| DBU | 1,8-diazabicyclo[5.4.0]undec-7-ene |
| DIBAL | Di-isobutyl Aluminum Hydride |
| DIPEA/Hunig's base | N, N-diisopropylethylamine |
| DDQ | 2,3-Dichloro-5,6-dicyano-1,4-benzoquinone |
| DME | Dimethoxyethane |
| LiHMDS | Lithium bis(trimethylsilyl)amide |
| NaHMDS | Sodium bis(trimethylsilyl)amide |
| nBuLi | n-Butyllithium |
| MS | Mass Spectrometry |

| | |
|-------|----------------------------|
| CatBD | Deutero Catecholborane |
| CatBH | Catecholborane |
| pinBH | Pinacolborane |
| COD | Cyclooctadiene |
| TMS | Trimethyl silyl |
| TBDMS | tert-Butyldimethylsilyl |
| TIPS | Triisopropylsilyl |
| ee | Enantiomeric excess |
| er | Enantiomeric ratio |
| de | Diastereomeric excess |
| dr | Diastereomeric ratio |
| Cy | Cyclohexyl |
| nbd | Norbornadienyl |
| M | Molarity |
| NMR | Nuclear Magnetic Resonance |
| DCE | Dichloroethane |
| DCM | Dichloromethane |

| | |
|------|-------------------------------------|
| THF | Tetrahydrofuran |
| ToEA | Tri-ethyl ortho acetate |
| TLC | Thin layer chromatography |
| RT | Room temperature |
| Rac | Racemic |
| J | Coupling Constant |
| Eq | Equivalents |
| Aq | aqueous |
| Me | Methyl |
| Et | Ethyl |
| DMAP | Dimethylaminopyridine |
| DCC | N,N'-Dicyclohexylcarbodiimide |
| HPLC | High Pressure Liquid Chromatography |
| Min | Minute |
| IR | Infrared |
| Hz | Hert |

Chapter 1- introduction

1.1 Chiral compounds and why it's important?

Although human body appears to be symmetrical, biological systems, in most cases, recognize a pair of enantiomers as different substances, and the two enantiomers will elicit different responses. Thus, one enantiomer of a chiral drug may have a desired beneficial effect while the other may be highly toxic.

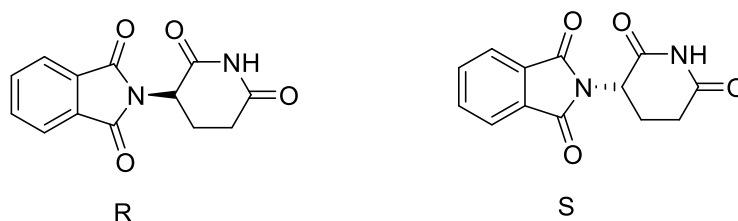


Figure 1 the enantiomers of thalidomide

For example, the well-known tragedy of thalidomide in which the R enantiomer is effective against morning sickness while the S enantiomers causes birth defects. For the organic chemists, the essential challenge is to develop efficient and reliable procedures to selectively synthesize the desired chiral drug molecules with control of absolute stereochemistry, that is, the efficient synthesis of products with high enantiomeric excess (% ee), instead of racemic mixtures that may cause unpredictable problems. There are several methods to obtain the enantiomerically pure molecules, the two major pathways are the resolution of racemic mixtures and the asymmetric synthesis. In this thesis, the asymmetric synthesis of chiral organoboronates will be

discussed.

Chiral organoboronates are powerful synthetic intermediates and useful building blocks in asymmetric synthesis. This is largely because (1) chiral organoboronates can be relatively prepared from common substrates in high yields and stereoselectivity, and (2) they display higher degree of chemical and configurational stability than many other organometallic reagents (e.g organolithiums and organomagnesiums).^[1] The functionalizations of organoboronates has been widely study in the past decades. Important advances have been made in C-C bond, C-O bond and C-N bond formation using the organoboronates for stereospecific conversion on the chiral center. Figure 1 highlights some examples of functional groups transformation with stereospecific conversion.

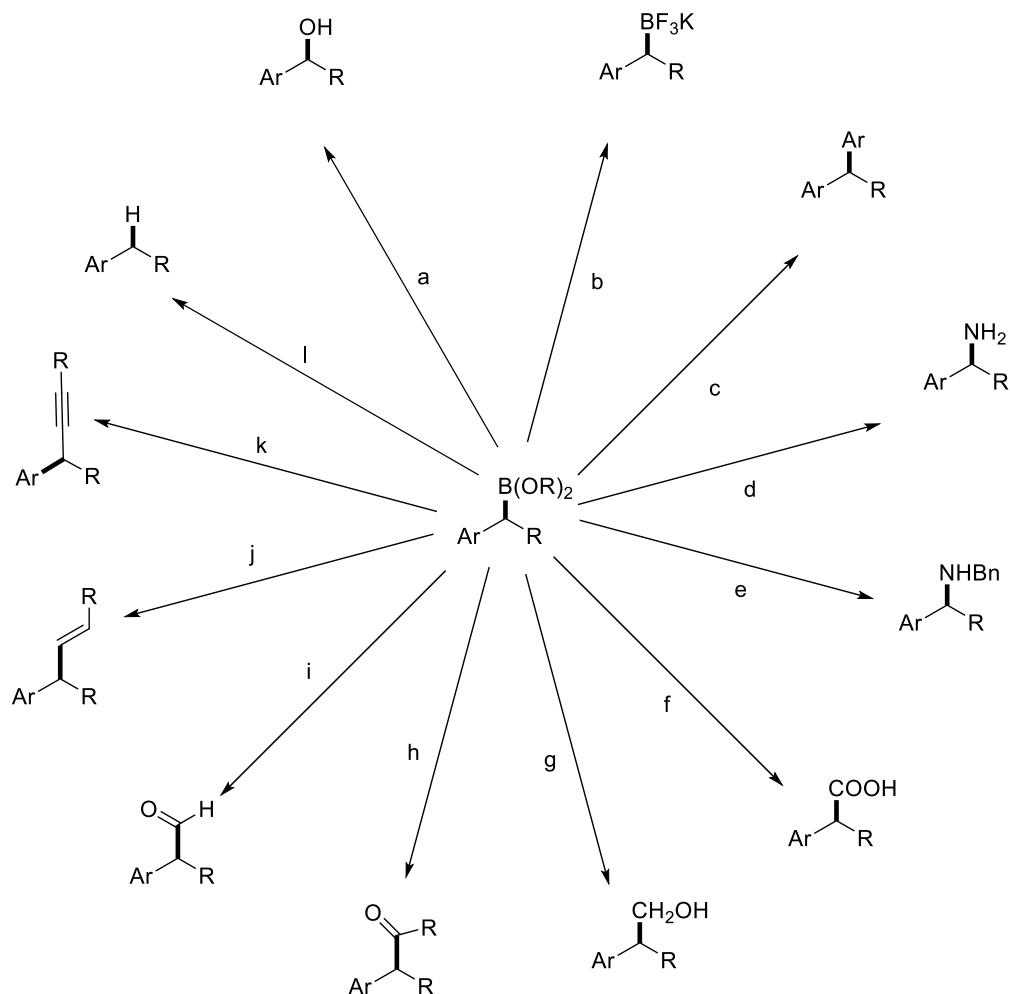


Figure 2 the functional groups transformation of organoboronates.

Conditions: (a) NaOH MeOH H₂O₂ ^[2]; (b) KHF₂, MeOH/H₂O ^[3]; (c) ArI Pd₂(dba)₃ Ph₃P, Ag₂O ^[4]; (d) MeMgCl, THF, H₂NOSO₃H ^[5]; (e) Et₂Zn, toluene, Benzyl amine, NaOCl. ^[6]; (f) LiCHCl₂ 1.5eq, ZnCl₂, THF, -100°C NaClO₂, NaH₂PO₄ ^[7]; (g) LiCHCl₂ 1eq THF, -78°C H₂O₂, NaOH ^[8]; (h) [Rh(cod)Cl]₂ 4-nitrobenzaldehyde dioxane /H₂O 80 °C, TEMPO oxidation; ^[9] (i) 1. THF, Me(CH₂)₄Me, 10 min, -100°C; 2. THF, -100 - -95°C; 2 h; 3. R:NaOH, H₂O₂, H₂O, 0°C; 2 h, rt ^[10]; (j) MeMgCl; ZniPr₂/ CuCN 2LiCl; allyl; (k); (l) Bu₄N⁺ •F⁻, EtCHEt, 2 h, 45°C; ^[11]

Consider the original methods and recent development in chiral organoboronates synthesis. In 1961, the first way to synthesize chiral molecules was reported using chiral hydroboration reagents in stoichiometric amounts. The milestone achievement of asymmetric hydroboration is H.C. Brown's demonstration of high enantioselectivity reaction on simple *Z*-alkenes.^[12] In their discovery, the chirality was originated from the easily accessible α -pinene derivative, diisopinocampheylborane (Ipc₂BH); with both enantiomers of the pinene available, both enantiomers of the product can be produced. The diisopinocampheylborane (Ipc₂BH) reagent was the first asymmetric hydroborating agent produced but it worked poorly with *E*-alkenes. In 1985, Masamune expanded the reaction substrate scope by introducing a new borane reagent so that the *E*-alkene and trisubstituted alkenes can be transformed to chiral boronic esters in this system.^[13] The stoichiometric hydroboration of 1,1-disubstituted alkenes was discovered by Sodequist's group by using 9-borabicyclo[3.3.1]nonane although the boron atom is not directly attached to the on the chiral carbon stereocenter.^[13b]

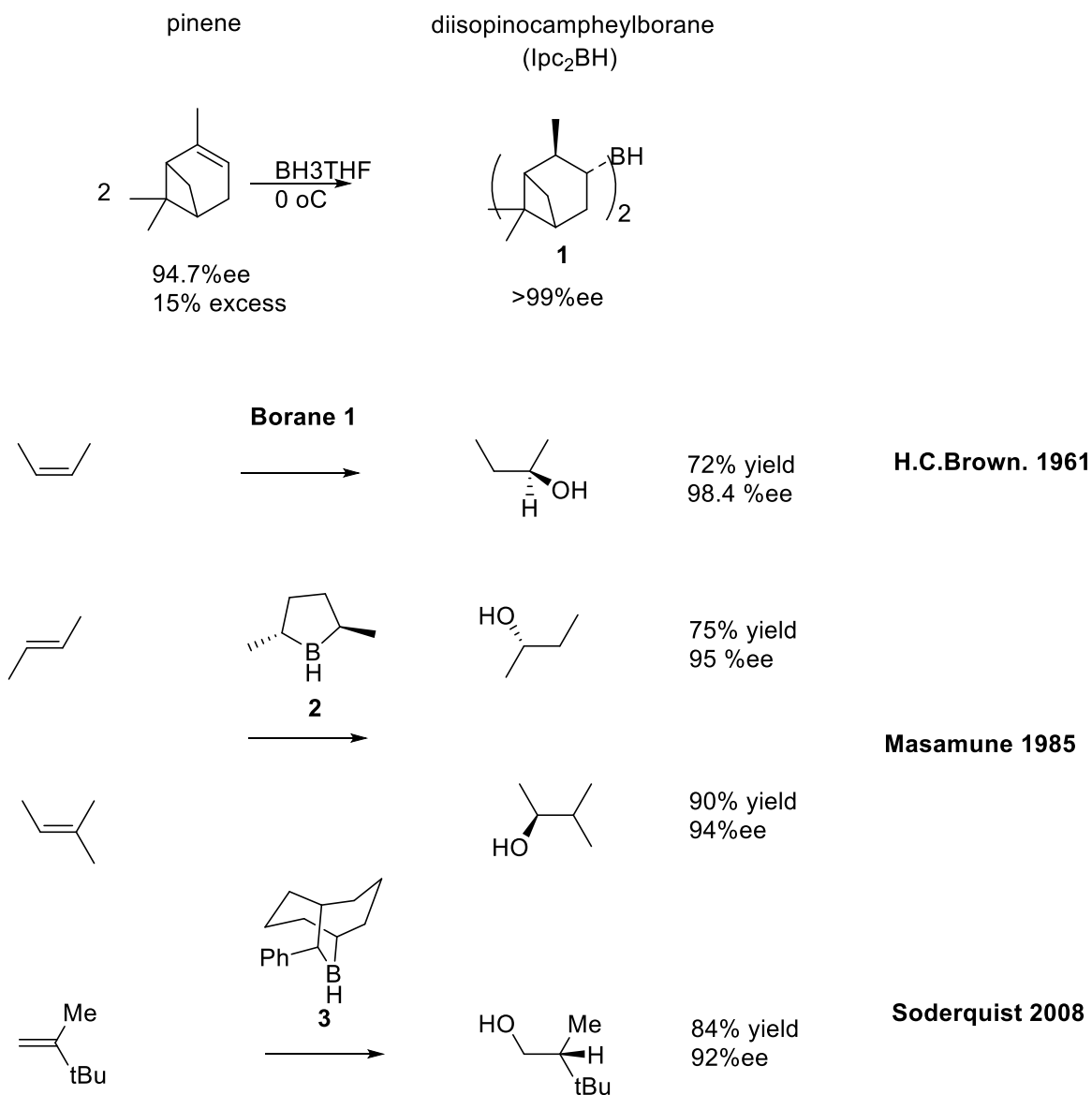


Figure 3 chiral borane reagents in stoichiometric asymmetric hydroboration

The reagent-controlled asymmetric hydroborations discussed above require a stoichiometric amount of chiral borane reagents which, although commercially available, are rather expensive and labile. Also, the alkene substrates that provide high stereoselectivity product are usually attached with simple substituents or rigid ring structures. To address these key limitations, the catalytic asymmetric hydroboration (CAHB) has been intensely investigated in recent years.

1.2 Catalytic asymmetric hydroboration

Transition-metal catalysis has seen an explosive increase of activity in the past several decades, especially in the synthetic chemistry community and especially for functional group transformations and catalytic enantioselective reactions. For example, the discovery of Sharpless enantioselective epoxidation using a tartrate-Ti complex^[14] and the now well-established enantioselective hydrogenation reactions with diphosphane-Pd complexes are notable examples.^[15] The importance of these two reactions was recognized by the 2001 Nobel Prize in Chemistry. In 2004, Grubbs received the Nobel prize for developing the highly active and versatile Ru catalysis for alkene metathesis,^[16] and the 2010 Noble chemistry prize was given to the Pd catalyzed cross-coupling reactions.^[17] All these achievements prove the powerful potential of the transition metal catalyzed chemistry in developing new synthetic methods and the discovery of new reactions.

1.3 Rhodium-catalyzed hydroboration

The first catalytic hydroboration reaction was reported by Männig and Nöth in 1985 using Wilkinson's catalyst (chloridotris(triphenylphosphane)rhodium(I)) to catalyze the reaction.^[18] The Rh(I) species in this catalyst is traditionally thought to undergo

oxidation addition of the borane reagent, e.g., catecholborane (CatBH), to the Rh(III) complex. This electron deficient species would facilitate the alkene substrate coordinate to the Rh and the ensuing alkene insertion step. The detailed mechanism of Rh catalyzed hydroboration is included in section 1.8 and figure 9.

There are crucial differences in terms of reactivity and regioselectivity of the reactions between the catalyzed and non-catalyzed conditions. For example, the 1mol% $\text{RhCl}(\text{PPh}_3)_3$ catalyzes hydroboration of γ,δ -unsaturated ketone react with CatBH to give the boronate product via alkene addition pathway. To the contrary, CatBH alone undergoes nucleophilic attack the carbonyl carbon effecting carbonyl reduction. Another profound difference between the catalyzed and non-catalyzed reactions, the non-catalyzed hydroboration of styrene gives the linear product as follows from the anti-Markovnikov addition rules. On the other hand, the Rh-catalyzed hydroboration gives the Markovnikov type branched product. (figure 4)

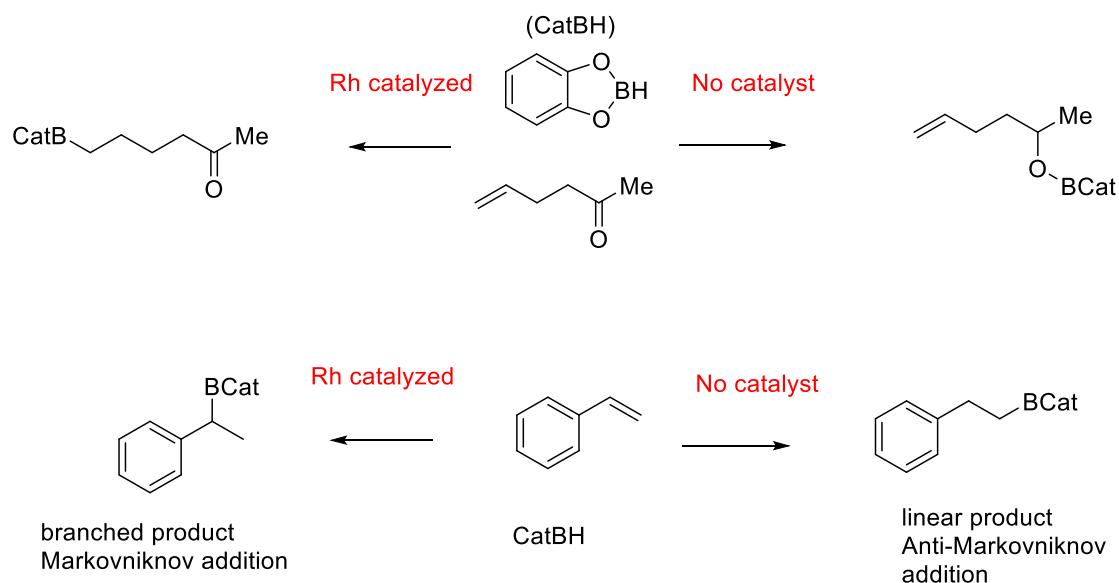


Figure 4. A comparison between catalyzed and uncatalyzed hydroboration reactions

1.4 Rh-catalyzed enantioselective alkene hydroboration

The first example of catalytic asymmetric hydroboration (CAHB) was reported by Burgess group in 1988^[19] and further developed by Hayashi^[2]. Norbornene, a 1,2-disubstituted with rigid and rather strained bicyclic structure, was subjected to hydroboration conditions with CatBH catalyzed by the combination of $[\text{Rh}(\text{cod})\text{Cl}]_2$ with the chiral diphosphine, DIOP. The reaction gives more than 90% boronated products. The enantioselectivity was checked after oxidizing the products and 64% ee indicates the ratio of two enantiomers in the product is about 4:1.

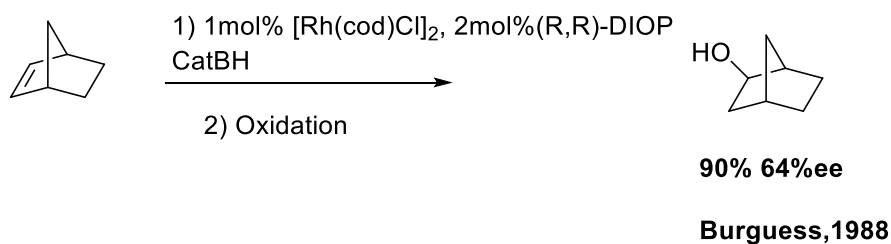


Figure 5 The early Rh-catalyzed enantioselective hydroboration reaction

Hayashi reported several new catalyst systems leading to improved enantioselectivity; for example, the cationic Rh/BINAP was found to be highly reactive. It catalyzes the hydroboration of styrene to completion in 30 min at low temperature. This is the 1st example that proves high level of enantioselectivity was attainable by CAHB. However, the hydroboration results catalyzed by BINAP exhibit limited substrate scope. ^[20] Knochel reported the new ligand, dicyclohexylbis(phosphane) that gave high chemo-, regio-, and enantioselectivity in the Rh catalyzed hydroboration. This ligand system can be employed on several ortho-, meta-, and para- substituted styrene to afford moderate to good enantioselectivity on boronate products. ^[21]

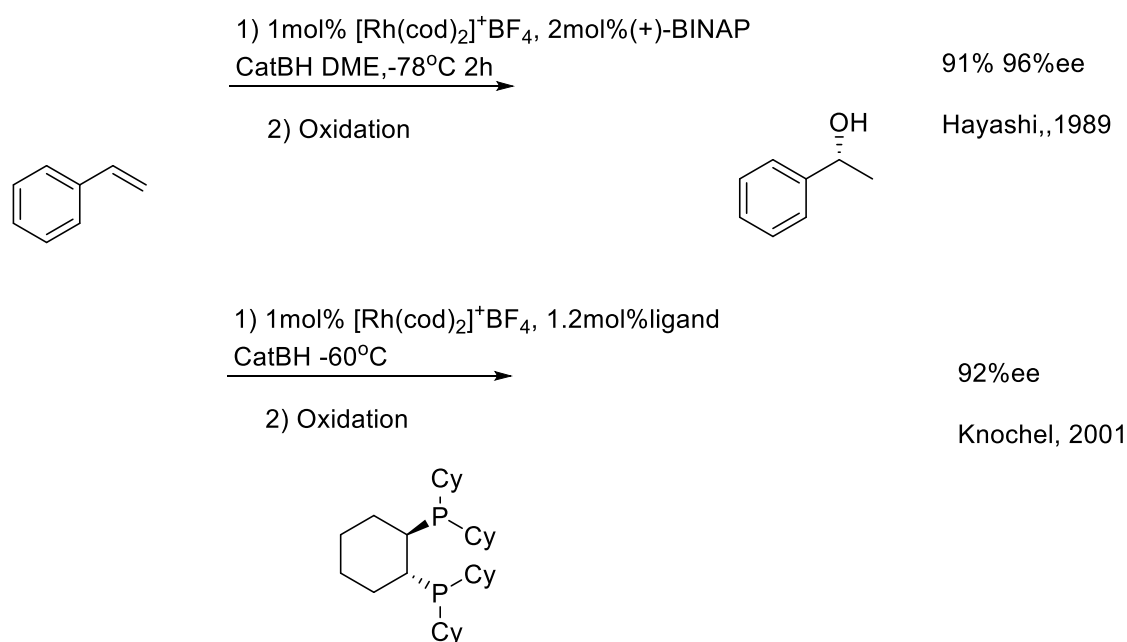


Figure 6. Examples of Enantioselective catalytic hydroboration

1.5 Enantioselective hydroboration catalyzed by transition metal other than Rh

The Rh is one of the better choices for the asymmetric hydroboration because other transition metal catalysts usually require longer time with low yield or enantioselectivity. For example, Micouin reported a hydroboration reaction that desymmetrize the meso of hydrazine, the Rh catalyst was very reactive even at -50 °C and reaction went to completion in 30 min. The boronate product was isolated in 91% yield with 84% ee. However, when an iridium catalyst was employed in the almost the same condition with higher temperature, they only got 40% boronate with 44% ee.^[22] Huang reported a cobalt-catalyzed enantioselective hydroboration of 1,1-disubstituted aryl alkenes using iminopridine-oxazoline ligands with robust reactivity as well as excellent enantioselectivity.^[23] The Lu group used similar ligands with Fe complex also discover promising results in 1,1-disubstituted alkene substrates, although the Fe catalyst loading is larger.^[24] Hoveyda reported CAHB using Cu complex with styrene derivatives. A high yield of boronate products with excellent % ee were observed. Hartwig developed asymmetric hydroboration on aliphatic internal alkenes with a directing group at the homoallylic position^[25]. CuCl and chiral ligands enables the highly regio- and enantioselective hydroboration which incorporate a wide range of functional groups in a regioselective and stereoselective manner. Despite the excellent results that complement the rhodium and iridium-catalyzed hydroboration, the drawback of these copper catalysts is the catalyst loading and reaction time (7.5 mol %,

48 h), both higher than other transition metal competitors.^[26]

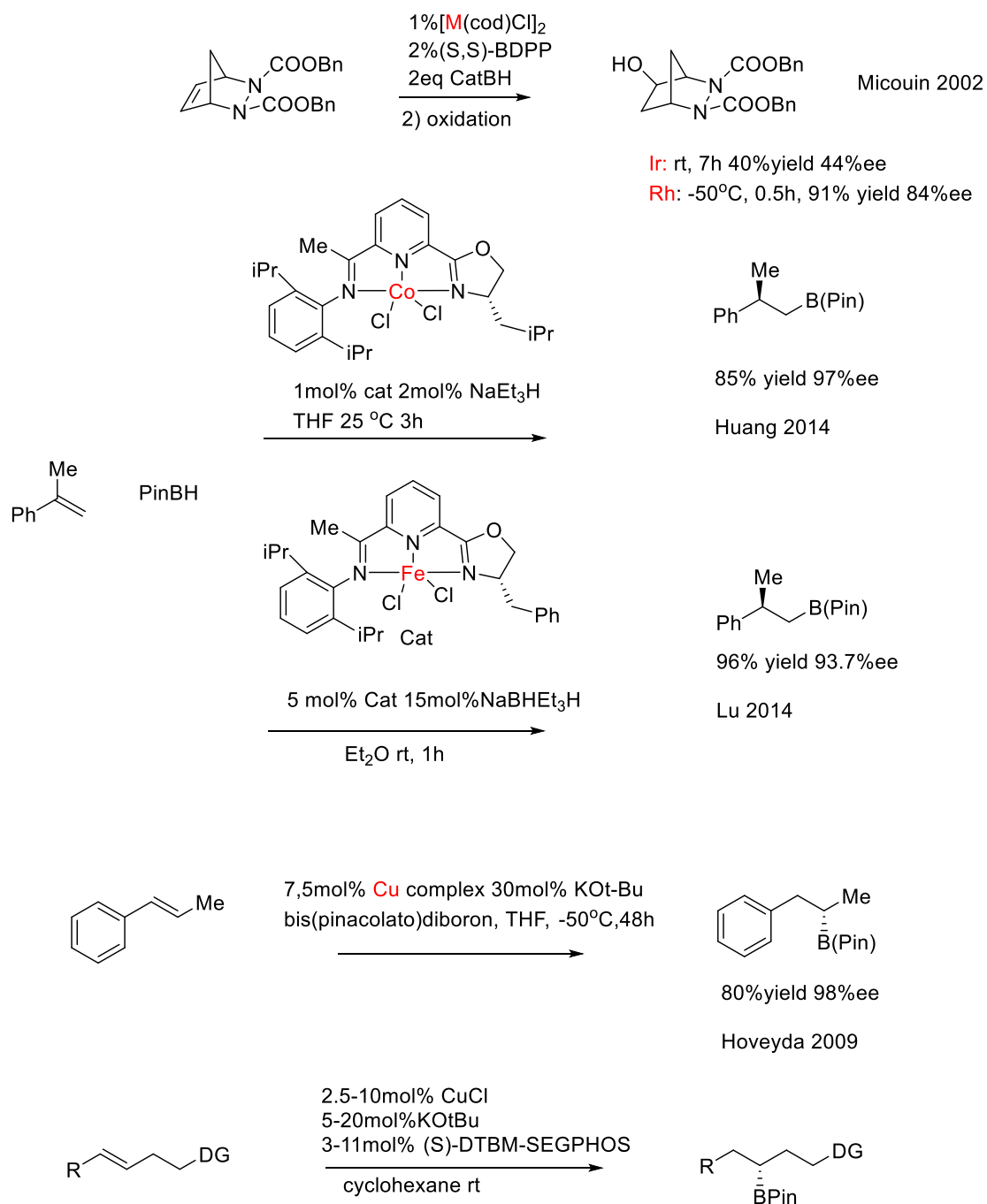


Figure 7. Catalytic asymmetric hydroboration catalyzed by other transitional metals

1.6 Substrates directed Rh-catalyzed enantioselective alkene hydroboration.

Despite all the developments achieved in a variety of area of preparing enantioenriched organoboronates, the utility of catalytic asymmetric hydroboration (CAHB) method has traditionally been compromised by a limited substrate scope. The examples mentioned above are exclusively showing effective enantioselective hydroboration on styrene and its simple derivatives. The severe lack of reactant structure flexibility significantly restricts this method's potential as building blocks and intermediates to construct the complicated bioactive natural molecules. As a consequence, the substrate directed CAHB has been investigated soon after the success of styrene hydroboration.

A substrate directed reaction involves part of the substrate interacting with reagents or catalyst through different intermolecular interactions, including covalent bonding, hydrogen bonding, electrostatic interaction, such that the reagents or catalyst can selectively approach and react a proximal part of the substrate molecule. To improve the regio- and stereoselectivity of CAHB, several useful directing groups were introduced to the alkene substrates. For example, Evans reported the first examples in which amide groups direct Ir-catalyzed hydroboration reactions.^[27] The high diastereoselectivity observed is apparently a consequence of two-point binding of the substrate, i.e., the carbonyl group on amide and alkene moieties coordinate to the Ir catalyst. Thus, *syn*-addition of the borane from the Ir complex is preferred. Fu later reported an efficient ether directed hydroboration; high levels of *syn*-stereoselectivity

indicate that the ether is a directing group.^[28] In 2003, a pendant ester was employed as the directing group by Gevorgyan. This discovery not only introduced another effective directing group to CAHB, but also provide a versatile functional group that can be transformed into other building blocks.^[29]

1.7 Recent development on amide directed CAHB

The Takacs group is responsible for recent studies of the substrate directed CAHB reactions by using TADDOL and BINOL derivatives as chiral monodentate ligands.^{[3,}

^{30]} For example, excellent yield and enantioselectivity are obtained by employing the phosphite and phosphoramidite ligands.^[30f] Because many asymmetric catalyst are highly substrate dependent and intolerant of small change on the structure, it is interesting to find that this catalyst system works well on both *E*- and *Z*-isomer of the substrate and afford the same product (Figure 9).

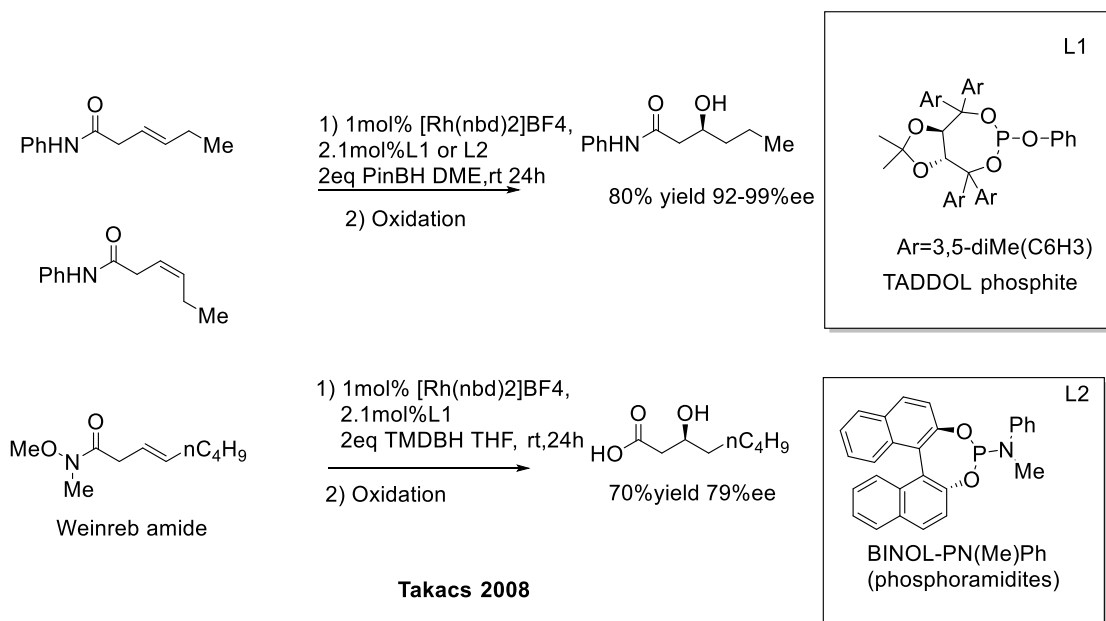


Figure 8. Highly regio- and enantioselective amide directed Rh catalyzed CAHB on β,γ -unsaturated amides

1.8 Mechanistic insights into the CAHB

Manning and Nöth proposed the first generally accepted mechanism of the rhodium-catalyzed hydroboration.^[18] The catalytic cycle begins with Wilkinson's catalyst; dissociation of one PPh₃ ligand forms Intermediate **I** coordinated with solvent. The Rh(I) Intermediate **I** is thought to oxidatively add the borane reagent giving the Rh(III) Intermediate **II** that can associate with the alkene substrate to form complex **III**. Alkene insertion into the Rh-H bond generates the Rh(III) Intermediate **IV** and/or its regioisomer. These two isomer intermediates lead to the branched and the linear products, respectively. The last step is the reductive elimination of the Intermediate **IV**, which means Rh(III) is reduced to Rh(I), while forming the carbon-boron bond to afford branched or linear boronate products.

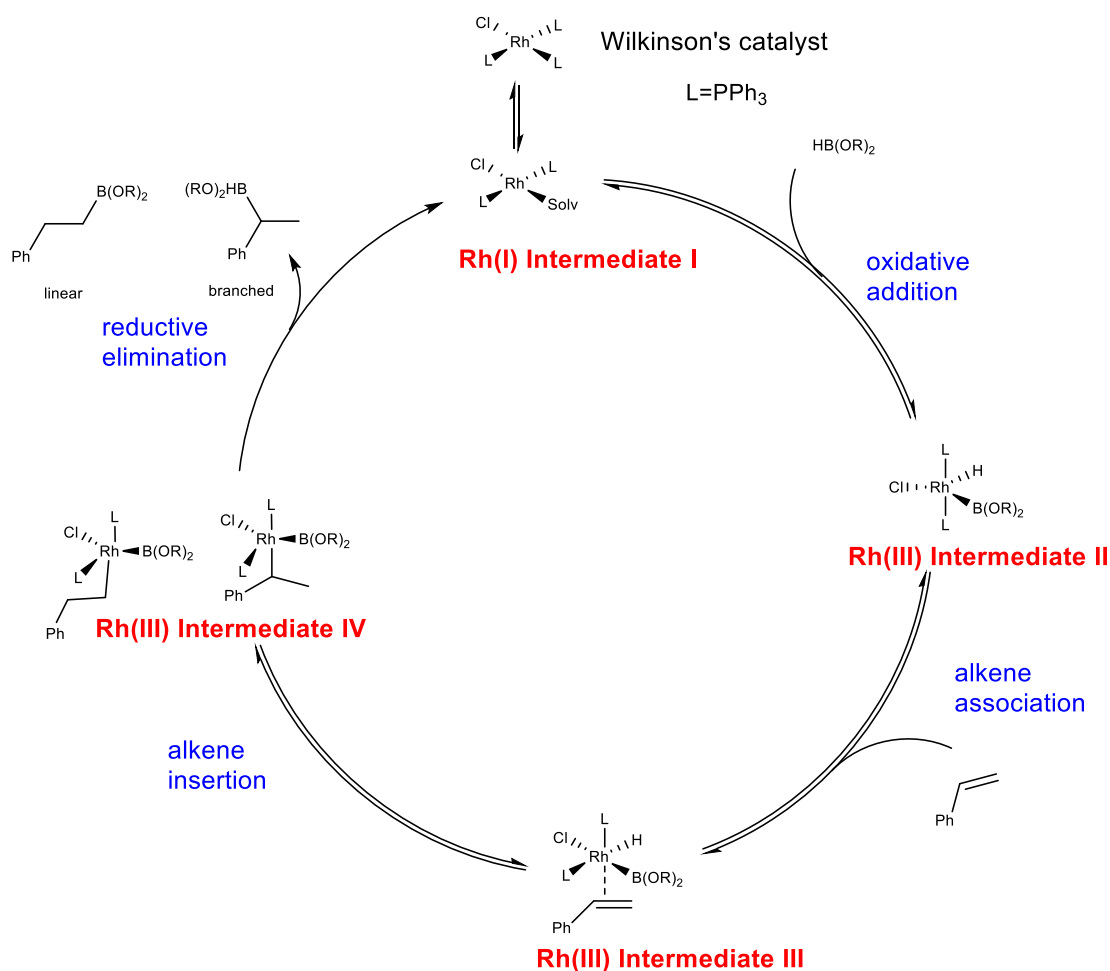


Figure 9 proposed catalytic cycle of the Rh-catalyzed hydroboration

In 1990, Evans reported a mechanistic investigation of the Rh-catalyzed hydroboration. According to their study, the possibility of heterogeneous, radical, and non-stereospecific reaction is eliminated.^[31] In the Deuterium labeling test by using CatBD, it was determined that the reversibility of alkene insertion step depends on the nature of alkene substrate. For example, in the hydroboration of 1-decene, there is deuterium scrambling found in both the alkene substrate and the boronate product which indicates both alkene insertion into the Rh-D bond and alkene complexation Rh are reversible for this substrate. However, when they subjected the styrene into the same reaction

conditions, no deuterium incorporation on starting material or doubly deuterated product was found. These results exclude the possibility of similarly reversible steps in the reaction mechanism.

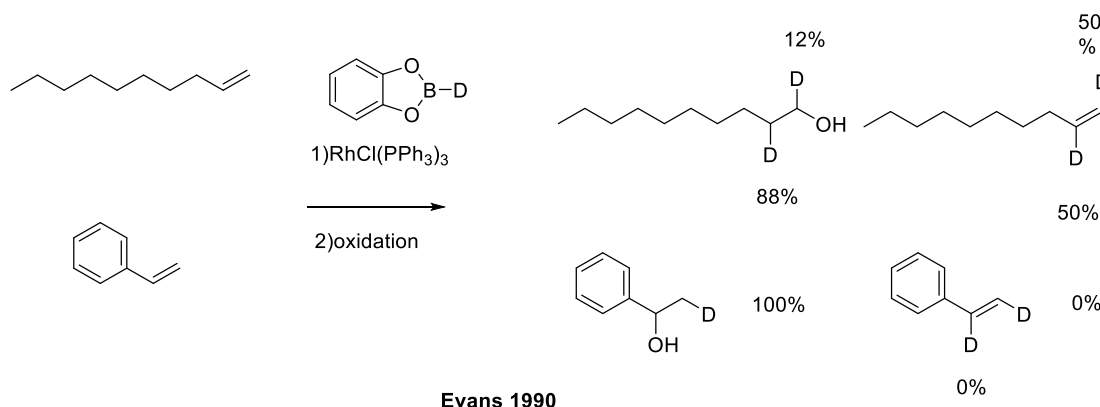


Figure 10 Mechanistic investigation by deuterium labeling.

Based on the results reported by Morokuma^[32] and Schleyer^[33], a computational study was carried out by Ziegler to exam the mechanism of Rh-catalyzed hydroboration.^[20] To reduce the computation, the simplified boranes and phosphane (i.e., PH_3) were employed into reactions. The study suggests that the alkene insertion step may involve in either inserting into Rh-B or Rh-H bond which are equal in energy for two potential pathways. The Takacs group reported a computational study of the two-point binding hypothesis which revealed several different mechanistic insights to previous studies.^[30g] Due to the nature of two-point binding substrates, the active intermediates in the catalytic cycle are six-coordinated instead of pentacoordinated. Two monodentate ligands involved in the intermediates which can form more complicated structures. Two coordinated groups in the substrate chelate to the Rh-complex leading to the *cis*-

configuration intermediate that supported by correlation with experimental results showing the formation of a major γ -borylated product. The two-point binding mechanism can better explain experimental results and observations for enantioselective reactions of CAHB on acyclic β,γ -unsaturated amides, compared with the previously reported one-point binding hypothesis.

1.9 Summary

There is an intensive study of chiral organoboronates as synthetic building blocks in the stereoselective synthesis as a result of recent developments and supplements to the methods available for their stereoselective hydroboration as well as stereospecific functionalization. These organoboronates are valuable intermediates to the pharmaceutical industry and can be widely applied to the synthesis of natural products. Therefore, tremendous amount of reports emerges to optimize the preparation of chiral organoboronates.

The catalytic asymmetric hydroboration (CAHB) of alkenes is an effective method for the synthesis of chiral organoboronates, however, the narrow substrate scope severely compromises the utility of this method. With limited exceptions, the application of CAHB is highly restrained to styrene derivative substrates or strained alkenes. Previously, Takacs group successfully expanded reaction scope to aliphatic β,γ -unsaturated amide. And cyclic γ,δ -unsaturated amides with high yields and enantioselectivity. However, acyclic γ,δ -unsaturated amides, which is an unstrained

alkene, have yet to be addressed.

Two topics would be covered in this thesis. (1) The effectiveness of previous CAHB catalyst system, Rh-phosphines or phosphoramidites, on acyclic γ,δ -unsaturated amide substrates. (2) The kinetic study to give a mechanistic insight of CAHB employing the reaction progress kinetic analysis. The discussion is based on our two-point binding mechanism hypothesis that the presence of a suitable directing group would increase the reactivity of the normally non-directed alkene substrates toward directed CAHB by virtue of two-point binding as is the case in catalytic asymmetric hydrogenation^[34]

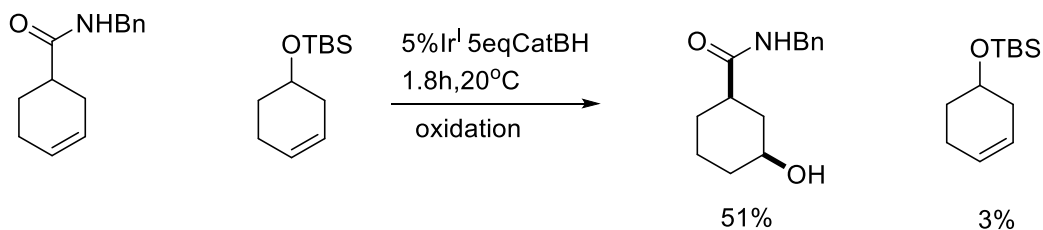
Chapter 2: Carbonyl-directed catalytic asymmetric hydroboration (CAHB) of 1,2-disubstituted γ,δ -unsaturated amide.

2.1 Background: amide directing asymmetric hydroboration of γ,δ -unsaturated 1,2 disubstituted alkene.

The numerous improvements made in catalytic asymmetric hydroboration (CAHB) of alkenes are primarily focusing on vinyl arene substrates and in a few cases strained alkenes.^[35] Despite the high regio-, stereoselectivity on vinyl arene substrates and strained alkenes, the enantioselective hydroboration of internal alkenes are rather limited^[26, 36]. New substrates containing other functional moieties that can tolerate the hydroboration conditions and could be converting further to other functional groups are therefore interesting fields to explore.

In 1992, Evans group reported the first highly regioselective amide directed hydroboration of a γ,δ -alkene catalyzed by iridium complex demonstrating that the carbonyl oxygen enhanced the reactivity of hydroboration for γ,δ -alkene.^[37] In a competition experiment, the γ,δ -cyclohexene phenyl amide is 10 times more reactive toward iridium-catalyzed hydroboration than its analogous cyclohexene lacking the carbonyl group having OTBS in its place. Since the OTBS group is remote to the alkene moiety, a steric or an electronic effect is unlikely to be the origin of its relative low

reactivity. The predominant 1,3-*syn*-product indicates the carbonyl group and alkene chelate to the catalyst, resulting in the *syn* coordination of carbonyl group with Rh-C bond before the reductive elimination to generate the observed 1,3-*syn*-product.

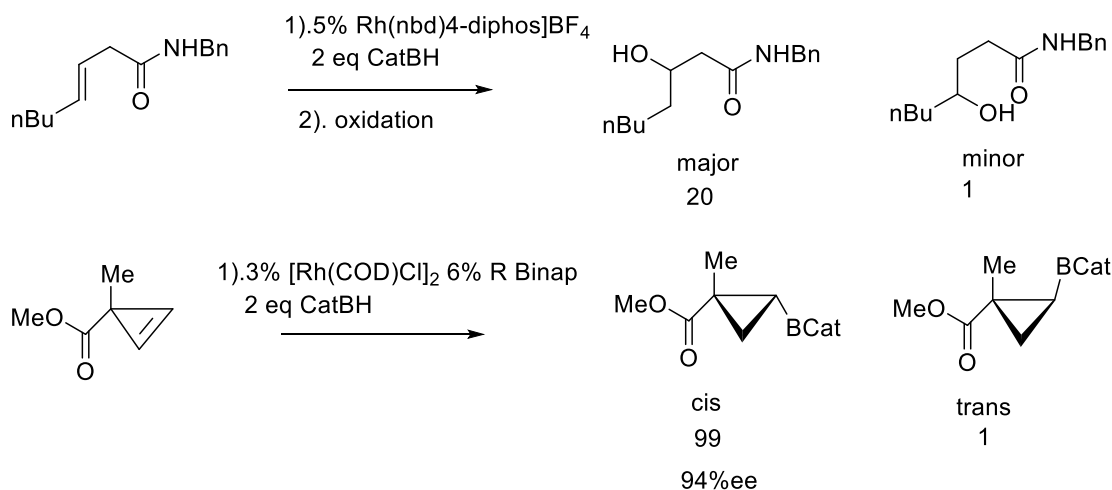


Evans 1992

Figure 11 The competition reaction of γ,δ unsaturated amide substrates.

An acyclic structure was also successfully subjected to regioselective hydroboration.^[27]

For example, the β,γ -unsaturated amide (figure 12) gave a good yield of β -borylated product with excellent regioselectivity (74% yield, 20 :1 regioisomer) presumably as a consequence of the two-point binding mechanism.



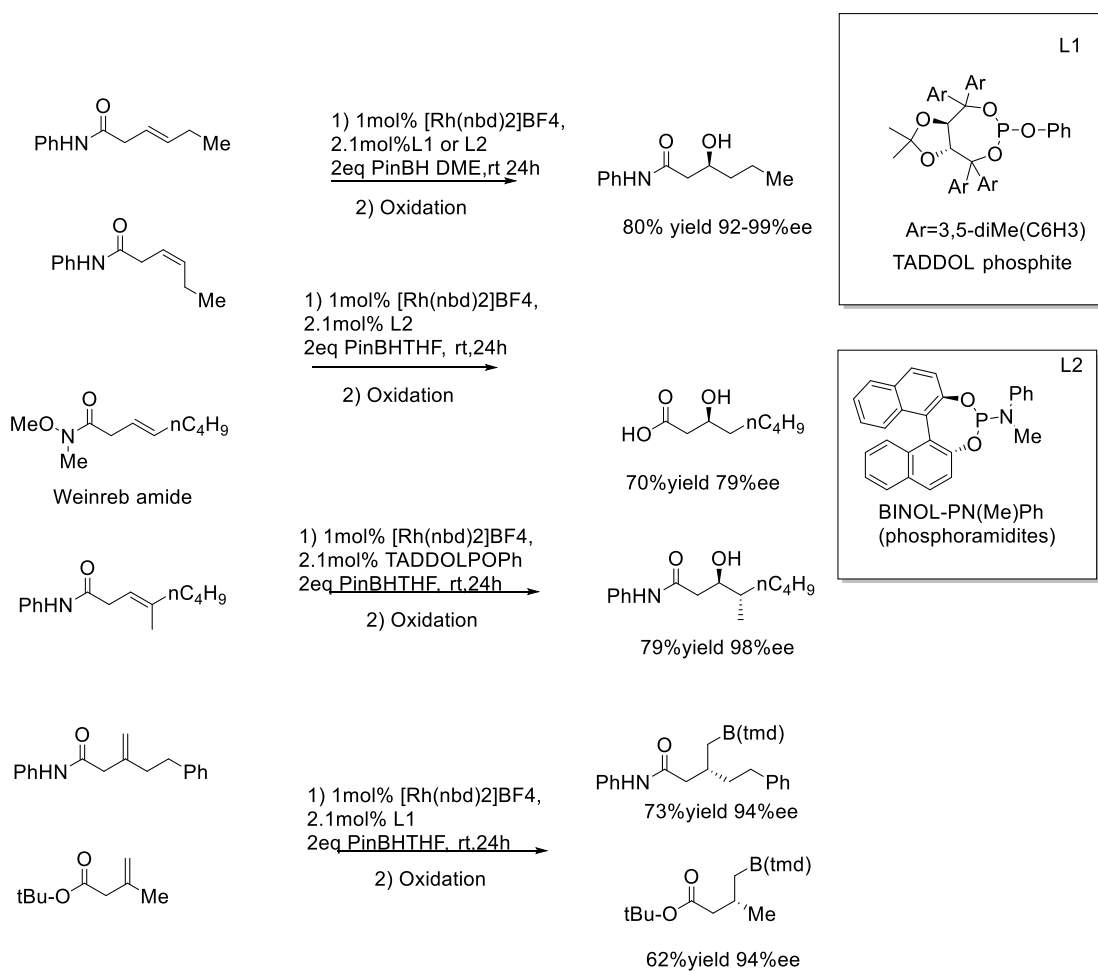
Evans 1991

Figure 12 The directed CAHB reaction of acyclic γ,δ -unsaturated amide and cyclic

unsaturated ester substrates.

In a study of CAHB on cyclopropenyl esters by Gevorgyan^[29], the strained nature of the symmetric molecule and an ester directing group contributed to the high regioselectivity and high enantioselectivity of the borylated product.

The results discussed above indicate that a carbonyl group like amide and ester are capable of chelating to Rh complex with olefin moiety. But the control of enantioselectivity needs to be improved particularly for acyclic structures. The Takacs group developed several amide or oxime directed β,γ -alkene substrates that perform well with the cationic Rh-TADDOL or -BINOL complexes.^[3, 30f] Even the less reactive trisubstituted ^[30d, 30e] and the challenging 1,1-disubstituted substrates ^[30c] proceed with high regio- and enantioselectivity.

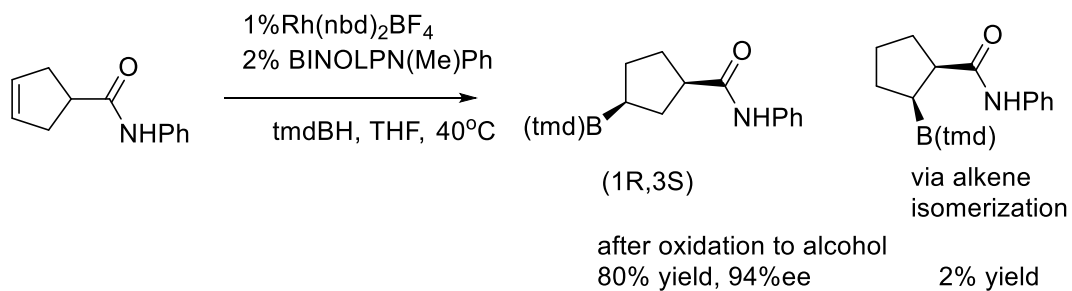


Takacs Group

Figure 13. Examples of amide directed β,γ -unsaturated amide CAHB.

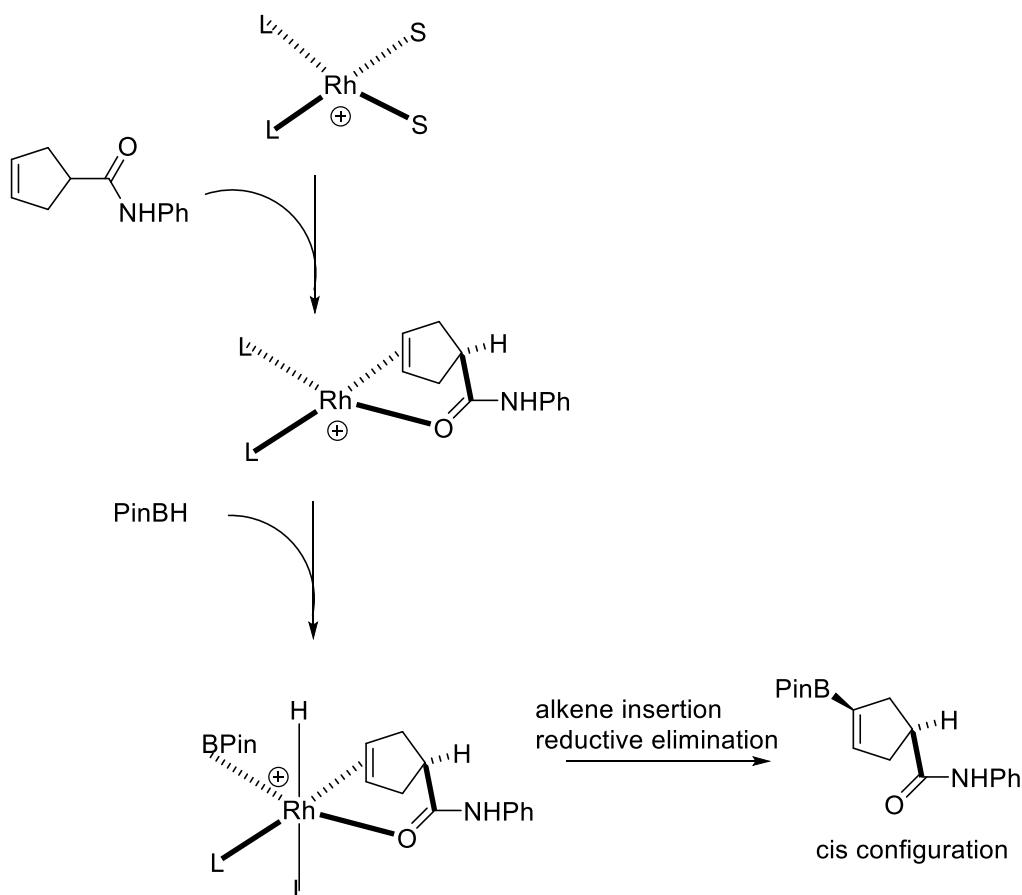
The success of β,γ -unsaturated amide substrates makes this catalytic system promising for expanding the substrate scope of directed CAHB. The Takacs group carried out several investigations on the CAHB of a cyclic γ,δ -unsaturated amide.^[30g] The proposed two-point binding mechanism is supported by a parallel computational study^[30g] that suggests the alkene and amide carbonyl oxygen on the substrate can chelate the cationic Rh(I) catalyst. This study suggested that the major γ -borylated product (1R*,3S*)-2 should result from the cis relative configuration after the chelation of substrate to the cationic Rh(I). The predicted cis configuration is supported by the experimental results.

To form the final borylated products, several potential pathways are possible including alkene isomerization via β -hydride elimination, reductive elimination and a newly discovered most energy-favored amide rotation followed by reductive elimination.



Takacs Group 2015

Figure 14 Computational study experimental results.



Takacs Group 2015

Figure 15. Mechanistic interpretation of CAHB on cyclic γ,δ -amide

2.2 Motivation on study of directed CAHB of γ,δ -unsaturated amide.

The previous studies of CAHB on γ,δ -unsaturated amide are mainly focused on a simple substrate containing symmetric ring structure. We would like to further investigate in this γ,δ -unsaturation pattern because of the following considerations.

- 1) The Rh catalytic system developed in our group is successful on β,γ -substrates and had showed promising results in the cyclic amide directed CAHB case. Thus, it is highly possible we would make breakthrough on general γ,δ -unsaturated amide substrates for which the directing group and the alkene moiety are but one carbon further removed.
- 2) Chiral organoboronates are useful synthetic intermediates. At the moment, several synthetically-useful, stereospecific transformations of organoboronates have been developed.^[38],^[10a]. Thus, building enantioenriched γ - or δ -borylated products could enhance the potential utility of organoboronates in synthetic chemistry, in particular, by creating a versatile platform for hydrofunctionalization that produces molecules containing C-N, C-halogen and C-C bonds.
- 3) The development of C-N activation makes the amide moiety on alkene substrate more than just a directing group. The amide group is an active site for a variety of

subsequent transformations. For example, the Boc-protected benzylamide can be transformed into the ester^[39] or ketone^[40] in high yields in a Ni-catalyzed reaction; the latter are very practical functional groups in organic synthesis.

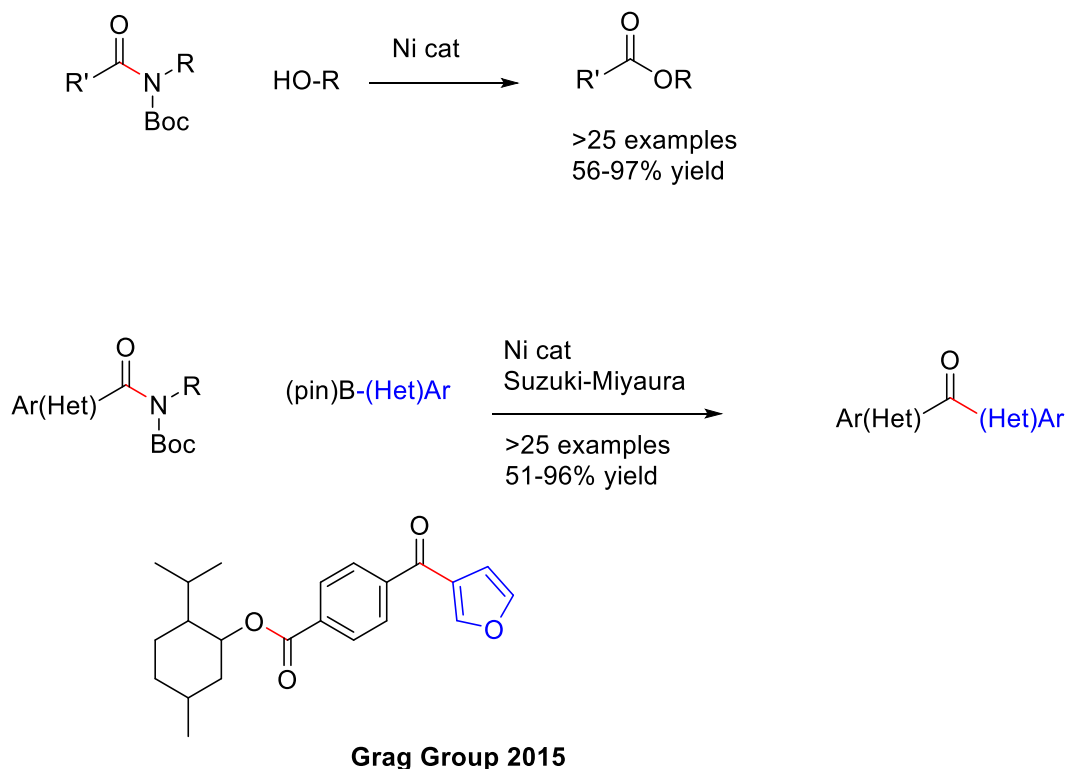


Figure 16 Examples on amide functionalization from the organoboronates.

2.3 Rh-catalyzed asymmetric hydroboration of two-point binding substrates: condition optimization

For the reasons discussed above, we began investigation into the CAHB on γ,δ -unsaturated amides. The Takacs group had previously reported rhodium-catalyzed carbonyl-directed catalytic hydroboration (directed CAHB) for a variety of β,γ -unsaturated amides and esters. Recently, the enantioselective desymmetrization of a

cyclic symmetric γ,δ -unsaturated amide was discovered by using the same catalyst systems. The products were β - and γ -borylated carbonyl compound with high regio- and enantioselectivity.

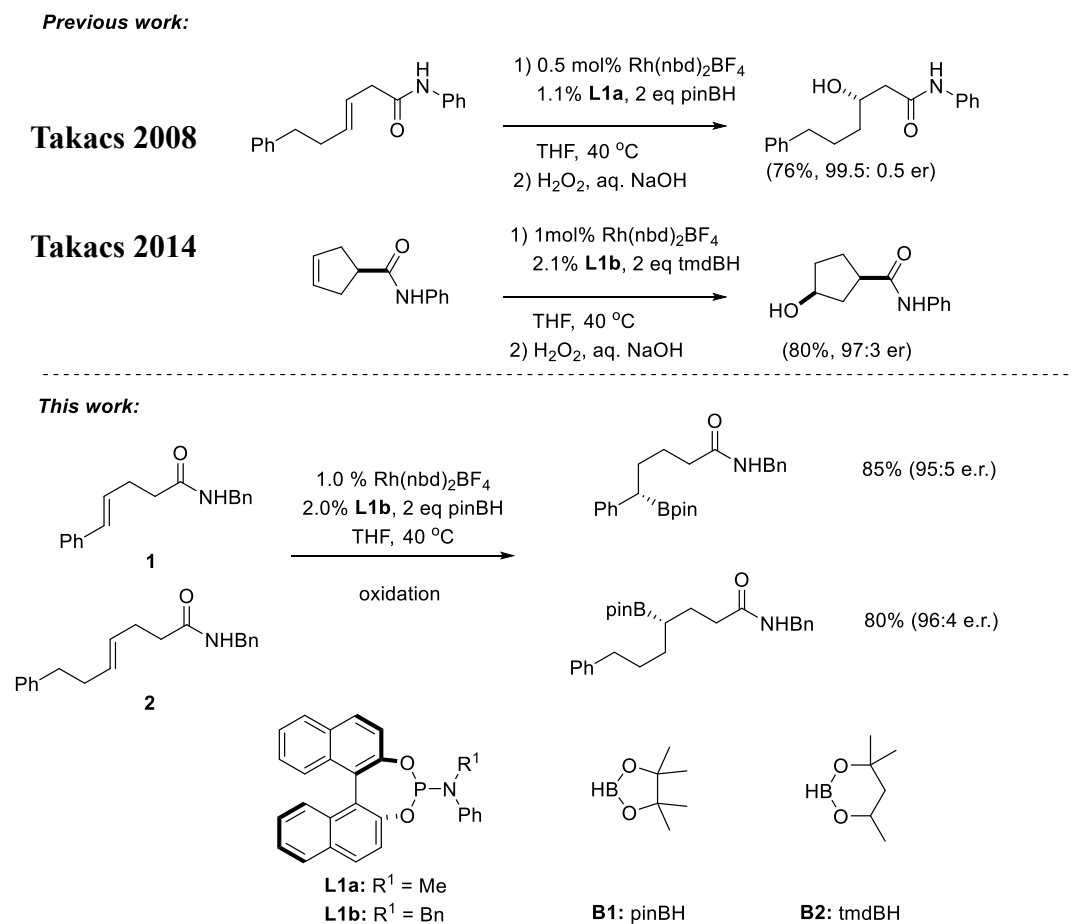


Figure 17 comparison between previous CAHB results and the topic in this thesis.

To further expand the substrate scope on γ, δ -unsaturated amide system, we investigated CAHB of the acyclic γ,δ -unsaturated amide substrates. For example, the unsaturated amide substrates **1** and **2** undergo carbonyl directed CAHB with pinacolborane (PinBH) using Rh(nbd)₂BF₄ in conjunction with phosphoramidite ligand, e.g., BINOL(PN)BnPh,

to give the γ - or δ -borylated hydroboration product in 80% yield and 91% ee; the percent ee is determined by chiral HPLC for its hydroxy derivatives after oxidation.

The product of CAHB on the alkyl-substituted acyclic γ,δ -unsaturated amide substrate is predominantly chiral secondary γ -borylated amide in 80% yield and 92% ee. The aromatic-substituted substrate affords δ -borylated product with 85% yield and 90% ee. the regioselectivity is greater than 20:1 in most cases.

2.4 Optimization studies on CAHB of substrate

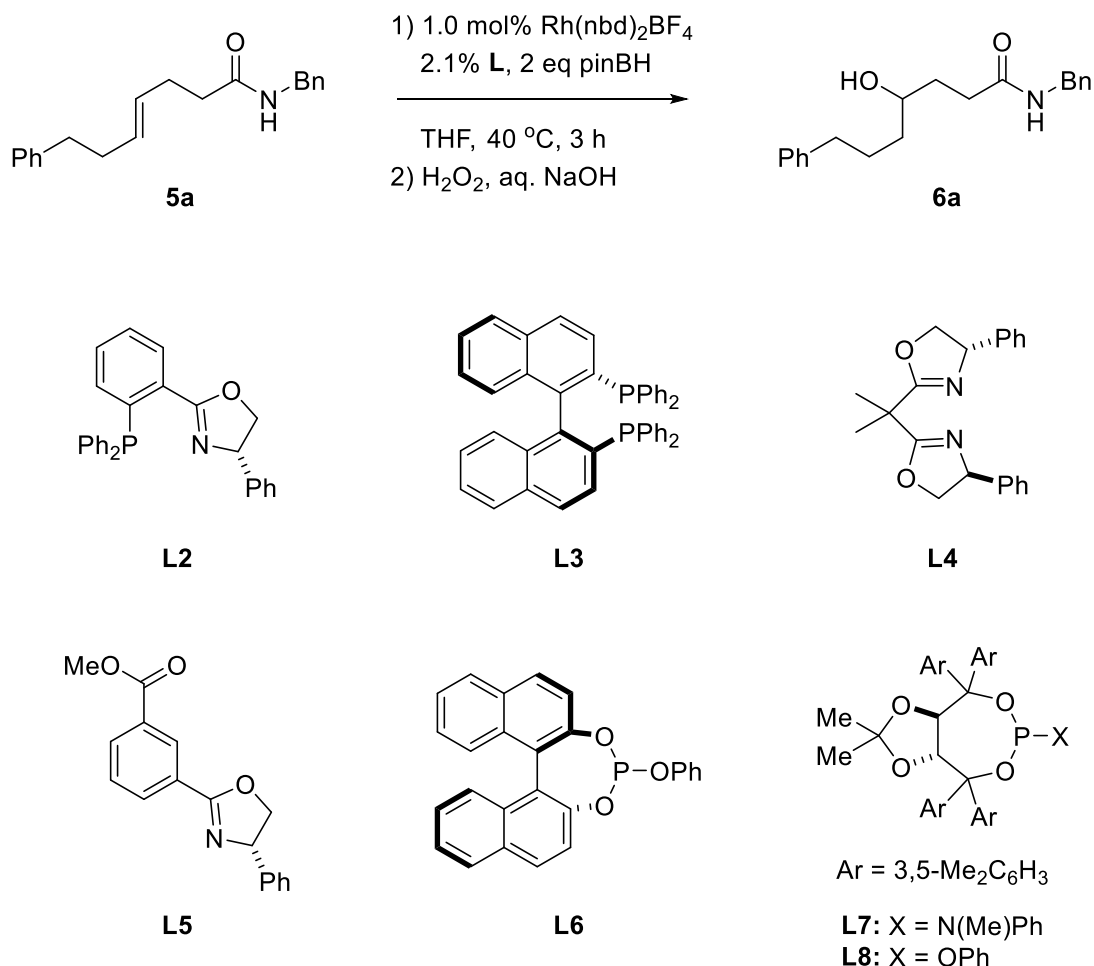


Figure 18 The ligand optimization of amide directed CAHB on γ,δ -unsaturated amides

The effect of ligand structure on the CAHB was surveyed with several common ligand

motifs for *N*- and *P*-ligands either monodentate or bidentate. The summarized results are shown in the table below.

Table 1 ligand optimization of amide directed CAHB on γ,δ -unsaturated amide

| Entry | Ligand | Conversion (%) | Yield of 6a (%) ^b | er of 6a ^c |
|-------|--------|----------------|-------------------------------------|------------------------------|
| 1 | L1a | 99 | 90 | 97:3 |
| 2 | L1b | 99 | 95 | 96:4 |
| 3 | L2 | 16 | Trace | NA |
| 4 | L3 | 99 | 16 | ND |
| 5 | L4 | 99 | 24 | ND |
| 6 | L5 | 20 | Trace | NA |
| 7 | L6 | 99 | 70 | 72:28 |
| 8 | L7 | 99 | 88 | 56:44 |
| 9 | L8 | 99 | 85 | 73:27 |

Phosphinooxazoline ligand **L2** is a bidentate ligand which is typically used in asymmetric allylic substitution (i.e., Tsuji-Trost reaction^[41], aminations^[42], sulfonylations^[43]) and asymmetric hydrogenation.^[44] However, most of the effective catalyst systems are Ir, Ru, Ni^[45] or Pd. We find low (16%) conversion of starting material also proves that the complex of cationic Rh and phosphinooxazoline is not a good choice for CAHB. BINAP (**L3**) is widely used in the transition metal catalyzed asymmetric synthesis due to its C₂ axial chirality.^[46] In our ligand screening, BINAP-

Rh complex showed high reactivity toward alkene substrate but very low chemoselectivity with only 16% of the γ -borylated product generated. The bidentate bis(oxazoline) (i.e., BOX) ligand has a wide substrate scope in asymmetric catalysis.^[47] The C_2 -symmetry of this ligand often results in high π -facile selectivity. However, only 24% γ boronate was isolated from the reaction. The other bidentate ligands above (L2-L4) similarly failed to show promising results. Monodentate oxazoline ligand (L5) is used to build supramolecular catalyst for catalytic asymmetric hydrogenation^[47] and hydroboration^[48]. It gave low reactivity on alkene substrate (20% conversion after 3h). The TADDOL-derived phosphoramidite (L7) and phosphite (L8) ligands showed good chemo- and regioselectivity (85-88% γ -borylated product) while only low to modest enantioselectivity (12-46% ee). Finally, the BINOL(PN)MePh (**L1a**) and BINOL(PN)BnPh (**L1b**) gave excellent yield (90-95%) and good enantioselectivity (92-94% ee). The BINOL-derived phosphite family catalysts worked best for γ,δ -substrate in this screen, which is also the optimal ligand in the previous β,γ -unsaturated amide CAHB study. The major side product in the optimal condition is the reduced product.

2.5 The substrate scope of CAHB on γ,δ -unsaturated amide

To explore the generality of the optimized catalyst system, a series of gamma delta unsaturated amide was prepared via one of the 3 synthetic pathways listed below.

2.5.1 General information on preparation of γ,δ -unsaturated amide substrate

The first pathway is the general method to prepare all the γ,δ -unsaturated amide series substrates. The long synthetic procedure is a reliable way to prepare the γ,δ -unsaturated amide although it limits the overall yield and material throughput. Another drawback of this method is that the allylic carbonate substitution step requires the expensive Pd(PPh₃) reagent as the catalyst. The pronucleophile in this Pd-catalyzed allylic substitution reaction is the malonate which could be sequentially deprotonated twice by NaH under the reaction conditions. Thus, the malonate-allylic adduct could act as nucleophile again to substitute the carbonate group at allylic position; double allylation reduces the product yield. The reaction time varies among the sought-after derivatives and yet reaction time is crucial to control the chemo-selectivity in this reaction. To avoid the side product results from the second nucleophilic substitution, TLC (Thin Layer Chromatography) was used to monitor the reaction progress. The γ,δ -unsaturated dimethyl malonate intermediate was hydrolyzed under NaOH/EtOH condition to form the unsaturated diacid. The decarboxylation and amination was followed by using CDI (carbonyldiimidazole) and benzyl amide. The overall yield for this pathway is about 25%.

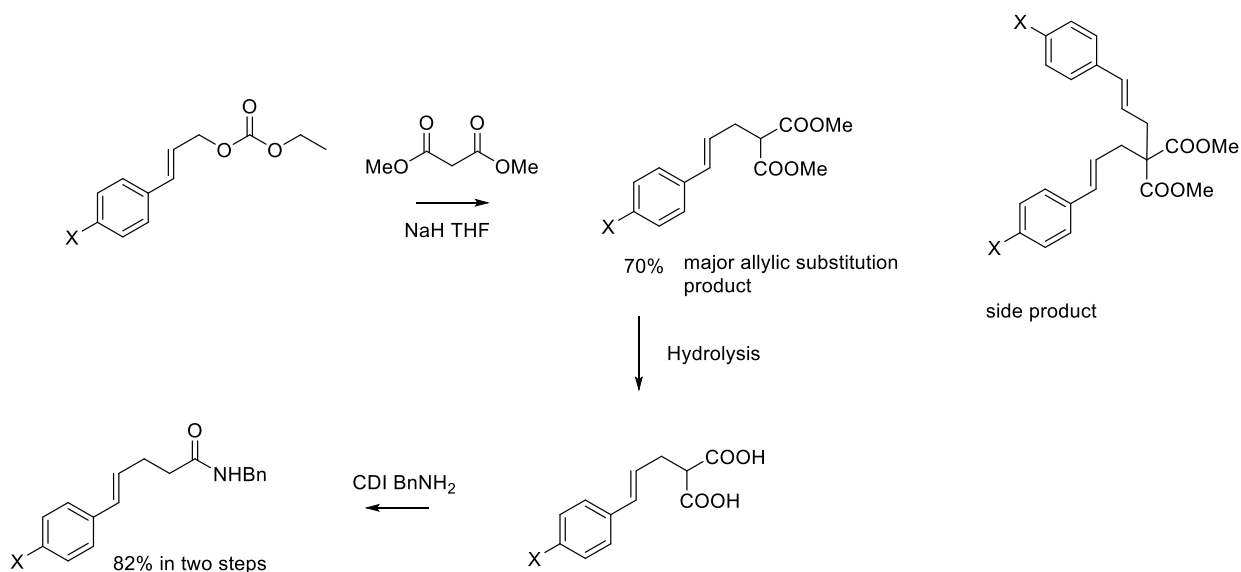


Figure 19. The preparation of γ,δ -unsaturated amide by Pd catalyze allylic substitution

The second method to introduce the γ,δ -unsaturated subunit is by the Claisen-Ireland rearrangement. The allylic alcohol is easily prepared by Grignard reaction then treated by excessive amount of ToEA (tri-ortho ethyl acetate) to form the allylic ester intermediate which undergo the Claisen-Johnson rearrangement promoted by the catalytical amount of propionyl acid at reflux condition. This facile reaction went to completion in about 30 min when the by-product EtOH was no longer collected by distillation. The remaining ToEA is removed by stirring overnight with HCl solution. Finally, the isolated γ,δ -unsaturated ester product is treated with TMA (trimethyl aluminum) and the requisite to afford the desired amide substrate.

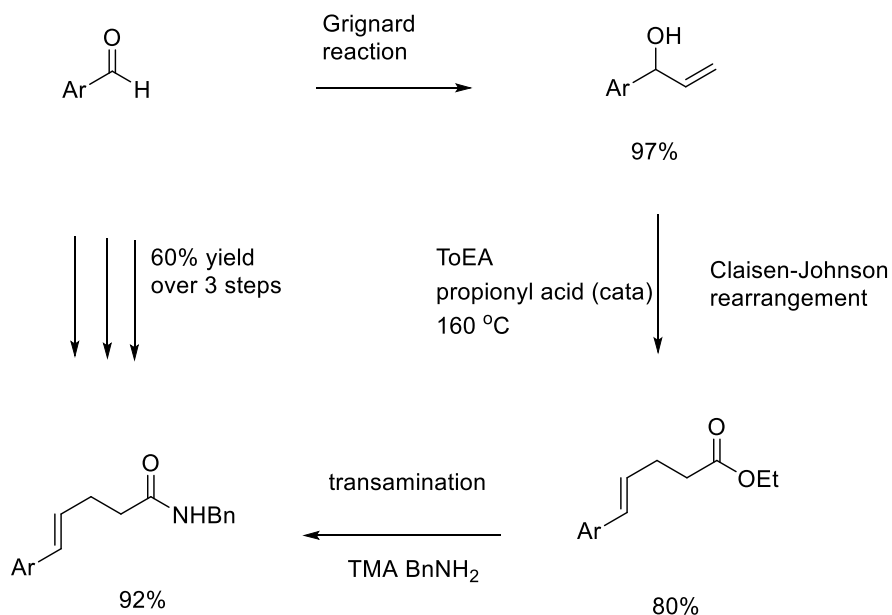


Figure 20. The preparation of γ,δ -unsaturated amide by Claisen-Johnson rearrangement.

The main advantage of this second method is its short preparation throughput time and high yield, generally over 60% in 3 steps. The only major drawback is the difficulty in completely separating the unsaturated ester from the *ToEA*; the latter competes to consume *TMA* and BnNH_2 and generate an unwanted side product. The method has been tested to work perfectly with respect to with the substrates containing a phenyl substituent on the alkene (i.e., aryl-substituted) as well as those phenethyl-substituted (i.e., alkyl-substituted). However, it didn't work with the substrates containing a furan substituent on the alkene.

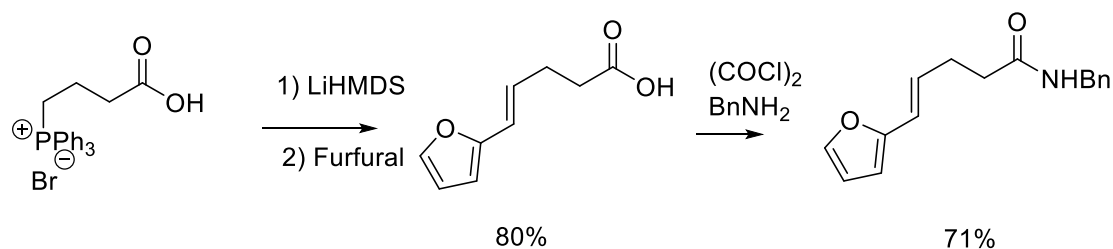


Figure 21 The preparation of γ,δ -unsaturated amide by Wittig reaction.

The furan-substituted alkene could be prepared by the first method described above; however, we chose a Wittig route instead. The Wittig salt can be prepared from 5-bromopentanoic acid. The following Wittig reaction with requisite aldehyde followed by amination from sequential treatment with $(\text{COCl})_2$ and BnNH_2 affords the furan-substituted γ,δ -unsaturated 2-benzyl amide. Although this 2 steps pathway provides high yield, the 5-bromopentanoic acid is expensive limiting the utility of this method to small test screening.

2.5.2 Substrate scope study with different substituents

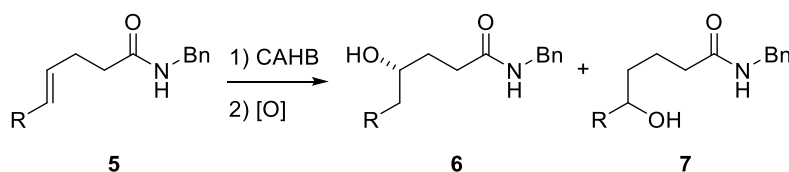


Figure 22 substrate scope study and the possible products

Table 2. Results of substrate scope study with different substituents

| entry | 5 | R | Alkene geometry | Yield of 6/7 (6:7) ^b | er ^c of 6/7 |
|-------|---|------------------------------------|-----------------|---|-------------------------------|
| 1 | a | CH ₂ CH ₂ Ph | <i>E</i> | 80 (20:1) | 96:4 |
| 2 | b | CH ₂ CH ₂ Ph | <i>Z</i> | 78 (20:1) | 93:7 |
| 3 | c | Ph | <i>E</i> | 85 (1:20) | 95:5 |
| 4 | d | para-F-Ph | <i>E</i> | 71 (1:20) | 90:10 |
| 5 | e | para-CF ₃ -Ph | <i>E</i> | 75 (1:20) | 90:10 |
| 6 | f | meta-OMe-Ph | <i>E</i> | 90 (1:20) | 95:5 |
| 7 | g | para-OMe-Ph | <i>E</i> | 88 (1:20) | 95:5 |
| 8 | h | Ortho-OMe-Ph | <i>E</i> | 68 (1:20) | 69:31 |

the electrons through resonance structures, its steric influence reduces both the hydroboration yield (68%) as well as the enantioselectivity (38% ee). In conclusion, the electronic effect plays a small role in the hydroboration process, the electron rich alkene generally shows higher regio- and enantioselectivity. The steric hindrance would have a large factor in the hydroboration process.

2.6 CAHB on morpholine amide

Morpholine amide is a good alternative to the Weinreb-amide as a versatile precursor to prepare ketones^[49] and aldehydes^[49b, 50] due to the high costs of MeNHOMe-HCl. In this study, the CAHB of γ,δ -unsaturated morpholine amide is also found to be quite effective. The unsaturated morpholine amide **8** can be converted to the γ -borylated product with BINOL phosphoramidite ligands in high yield (81-86%) and excellent enantioselectivity (90-95% ee). The optimal ligand in this case is the BINOL(PN)BnPh. However, for the 1,1-disubstituted alkene substrate **10**, the enantioselectivity is lower lower than that of 1,2-disubstituted derivative **8** using the same Rh catalyst complex. 1,1-Disubstituted alkenes are often challenging substrates for asymmetric hydroboration.^[51] The BINOL(PN)PhPh ligand provided best results among BINOL ligands we tested, 80% ee. Although the enantioselectivity on 1,1-disubstituted substrate needs further developments, the CAHB on 1,2 disubstituted substrate affords high yield and enantioselectivity of the borylated-morpholine amide which can be

readily refunctionalized at both boronate site and morpholine sites.

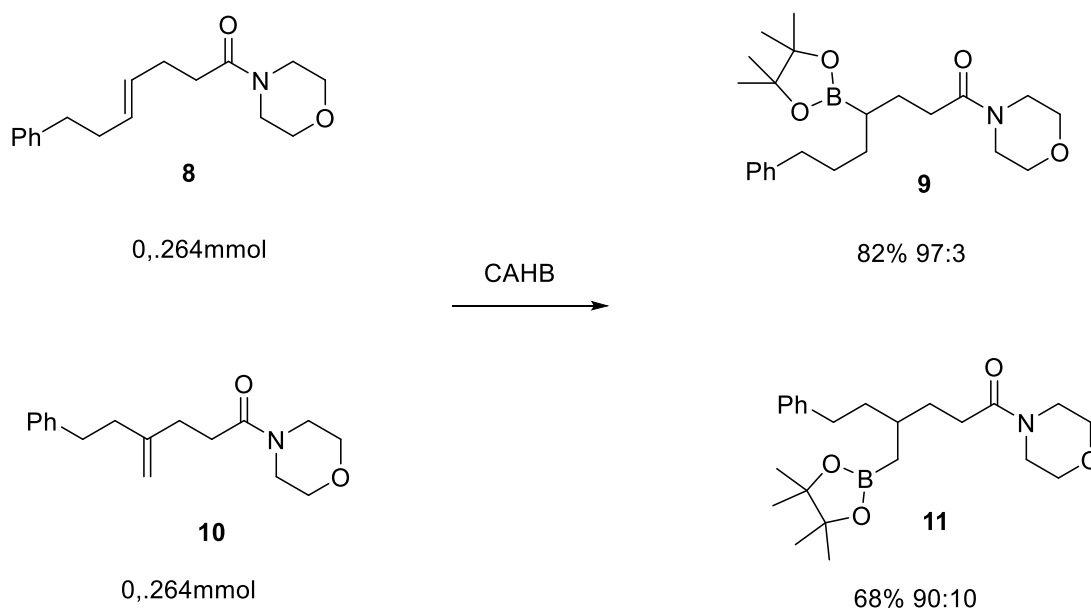


Figure 23 CAHB on morpholine amide

Table 3 CAHB on morpholine amide with BINOL series ligands

| entry | alkene | ligand | Yield of 9/11 | er ^c of 9/11 |
|-------|-----------|---------------------------------|----------------------|--------------------------------|
| 1 | 8 | (R) BINOL(PN)MePh | 81% | 95:5 |
| 2 | 8 | (R) BINOL(PN)BnPh | 82% | 97:3 |
| 3 | 8 | (R) BINOL(PN)PhPh | 86% | 95:5 |
| 4 | 10 | (R) BINOL(PN)BnPh | 82% | 65:35 |
| 5 | 10 | (R) BINOL(PN)PhPh | 68% | 90:10 |
| 6 | 10 | (R) 3,3'-diphenyl-BINOL(PN)MePh | 65% | 70:30 |

Reaction conditions: ^a CAHB conditions: 1% [Rh(nbd)BF₄], 2 eq PinBH, THF, 40 °C,

3h. ^b Isolated yield, an average of three experiments exhibiting a spread of ±2%. ^c

Enantiomer ratio (er) determined by chiral HPLC analysis.

2.7 The effect of an existing chiral center on CAHB

The previous achiral substrates gave good enantioselectivity and regioselectivity with a chiral catalyst. The amide directed two-point binding mechanism seems possible based on those results and the earlier successful β,γ -unsaturated amide case. However, it is under concern that whether the proposed two-point binding mechanism for β,γ substrate system is still plausible to the γ,δ -unsaturated structure when an existing chiral center is present. It is for this concern that we begin the investigation on how the pre-installed chiral substrate would affect the stereoselectivity and what insights the results can provide for the proposed two-point binding mechanism.

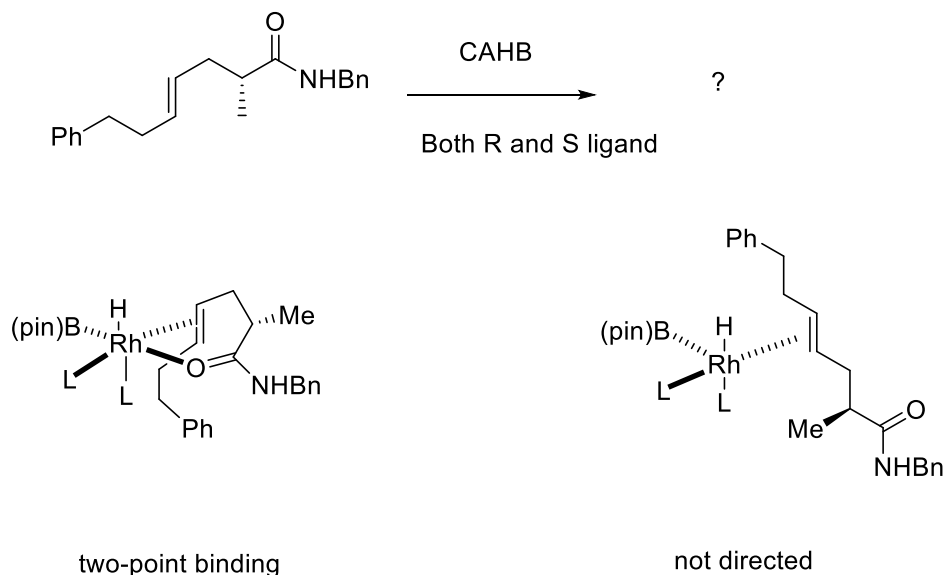


Figure 24. The two possible geometry models of intermediate after alkene association with Rh complex.

2.7.1 Motivation on study of pre-installed chiral substrate CAHB: A mechanistic investigation

We introduced a α -Me-substituent on the parent substrates described above for both aryl- and alkyl-substituted systems. The idea is if the carbonyl group and alkene moiety chelate to the Rh complex as we proposed, the substituent at α position would affect the stereoselectivity can cause matched/mismatched influences to enhance or decrease the selectivity obtained from enantiomers of chiral ligand. If the carbonyl moiety is far away from the Rh complex during the hydroboration process, the α -Me substituent might be expected to exert little effect on the enantioselectivity from enantiomeric catalysts.

2.7.2 Preparation of α -Me chiral substrate

The α -Me chiral substrate was prepared using Evans chiral auxiliary for asymmetric alkylation. The example of chiral α -Me chiral alkyl-substituted substrate is shown below. The two major components in this asymmetric alkylation are the propionyl oxazolidinone, as the nucleophilic component, and an allylic halide as the electrophilic component. The bromide was prepared from corresponding aldehyde followed by Horner-Emmons reaction to form an α,β -unsaturated ester followed by DIBAL-H (diisobutyl aluminum hydride) reduction to the allylic alcohol. The latter compound is treated with PBr_3 to afford the desired allylic bromide. The nucleophile's chiral auxiliary group starts from cheap natural chiral source, L-phenyl alanine. The amino

alcohol underwent cyclization reaction with diethyl carbonate (EtO)₂CO to generate the oxazolindione which is followed by acylation with propionyl chloride. The oxazolindione was deprotonated using the bulky base NaHMDS (-78°C) followed by addition of the allylbromide. The yield of desired product is not satisfactory and may reflect the fact that the reaction is relative moisture sensitive. The desired product was subsequently hydrolyzed and amidated to give the desired chiral methylated substrate **XX**. Despite the low yield, the HPLC analysis indicated the enantiomeric excess of the substrate is higher than 99% ee.

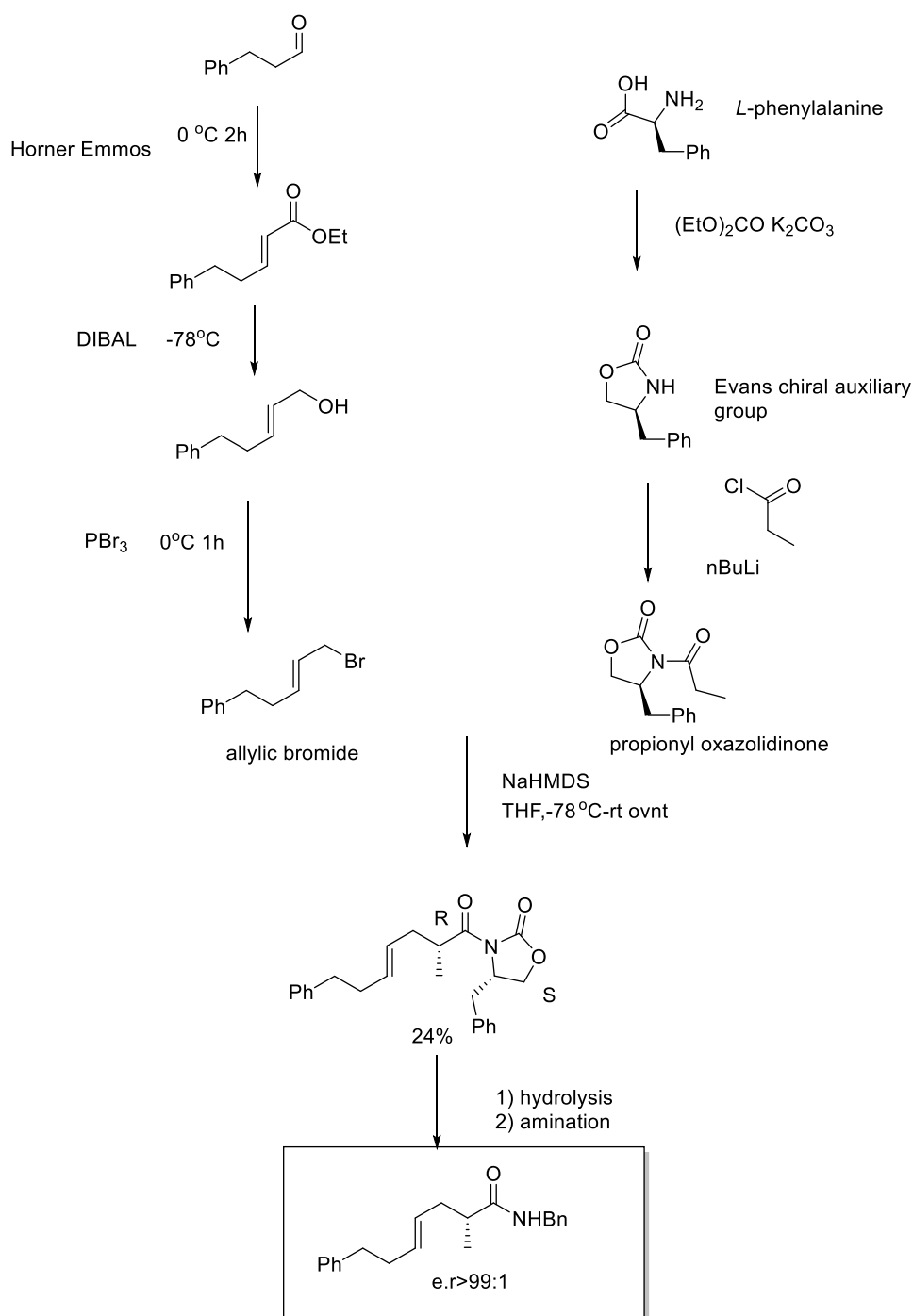


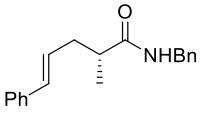
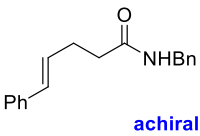
Figure 25. Preparation of an α -Me chiral substrate by using Evans chiral auxiliary group method.

2.7.3 The results of CAHB on preinstalled chiral substrates

For the phenyl substituted chiral substrate, after CAHB and oxidation, the ratio of two

diastereomers can be determined by ^1H NMR. The results are summarized in table 4.

Table 4. Results of CAHB on phenyl substituted γ,δ -unsaturated chiral substrate, and comparison with the achiral substrate.

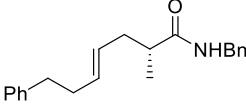
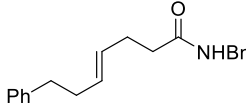
| | R Binol(PN)BnPh | S Binol(PN)BnPh |
|---|------------------------|--------------------------|
|  | 85% yield 1:8.7 d.r | 82% yield 8.6 : 1 d.r |
|  | 85% yield 95: 5 e.r | 76% yield 5: 95 e.r |

CAHB conditions: 1% [(**L1b**)₂Rh(nbd)BF₄], 2 eq PinBH, THF, 40 °C, 3h. Isolated yield (diastereomer ratios were determined by 700Hz NMR)

The major borylated product is at the benzylic position. Both the yield and the stereoselectivity of the major product in two conditions are roughly the same. However, the major diastereomer switched as the enantiomer of the ligand changed. It means the stereoselectivity of the reaction is controlled by the enantiomer of the ligand. There is no match and mismatch effect in this case. However, when we compare the result of the achiral homologous alkene (table 4, row 2), the chiral substrate has significantly decreased the stereoselectivity. The results indicate that the chiral α -Me group probably still interacted with the Rh complex.

Table 5 Results of CAHB on phenethyl substituted γ,δ -unsaturated chiral substrate and

comparison with the achiral substrate.

| | R Binol(PN)BnPh | S Binol(PN)BnPh |
|--|-------------------------|--------------------------|
|  | 72% yield 5.7: 1 d.r | 72% yield 10.7: 1 d.r |
|  achiral | 80% yield 96: 4 e.r | 80% yield 4: 96 e.r |

For the alkyl substituted chiral substrate (table 5, row one), two enantiomers of the ligand provide the same yield of γ -borylated product and the major diastereomer. However, S ligand gave a match result of 10.7: 1 d.r whereas the R ligand gave a mismatch result of 5.7: 1 d.r. The match and mismatch effect in this case suggests that the chiral α -Me group possibly interacted with the catalyst. The substrate would chelate to the Rh complex over the course of a reaction. The conclusion based on table 5 and 6 is that the γ,δ -unsaturated amides may follow the two-point binding mechanism.

2.7.4 Preliminary results for future directions on chiral substrate

CAHB

In the previous section, we discussed the influence of an α -Me-substituent in a simple chiral substrate on the stereoselectivity of CAHB with enantiomeric catalysts. It could be interesting if we install Me or OH groups at β position or on both α and β carbon. Substrates bearing such substituents are intriguing because those substituents occur as the common building blocks in natural products thus are valuable intermediates in

organic synthesis.^[52] If the asymmetric hydroboration of unsaturated chiral alcohols gives high diastereoselectivity, it would elevate the utility of this technique in total synthesis. Also, the OH groups can be protected by bulky silyl ether such as TMS (trimethyl silyl), TBDMS (tert-butyldimethylsilyl) and TIPS (triisopropylsilyl). This kind of steric chiral groups may have match and mismatch effect on stereoselectivity and could further our understanding of the mechanism of asymmetric hydroboration. Some preliminary progress was made toward evaluating these types of substrates.

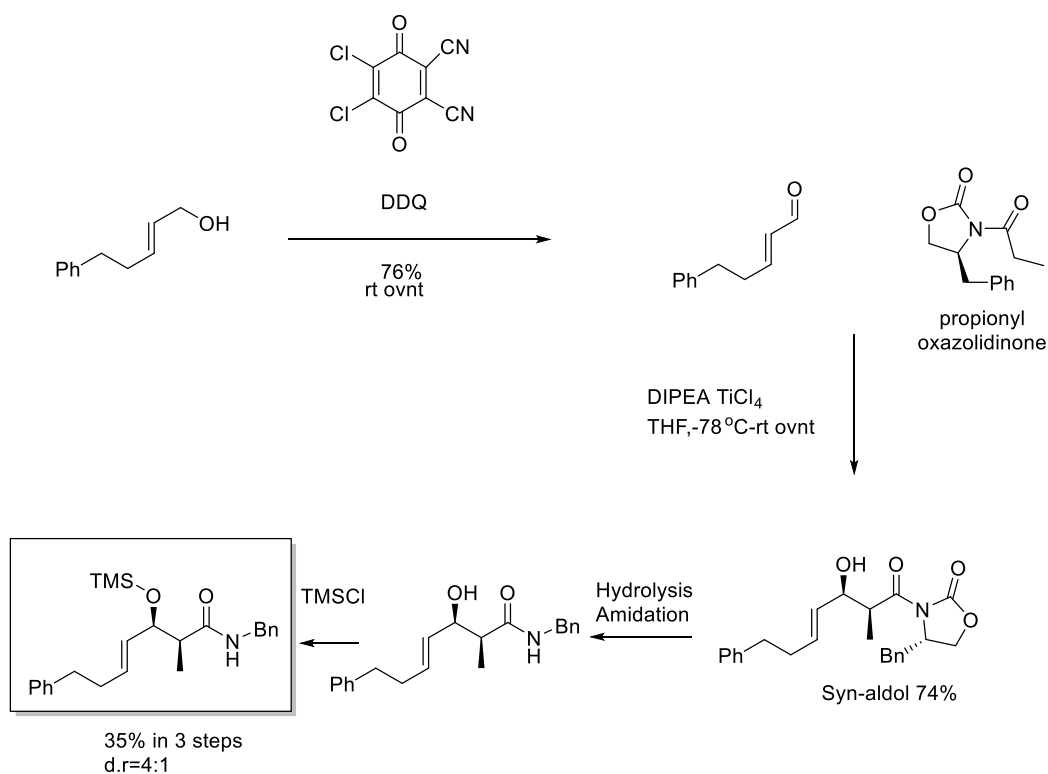


Figure 26 The preparation of α -Me, β -OH, γ,δ unsaturated amide chiral substrate.

The synthesis of a α -Me, β -OH chiral amide began with an allylic alcohol. Oxidation by DDQ (2,3-dichloro-5,6-dicyano-1,4-benzoquinone) afforded the α,β -unsaturated aldehyde **XX**. The propionyl oxazolidinone enolate adds to enone giving the *syn*-aldol

product **XX**. The latter was hydrolyzed and converted to unsaturated amide. However, the diastereomer ratio (d.r.) of these products is only 4:1 which was deemed marginally efficient for preliminary CAHB studies. To go forward with a preliminary assessment, the β -OH group was protected by TMS to prevent any coordination between that oxygen and Rh catalyst in CAHB and prevent its deprotonation under the CAHB reaction conditions. In the event, this substrate showed only low reactivity; only 30% starting material reacted under the standard CAHB condition. Despite low yield, optimization on this substrate could be helpful.

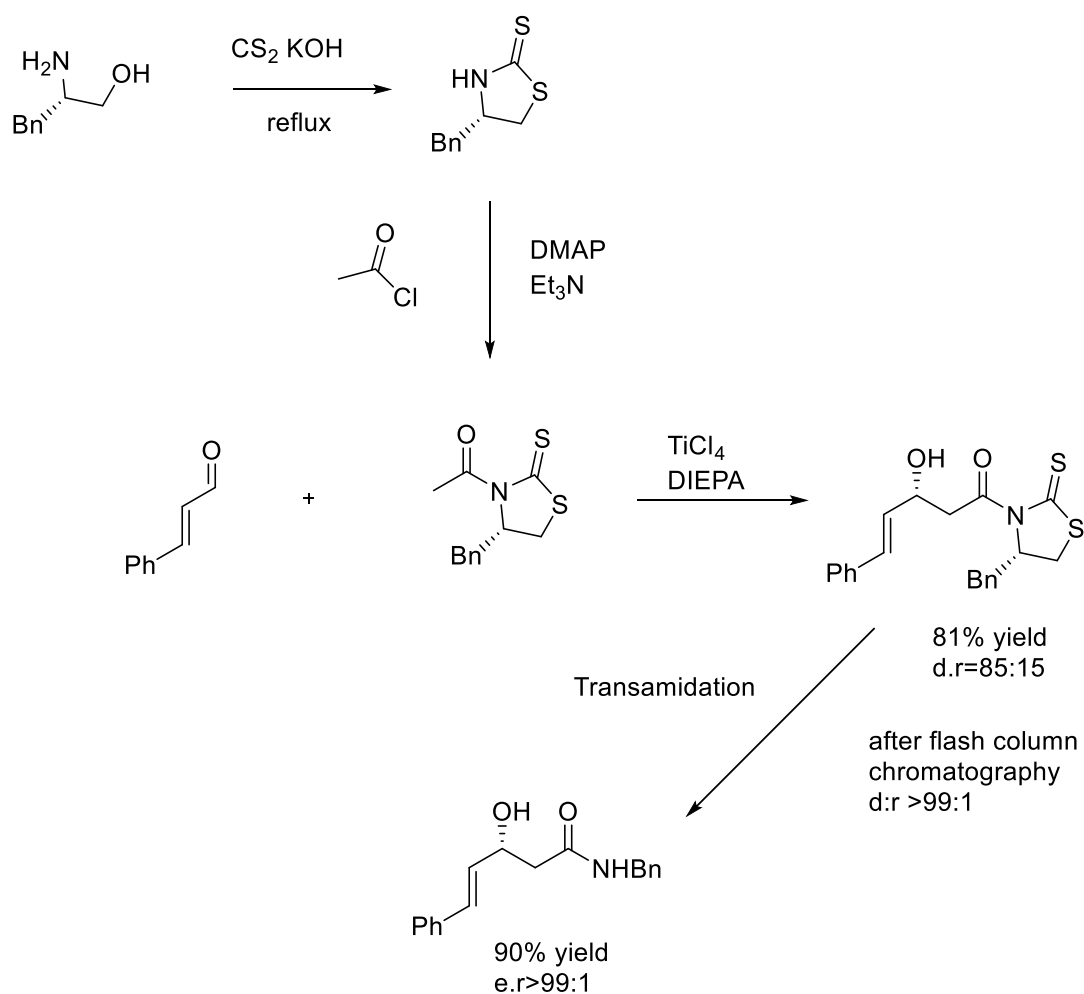


Figure 27. The preparation of β -OH, γ,δ unsaturated amide chiral substrate.

In contrast with low d.r. of α -Me, β -OH substrate **XX**, the chiral β -OH substrate can be synthesized relatively easily with higher diastereoselectivity (d.r. = 85:15) as illustrated in Figure 28; furthermore, the diastereomers of **XX** are readily separated by flash chromatography to afford satisfactory yield and excellent d.r. of the major diastereomer (67% yield, d.r. >99:1). The advantageous result is due to the thiazolidinethione chiral auxiliary group. The sulfur atoms not only provide the basis for the good separation of diastereomers but also weaken the amide bond after the aldol reaction. It is then possible for direct transamidation from the thiazolidinethione adduct to the β -OH γ,δ -unsaturated amide by simply mixing the adduct and BnNH_2 under aqueous conditions. The enantiomeric ratio of β -OH γ,δ -unsaturated amide is examined by HPLC and found to be more than 99:1.

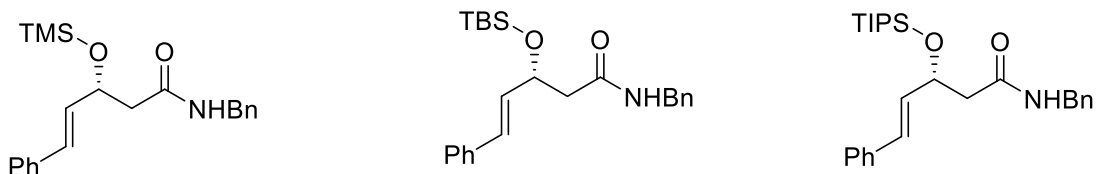
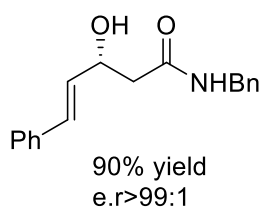


Figure 28 Three different chiral silyl ether substrates for CAHB

The β -OH product was converted into silyl ethers before the CAHB. The idea for this

chiral β -OH substrate design is to compare the results with α -Me chiral substrate. Both substrates are single enantiomers with high enantiopurity. Their hydroboration results would be important to help us understand the geometry of intermediates in the catalytic cycle. The corresponding β chiral silyl ethers substrates were expected to work in CAHB reaction because the α -Me, β -silyl ether had some reactivity. Unfortunately, the substrates shown no reactivity at all in the CAHB screening. It is suspicious that the substrates may in fact be contaminated with some silylated impurity that is not easy to separate by column chromatography. Although these chiral substrates did not under CAHB, they have the potentials to contribute understandings to the mechanism of CAHB on unsaturated γ,δ -amide.

2.8 Employing the Tropos ligand into the CAHB study.

The word “tropos” means “turn” in Greek. The commonly used chiral phosphoramidites and phosphites ligands in our CAHB study like BINOL(PN)MePh or TADDOLPOPh are typical “atropos” ligands. They have a fixed dihedral angle and not able to “turn” to the opposite sense of axial chirality. Unlike to the classical stereochemically stable catalyst, a tropos ligand can in principle be under dynamic stereoisomerization at room temperature.^[53] If the racemic catalyst (i.e., one bearing a the tropos ligand) is under fast equilibrium, the addition of a chiral reagent, either stoichiometric or catalytic amount, can activate one catalyst enantiomer and provide an enantioenriched chiral product. That is, this chiral activator not only promotes catalytic

activity but also controls the dynamic kinetic resolution of the racemization of tropos complexes.^[54]

In the present case, the chiral substrate is to be the activator that promotes the dynamic kinetic resolution of tropos ligand and thereby fosters CAHB with good enantiomeric excess. The **L9** ligand is used at two different temperatures; the one in 40°C gives a higher yield of γ -borylated product and higher diastereoselectivity (71% yield, 3.6:1 d.r.), while the one at 80 °C gives more alkene reduction and lower diastereoselectivity for the borylated product **XX** (58% γ borylated 2.3:1 d.r.). This suggests at higher temperature, the equilibrium of tropos ligand racemization is faster, however, both enantiomeric catalysts react. The tropos ligand **L10** gives good yield for hydroboration but the diastereoselectivity is modest (87% yield, 3.3:1 d.r.) compared with **L1b** (78% yield, 5:1 d.r.).

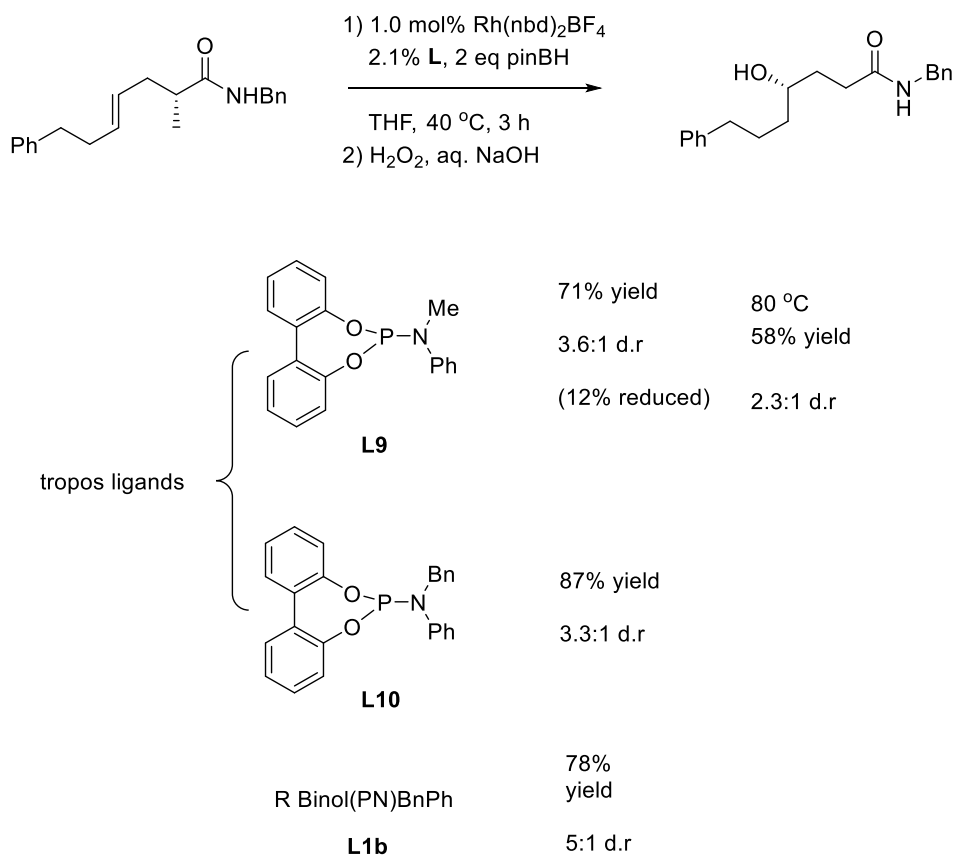


Figure 29 the CAHB on α -Me chiral substrate with tropos ligand catalyst.

The results indicate that although phosphoramidite tropos ligands examined do not induce high diastereoselectivity for CAHB reaction under the conditions examined, our α -Me chiral γ,δ -unsaturated amide substrate indeed activates the tropos ligand, showing some promise for the future design and evaluation of other tropos ligands and other possible chiral activator for CAHB.

2.9 Conclusion:

The carbonyl-directed CAHB of acyclic γ, δ -unsaturated amides proceed with high π -facial selectivity in introducing the boron group to the alkene moiety. The $[\text{Rh}(\text{nbd})_2\text{BF}_4$

+ BINOL(PN)BnPh] gives excellent yield and good enantioselectivity. The amide directed aliphatic alkene provides γ -borylated product while δ -borylated (benzylic position) is predominantly formed in the aromatic alkene. The CAHB on chiral α -Me substrates

Chapter 3: Investigations of Rh-catalyzed asymmetric hydroboration on a 1,2-disubstituted γ , δ -unsaturated amide informed by reaction progress kinetic analysis.

3.1 The introduction on Reaction Progress Kinetic Analysis (RPKA):

3.1.1 The definition of RPKA

The Reaction Progress Kinetic Analysis (RPKA) is a kinetic methodology that employs virtually continuous reaction progress data over the course of a reaction. The data can be collected by using a variety of modern *in-situ* kinetic tools, e.g., NMR or React-IR, and can provide mechanistic insights into simple or complex catalytic reactions. ^[55]

There are two features in this method. (1) The reaction rates over the majority part of the reaction can be analyzed so that only 2-3 reactions are sufficient to determine the reaction order of the reagents. (2) The data arise using concentrations of reagents in the realistic reaction conditions.

In the classical kinetic study, the most common method employed is that of “initial rates”, which means collecting the rates at the very beginning of reactions and discarding the remaining parts of data. There are two drawbacks in this method. (1) It

requires multiple reaction conditions for each reactant of interest. (2) Most reagents of a reaction are in the excessive amounts compared with the reactant of interest, leading to the assumption that the excessive reagents are present in essentially constant concentration over the course of a reaction.

3.1.2 What can RPKA provide?

Unlike the classical kinetic analysis, the RPKA extracts maximum information from a minimal number of experiments, designed to be mathematically independent, via graphical manipulations of time course data.^[56] For example, the PRKA can provide the reaction order and can be used to assess catalyst stability from data collected using *in-situ* monitoring tools. The more accurate and data rich profiles of the rate versus the substrate concentration disappearance can be obtained in just a single experiment whereas classical methods require perhaps 10 to 20 experimental variations. Additionally, the reaction profiles could be summarized as mechanistic fingerprints that not only for simple catalytic reactions but also for the complex one, e.g., reactions involving off-cycle equilibria,^[57] competitive side reactions,^[58] product acceleration^[59] or inhibition^[60] to the catalytic cycle.

3.1.3 The key parameter in PRKA: “excess”

RPKA relies on the key parameter called “excess” ($[xs]$) for mathematical and graphical manipulation; xs is the initial concentration difference between two reagents. For example, consider a bimolecular elementary reaction:



If one mole of A would react with one mole of B, and those two substrates have no side reactions, then over the course of the reaction, their difference in concentration (x_s) would remain the same over the course of the reaction.

$$[x_s] = [B_0] - [A_0] = [B] - [A]. \quad (1)$$

The two types of experiment that using this parameter are called “the different excess” and “the same excess”; these are intensively employed in the analysis and will be discussed later in the thesis.

3.1.4 The *in-situ* tools for the RPKA:

The power of RPKA is based the ability of continuously monitoring the change of substrates in accuracy over the course of the reaction, and there are plenty of options to accomplish this goal. The most commonly used tools are reaction progress NMR, *in-situ* FT-IR (e.g., React-IR) and reaction calorimetry. To confirm the validity of results, monitoring the reactions by more than one independent methods is recommended. ^[59]

3.1.4.1 NMR spectrometer

NMR spectroscopy is the method we used to monitor the reaction progress in this thesis. By setting up the reaction in an NMR tube and scanning multiple times, the substrate consumption and the formation of the products can be recorded over the course of a reaction. The primary data collected are transformed into the concentration vs. time.

This data can be curve fitted into a polynomial equation from which the rate vs. time can be obtained by taking the first derivative of the fitted equation. The drawback of this technique is that the reaction must be homogeneous. In addition, the reaction has to be initiated before its scanning in the NMR. This means the reaction information at the very beginning (usually from 0 to 1 min) are inevitably lost.

3.1.4.2 Infrared spectroscopy

In-situ infrared spectroscopy, for example, React-IR, is also widely used in RPKA kinetic studies. It uses intensity data from distinctive absorbances in the IR spectral region. If we can locate the reactant's and product's characteristic signals and they are not overlapped with each other, the intensity of signals can be collected. These intensities are directly proportional to the concentration according to the Beers' law. The *in-situ* infrared technique can collect the data from the beginning of a reaction. Thus, it may help, for example, to determine whether there is a catalyst activation step in a reaction.

The problem of this technique is determining unique, assignable absorptions. More specifically, it is unlikely to identify readily assignable frequency bands suitable to effectively monitor the reaction. For example, although the fingerprint region of the IR spectral window gives distinctive peaks to each molecule, the low intensity and high chances of signal overlapping make this area not easy for the quantitative analysis. A carbonyl group shows high IR intensity with a sharp peak to follow at ca. 1700 cm^{-1}

making it to be one of the best target to track the reaction. However, not all the substrates of interest contain carbonyl groups or sometimes there is an overlap of product's and starting material's carbonyl peaks in the spectrum of the reaction mixture. Despite those drawbacks, the *in-situ* IR instrument is still the best technique at the moment that can provide a complete kinetic picture of a reaction. ^[61]

3.1.4.3 Reaction calorimetry

The calorimetry can measure the instantaneous heat flux of the reaction that relates to the enthalpy change for the reaction. The data collected are proportional to the instantaneous reaction rate.

$$q = \Delta H \cdot (\text{volume}) \cdot \text{rate} \quad (2)$$

Reaction calorimetry has been applied to both parallel and consecutive mechanistic pathways. ^{[62], [63]}. This technique is very sensitive to the reaction time. The measurement may be inaccurate due to the time lag of reaction heat flows through the reactor sensor walls. However, if the reaction time is too long, the signal would be too low to provide accurate data. ^[64].

3.1.5 How to determine the orders of reactants by PRKA.

As we mentioned earlier, the key parameter to the graphical analysis is called the excess (xs), and there are two different experiment protocols: the different excess and the same excess protocol.

3.1.5.1 The different excess:

It is to determine the order of reagents. For a bimolecular elementary reaction:



The rate equation should be:

$$\text{rate} = k \cdot [\mathbf{A}]^m \cdot [\mathbf{B}]^n \quad (3)$$

The numbers “m” and “n” are the orders of **A** and **B** which are to be determined in this analysis via graphical evaluation of the data. The reaction rate is determined from the first derivative of the curve for product formation versus time. **[A]** and **[B]** are from the experiment conditions. In the different excess experiments, we collect data from two reactions, one in which the difference in concentration of the two reagents (i.e., the excess) is equal to 0.41 M and a second reaction in which the excess is equal to 0.21 M. After we plug the data into the rate equation (3), the reaction profile of the rate vs. **[A]** is shown in figure 30.a

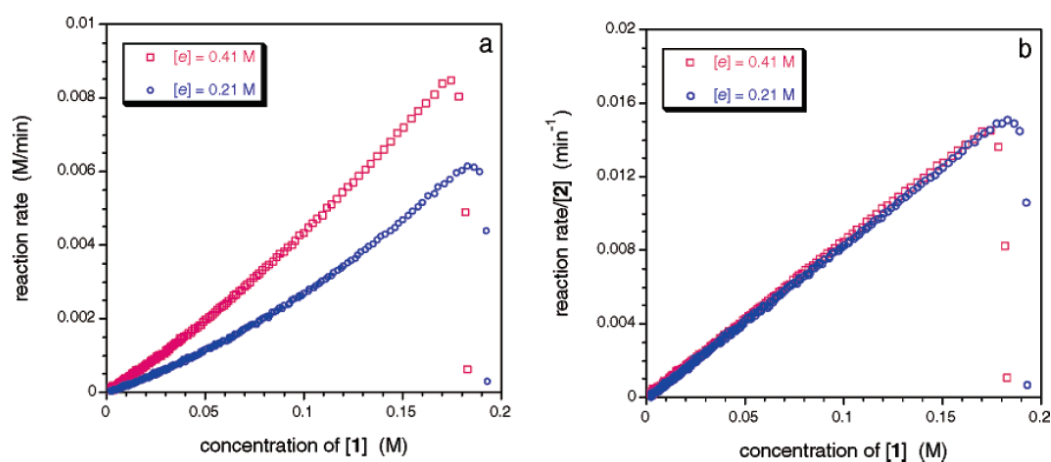


Figure 30 Examples of “different excess” overlay in the RPKA

Adapted from Ref 64 with permission. Copyright 2006 American Chemical Society.

The figure 31.a shows the reaction rate vs. $[A]$ from two different excess experiments. To investigate the order of each reactant, we rearrange the rate equation (3) to normalized reaction rate equation (4):

$$\text{“normalized rate”} = \frac{\text{rate}}{[B]^n} = k \cdot [A]^m \quad (4)$$

The figure 31.b shows the normalized rate vs. $[A]$ of two different excess experiments. By carefully adjusting the arbitrary numbers “n” and “m”, we can find correct numbers for each reactant. For example, in figure 31.b, when lines are straight, the y-axis values are proportional to $[A]^1$, which means the A behave as first order. If lines are not straight, it means y-axis values are not linear to $[A]^1$, thus A is not 1st order. When lines fall on top of another, it means the normalized rate “ $\frac{\text{rate}}{[B]^n}$ ” is independent of $[B]^n$. The instantaneous “n” is the order of B.

3.1.5.2 Same excess:

We use the “same excess” experiment to analyze the robustness of catalyst and make conclusions based on the reaction rate vs. [reactant] plots. There are two reaction conditions with the same excess parameter and the same catalyst concentration but the different initial concentrations of two reactants. The idea of the “same excess” experiment is that the second reaction condition is a simulation of the first one at partial conversion. If the catalyst is deactivated, (figure 32.a) the rate of the second reaction should be higher than that of the first one at the same reactant concentration, i.e., the x-axis value. However, if the catalyst is not deactivated over the course of a reaction,

(figure 32.b) the second reaction rate should be the same to the first one at the same reactant concentration. [64]

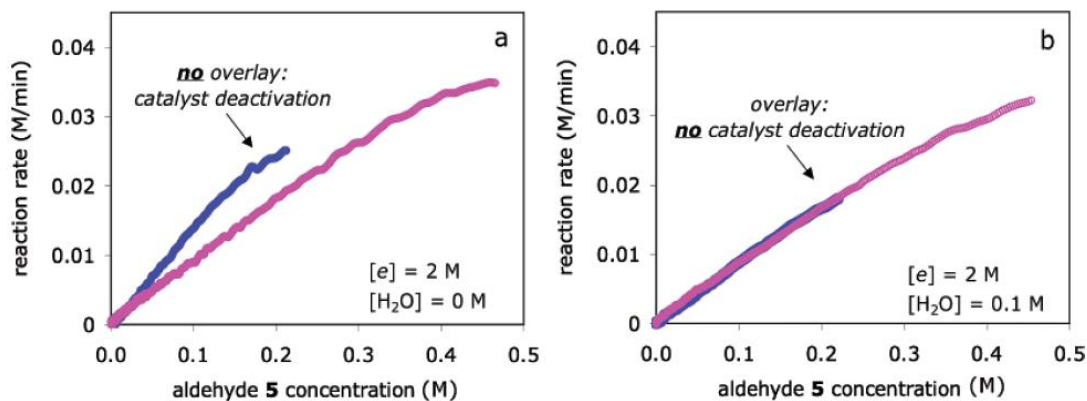


Figure 31 Examples of “same excess” overlay in the RPKA

Adapted from Ref 64 with permission. Copyright 2006 American Chemical Society.

3.2 PRKA on CAHB of 1,2-disubstituted γ,δ -unsaturated amide

3.2.1 The experimental design:

In our kinetic study, we decide to use para-CF₃-phenyl substituted 1,2-disubstituted γ,δ -unsaturated amide as sample substrate. The standard reaction condition is listed below.

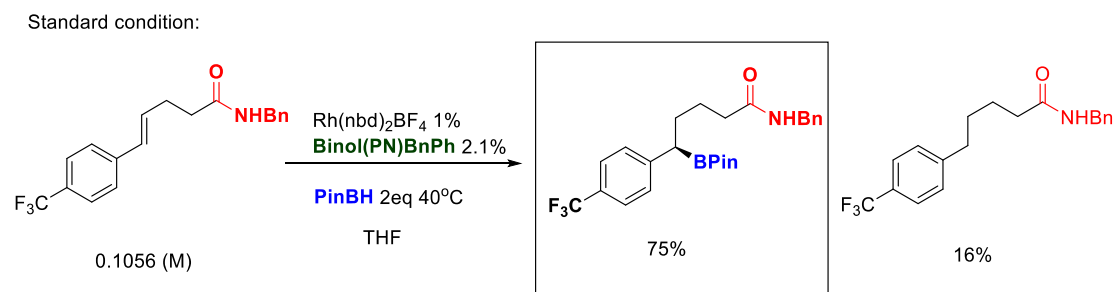


Figure 32 The standard condition used in the PRKA study.

| | |
|-----------------------|--------|
| Reaction total volume | 0.5 mL |
|-----------------------|--------|

| | |
|--------------------|--|
| Solvent | THF |
| [alkene substrate] | 0.1056 M |
| [PinBH] | 0.2112 M |
| [Catalyst] | 1.0 mol% Rh(nbd) ₂ BF ₄ + 2.0 mol% BinolPN(Bn)Ph |

The key parameter “excess” is designated as the concentration difference between PinBH and alkene substrate.

$$\text{Excess: } [xs] = [\text{PinBH}] - [\text{Alkene}]$$

We set up the reaction in an NMR tube, then kept scanning ¹⁹F NMR spectroscopy for every 30 s. The consumption of alkene substrate as well as the formation of boronic ester can be monitored by integrating their signals and correlating with the reaction time.

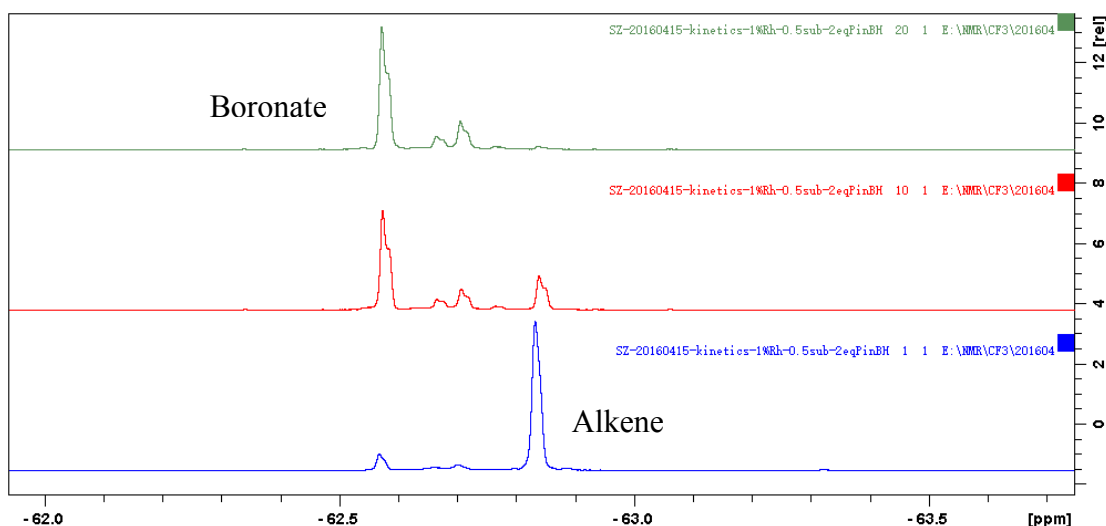


Figure 33 The multiple displays of ¹⁹F NMR spectra.

For example, the multiple displays of ¹⁹F NMR spectra from a single reaction at the different reaction time (Figure 33) show a good resolution of signals of the alkene

substrate (the very right peak) and the boronic ester (the very left peak). The time scale is from bottom to top. The hydroboration process rate equation is:

$$\text{Hydroboration rate} = k \cdot [\text{Alkene}]^m \cdot [\text{PinBH}]^n \quad (5)$$

The hydroboration rate data is from the first derivative of the function of the boronic ester formation vs. time. The **[Alkene]** is directly from the raw data and the **[PinBH]** is equal to **[xs]** + instantaneous **[Alkene]**.

There are three types of experiments in this kinetic study:

1. The same excess experiment: to study the robustness of the catalyst.
2. The different excess experiment: to study the order of reactants.
3. The study of catalyst order.

The detailed reaction conditions and results of these three types of experiments will be included in section 3.4 of this chapter.

3.3 The general procedures of data processing.

3.3.1 Peaks integration.

Integrate the peaks over all spectra of a reaction by using Topspin software and export the data to a single text file. (figure 34)

```

C:/Users/jmt/Desktop/Shuyang/CF3/201607/SZ-20160729-kinetics-1.5%catalyst-1s2b/1/pdata/1/integrals.txt
 1  -63.114  -63.160    0.0427282
 2  -63.214  -63.249    0.0201223
 3  -63.249  -63.289    0.0698678
 4  -63.375  -63.429    1.29587
 5  -63.708  -63.784     1

C:/Users/jmt/Desktop/Shuyang/CF3/201607/SZ-20160729-kinetics-1.5%catalyst-1s2b/2/pdata/1/integrals.txt
 1  -63.114  -63.160    0.0763294
 2  -63.214  -63.249    0.026166
 3  -63.249  -63.289    0.0789372
 4  -63.375  -63.429    1.16475
 5  -63.708  -63.784    0.945126

C:/Users/jmt/Desktop/Shuyang/CF3/201607/SZ-20160729-kinetics-1.5%catalyst-1s2b/3/pdata/1/integrals.txt
 1  -63.114  -63.160    0.12946
 2  -63.214  -63.249    0.0338773
 3  -63.249  -63.289    0.0956563
 4  -63.375  -63.429    1.0756
 5  -63.708  -63.784    0.936397

C:/Users/jmt/Desktop/Shuyang/CF3/201607/SZ-20160729-kinetics-1.5%catalyst-1s2b/4/pdata/1/integrals.txt
 1  -63.114  -63.160    0.187463
 2  -63.214  -63.249    0.0390434
 3  -63.249  -63.289    0.116572
 4  -63.375  -63.429    0.951394
 5  -63.708  -63.784    0.960109

```

Figure 34 The integrals from NMR spectra.

3.3.2 Transform the raw data to concentrations.

The raw data (figure 35, left part columns) is converted to the concentration data (figure 35, right part columns) after normalizing to the percentage (figure 35, central part columns) and multiply with the total concentration of the reaction. The graph in the central is the concentration of each reaction component vs. reaction time. Each line is a component of the reaction. For example, the purple line is the consumption of alkene starting material, the blue line is the borylated product, the green line is the reduced product and the red line is the unidentified byproduct.

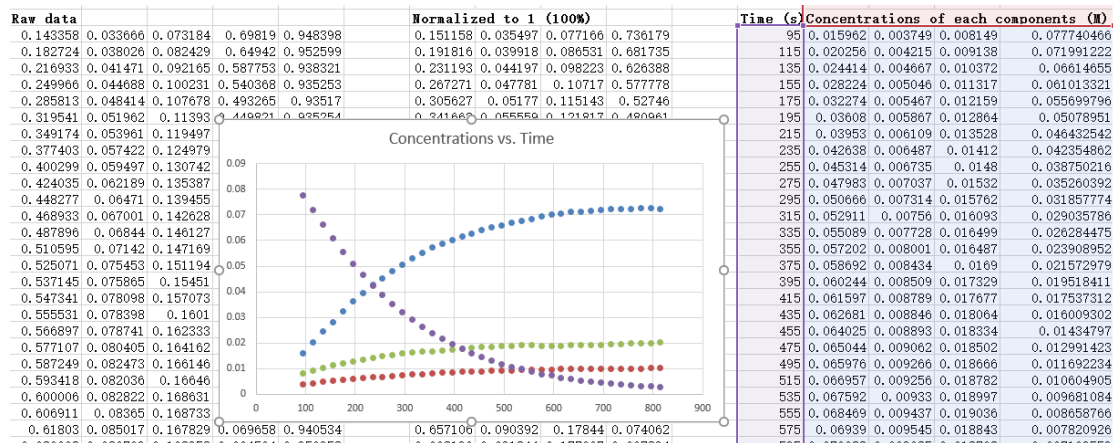


Figure 35. The transformation of raw data to the concentration.

3.3.3 Curve fitting of the concentration data.

In order to calculate the rate of the hydroboration process, the data were curve fitted into a 6th-degree polynomial equation. Based on the reaction time (figure 36, column A) and coefficients of boronic ester (figure 36, column B), we can regenerate the concentration (figure 36, column C) and the hydroboration rate (figure 36, column D) for each NMR scan. The hydroboration rate is from the first derivative of the 6th-degree polynomial equation.

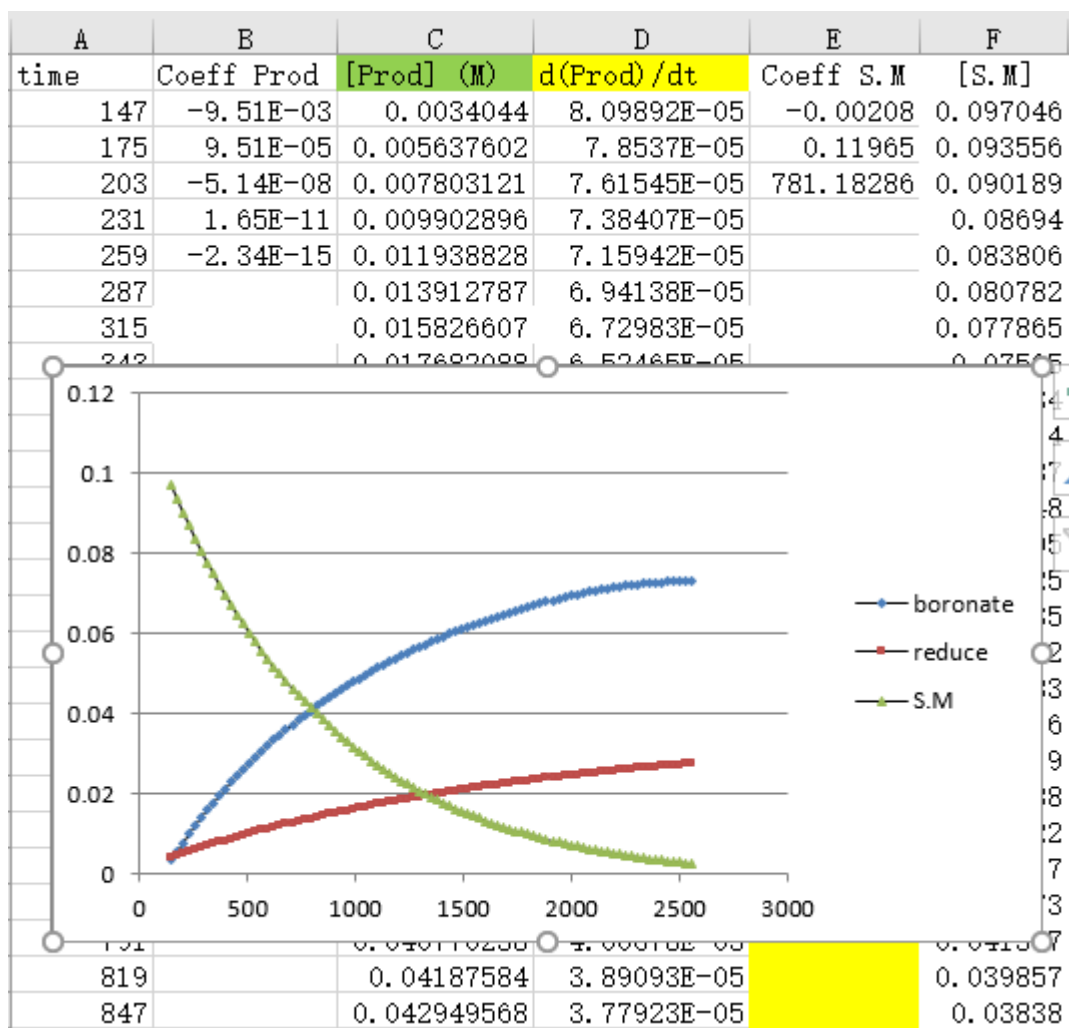


Figure 36 Curve fitting of the raw data

3.3.4. Transform the rate equation to normalized rate functions.

According to the normalized rate equation (xx), the hydroboration rates (figure 36, column D) were rearranged to normalized rate functions. For example, column L (figure 37) is to study the order of alkene starting mater, column M (figure 37) is to PinBH.

The arbitrary numbers of “n” and “m” can be adjusted in column H and column K (figure 37).

| G | H | I | J | K | L | M |
|-----------|-------|----------|----------|-----|-----------------|---------------|
| $[S.M]^m$ | m | [B] | $[B]^n$ | n | rate/ $[S.M]^m$ | rate/ $[B]^n$ |
| 0.097046 | 1 | 0.202646 | 0.125534 | 1.3 | 0.000834542 | 0.00064516 |
| 0.093556 | 0 | 0.199156 | 0.12273 | 1 | 0.000839463 | 0.00063991 |
| 0.090189 | #REF! | 0.195789 | 0.12004 | 1 | 0.000844388 | 0.00063441 |
| 0.08694 | #REF! | 0.19254 | 0.117457 | 1 | 0.000849325 | 0.00062866 |
| 0.083806 | #REF! | 0.189406 | 0.114977 | 1 | 0.000854283 | 0.00062268 |
| 0.080782 | 0 | 0.186382 | 0.112597 | 1 | 0.000859271 | 0.00061648 |
| 0.077865 | #REF! | 0.183465 | 0.110311 | 1 | 0.000864298 | 0.00061008 |
| 0.07505 | #REF! | 0.18065 | 0.108116 | 1 | 0.000869373 | 0.00060349 |
| 0.072334 | #REF! | 0.177934 | 0.106008 | 1 | 0.000874509 | 0.00059672 |
| 0.069714 | 0 | 0.175314 | 0.103983 | 1 | 0.000879716 | 0.0005898 |
| 0.067187 | 0 | 0.172787 | 0.102038 | 1 | 0.000885007 | 0.00058273 |
| 0.064748 | 0 | 0.170348 | 0.10017 | 1 | 0.000890394 | 0.00057553 |
| 0.062395 | 0 | 0.167995 | 0.098375 | 1 | 0.000895891 | 0.00056822 |
| 0.060125 | 0 | 0.165725 | 0.096651 | 1 | 0.000901511 | 0.00056082 |
| 0.057935 | 0 | 0.163535 | 0.094993 | 1 | 0.00090727 | 0.00055333 |
| 0.055822 | 0 | 0.161422 | 0.093401 | 1 | 0.000913184 | 0.00054577 |
| 0.053783 | 0 | 0.159383 | 0.09187 | 1 | 0.000919267 | 0.00053816 |
| 0.051816 | 0 | 0.157416 | 0.090399 | 1 | 0.000925538 | 0.00053051 |
| 0.049919 | 1 | 0.155519 | 0.088985 | 1 | 0.000932014 | 0.00052284 |
| 0.048088 | 0 | 0.153688 | 0.087626 | 1 | 0.000938713 | 0.00051515 |
| 0.046322 | 0 | 0.151922 | 0.086319 | 1 | 0.000945654 | 0.00050747 |
| 0.044617 | 0 | 0.150217 | 0.085062 | 1 | 0.000952855 | 0.0004998 |
| 0.042973 | 0 | 0.148573 | 0.083854 | 1 | 0.000960339 | 0.00049215 |
| 0.041387 | 0 | 0.146987 | 0.082692 | 1 | 0.000968124 | 0.00048454 |

Figure 37 The normalized rate data.

3.3.5. Prepare the plot of the normalized rate equation.

The normalized rate plot was generated by either column L vs. column J or column M vs. column G. (figure 37) For example, to study the order of PinBH, column M vs. column G was used. (figure 38)

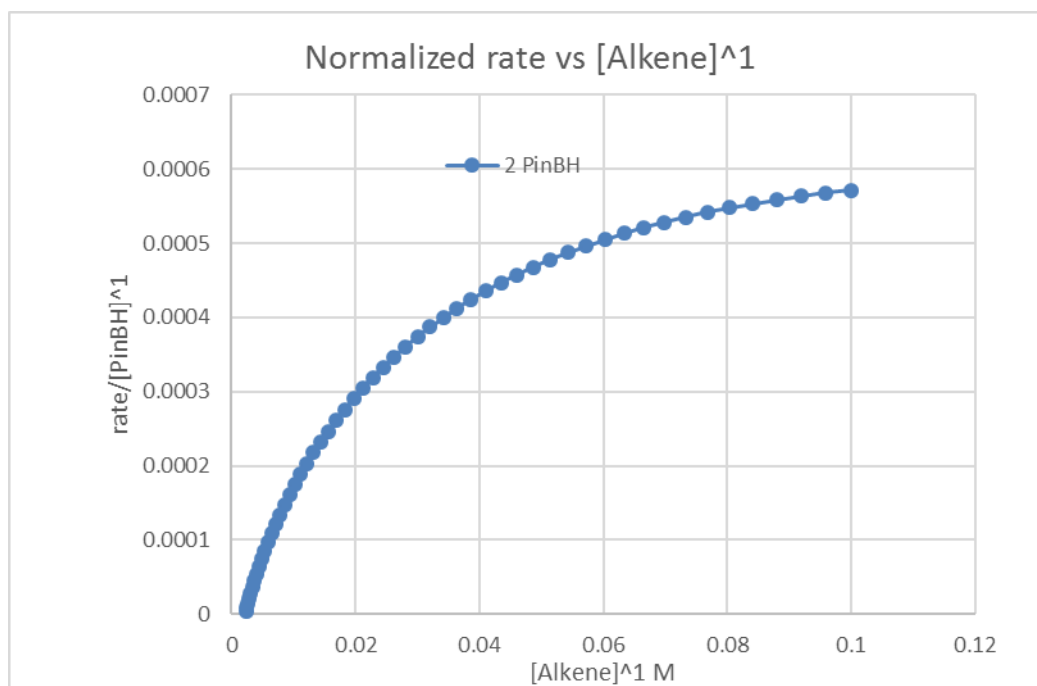


Figure 38 The plot of normalized rate vs. [Alkene] from 1 reaction.

3.3.6. Summarize the data from different reaction conditions in one plot.

After finishing operations above, we need to repeat on other reaction conditions and summarized the data in one plot so that we can carefully adjust the arbitrary numbers and discuss the shape of lines. (figure 39)

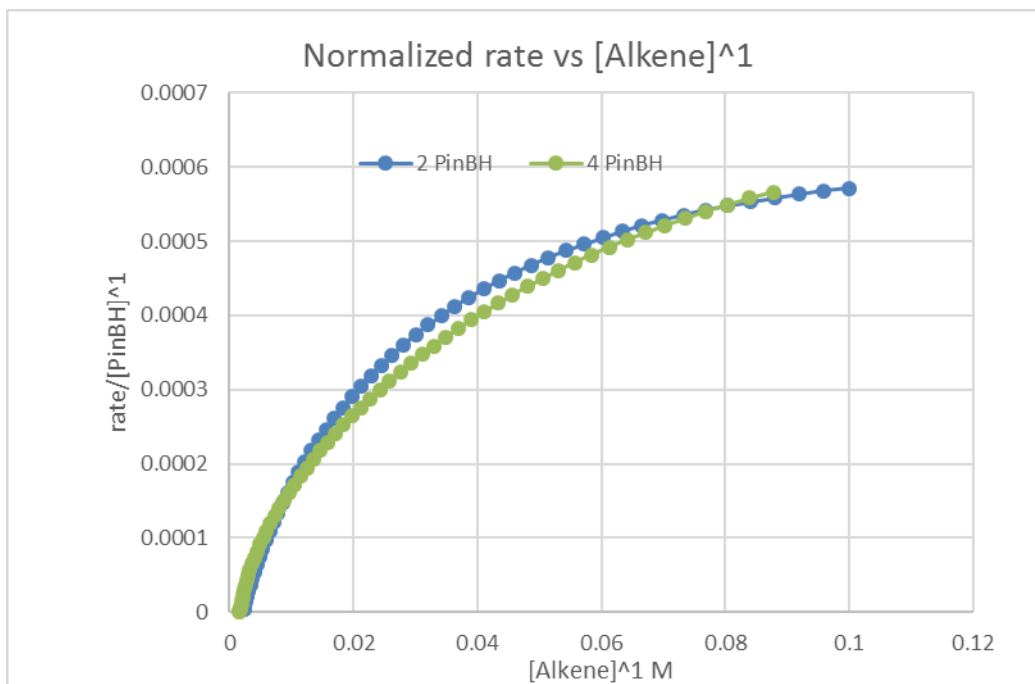


Figure 39 The plot of normalized rate vs. [Alkene] from 2 different reactions.

The experiment set includes the standard reaction (0.1056 M alkene substrate, 0.2112 M PinBH, [xs]=0.1056 M) and the one with 50% initial substrate (0.0528 M alkene, 0.1584 M PinBH, [xs]=0.1056 M)

The second part is “different excess” experiments. To investigate the order of alkene substrate and PinBH, we defined two sets of conditions along with the standard one; i.e., changing the [PinBH] so that [xs]=0.1584 M and [xs]=0.3168 M. and changing the [Alkene substrate] so that [xs]=0.1584 M and [xs]=0.0528 M. In the best scenario, only one set of experiments is enough to determine the reaction orders on reagents. The reason that we used two conditions here is to validate the results by manipulating the concentration of two reagents separately.

3.4 The detailed reaction conditions and results of the kinetic study:

3.4.1 The same excess experiment: the stability of the catalyst

To start the investigation, the first experiment is the “same excess” which can determine the robustness of the catalyst complex. This is important because we need to establish from the beginning whether the catalyst deactivation will be an issue in the reaction. To investigate the robustness of Rh catalyst in the CAHB, 1.0 mol% Rh was used in the experiments. The detailed conditions are listed below. The concentration of 0.1056 *M* is considered as “1 equivalent” for convenience.

Table 6 experimental design for the “same excess” experiment

| | [Alkene] <i>M</i> | [PinBH] <i>M</i> | “Excess” <i>M</i> |
|------------------|-------------------|------------------|-------------------|
| 1 Sub, 1.5 pinBH | 0.1056 (1 eq) | 0.1584 (1.5eq) | 0.0528 |
| 1.5 Sub, 2 pinBH | 0.1584 | 0.2112 | 0.0528 |

Kinetic results:

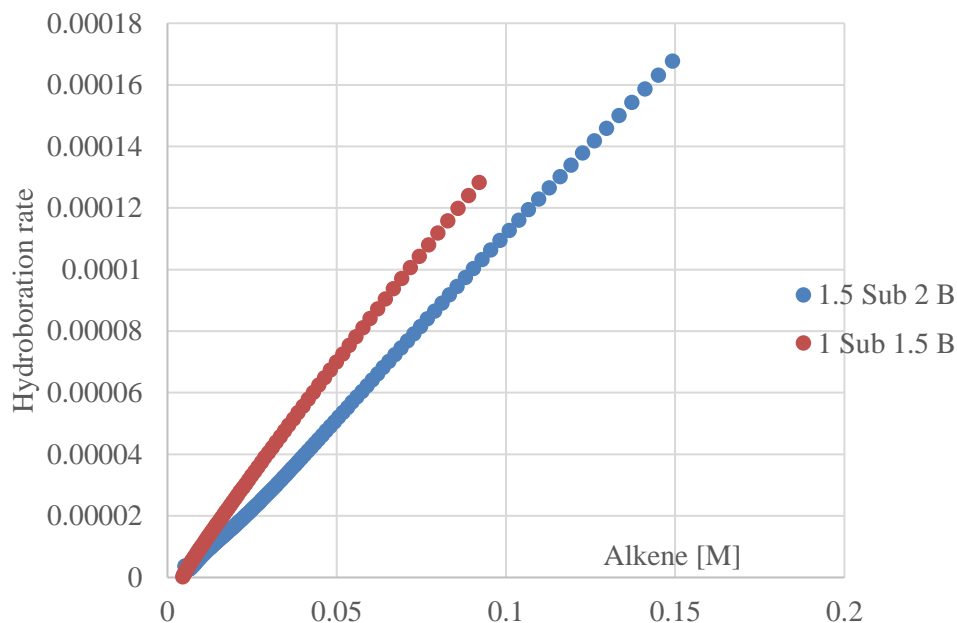


Figure 40 Data from "same excess" experiments, rate vs time in two experiments.

As we mentioned earlier, in the same excess experiment, the second condition is a simulation of the first one at partial conversion. For example, (figure 40) when the blue line reaction consumes 0.0528 M of alkene substrate which is 33% conversion, the instantaneous reaction condition should be the same to the initial condition of the red one. However, the lines of the two reactions are not overlapping. This means the reaction rate under the second conditions (1 Substrate, 1.5 pinBH) is higher than that of under the first conditions (1.5 Substrate, 2.0 pinBH) at the same alkene concentration. The rate difference is attributed to fresher catalyst under the second conditions. Based on the results, our conclusion is that there is a catalyst deactivation over the course of a CAHB reaction.

3.4.2 The order of PinBH.

The major two plots for the order analysis are the reaction rate vs. time and the “normalized rate” vs. [reagent]. The former may imply the possible order of a reactant which could be further tested by the latter graphical analysis. In this “different excess” study, we designed three reactions conditions only differing in the concentration of PinBH. More specifically, they have the same alkene concentration (i.e., 0.1056 *M*) and 1.0, 2.0, and 4.0 equivalents of PinBH (Table 6).

Table 7 The experimental design for the "different excess" experiment with 1mol% Rh catalyst loading.

| | [Alkene] <i>M</i> | [PinBH] <i>M</i> | “Excess” <i>M</i> |
|----------------|-------------------|------------------|-------------------|
| different xs 1 | 0.1056 | 0.1056 | 0 |
| Standard | 0.1056 | 0.2112 | 0.1056 |
| different xs 2 | 0.1056 | 0.4224 | 0.3168 |

Kinetic results:

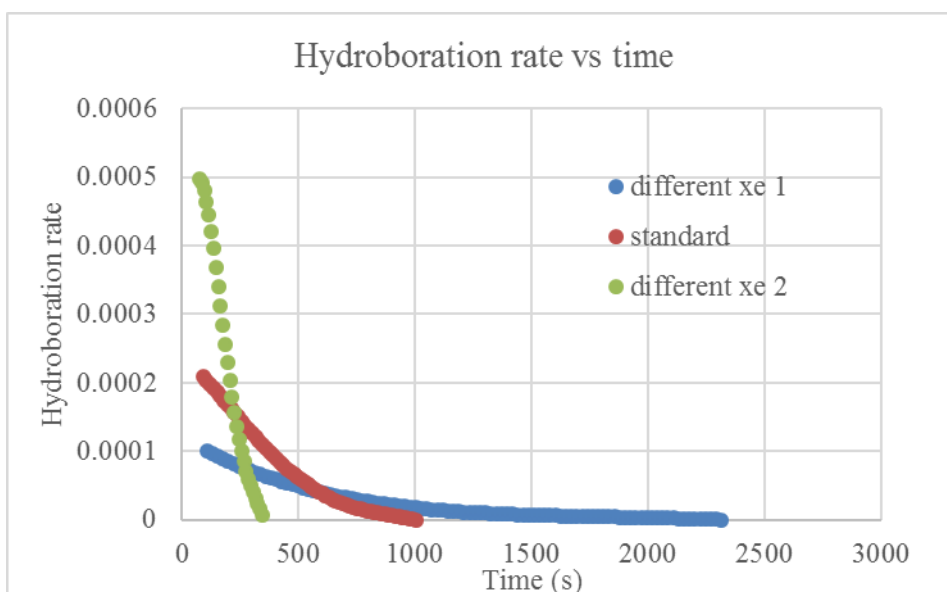


Figure 41 The "different excess" experiments, rate vs time under three reaction conditions.

From the hydroboration rate vs. time plot, the ratio of the three initial rates is roughly 1:2:4. Considering the ratio of PinBH in these three conditions is also 1:2:4, it implies the order of PinBH should be the 1st. The "normalized rate" versus [alkene] will provide the more definitive conclusion.

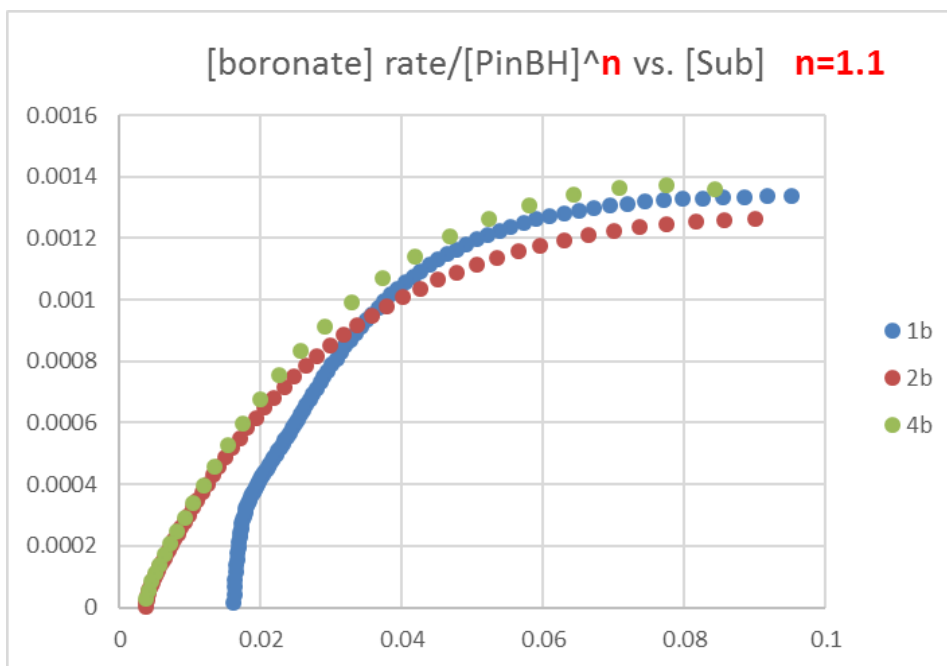


Figure 42 The "different excess" experiments, normalized rate vs. [alkene] substrate

According to hydroboration rate equation:

$$\text{Hydroboration rate} = k \cdot [\text{Alkene}]^m \cdot [\text{PinBH}]^n \quad (5)$$

We rearrange the equation (5) to normalized rate equation:

$$\text{Normalized rate} = \frac{\text{hydroboration rate}}{[\text{PinBH}]^n} = k \cdot [\text{Alkene}]^m \quad (6)$$

All the analysis below in this section is based on equation (6). After careful adjusting the arbitrary number of "n", we found that when "n" equals to 1.1, the lines from 3 different conditions give the best overlapped with each other. The adjusting process is shown below. The arbitrary "n" is increased from 0 to 1.5.

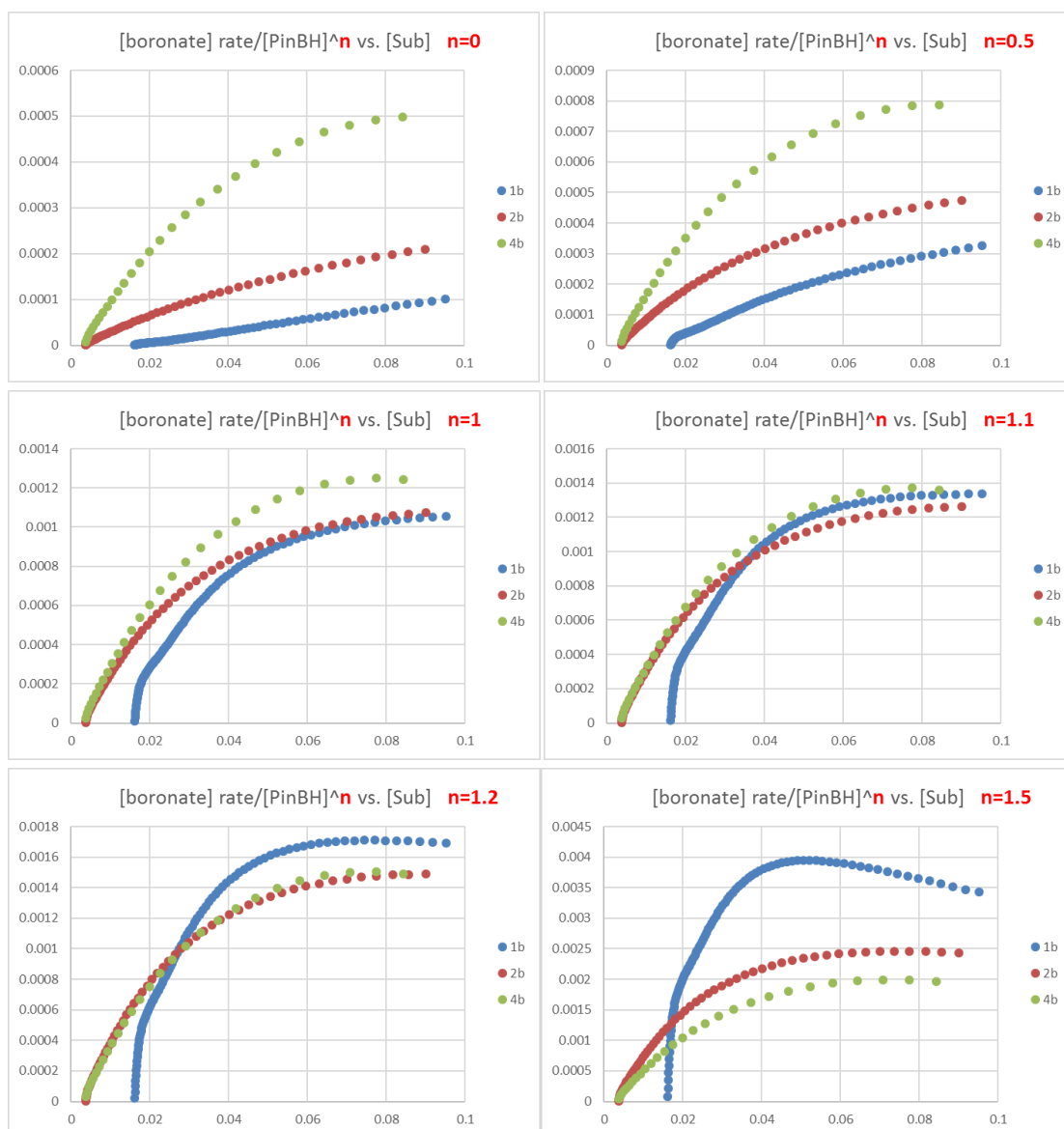


Figure 43 The adjusting on "n"

When we increase the “n” from 0 to 1, the lines are gradually gathering together. They show the best overlay when “n” is 1.1. There is a significant deviation at the bottom left part of “n” = 1.1 figure, which is probably due to low concentrations of both reactants leading to the slowdown of the rate at the end of the reaction (1:1 equivalent of alkene to PinBH). When we increase the “n” to 1.5, the lines are separated again.

Although the lines are overlapped with each other best when “n” = 1.1, the lines are not

straight which means the normalized rate is not proportional to $[\text{Alkene}]^1$. Thus, based on the rate equation (5) and (6), it's safe to say that the alkene substrate does not behave as the 1st order in the CAHB process. This result is very close to a published example which drew a similar conclusion from the RPKA. (figure 44)

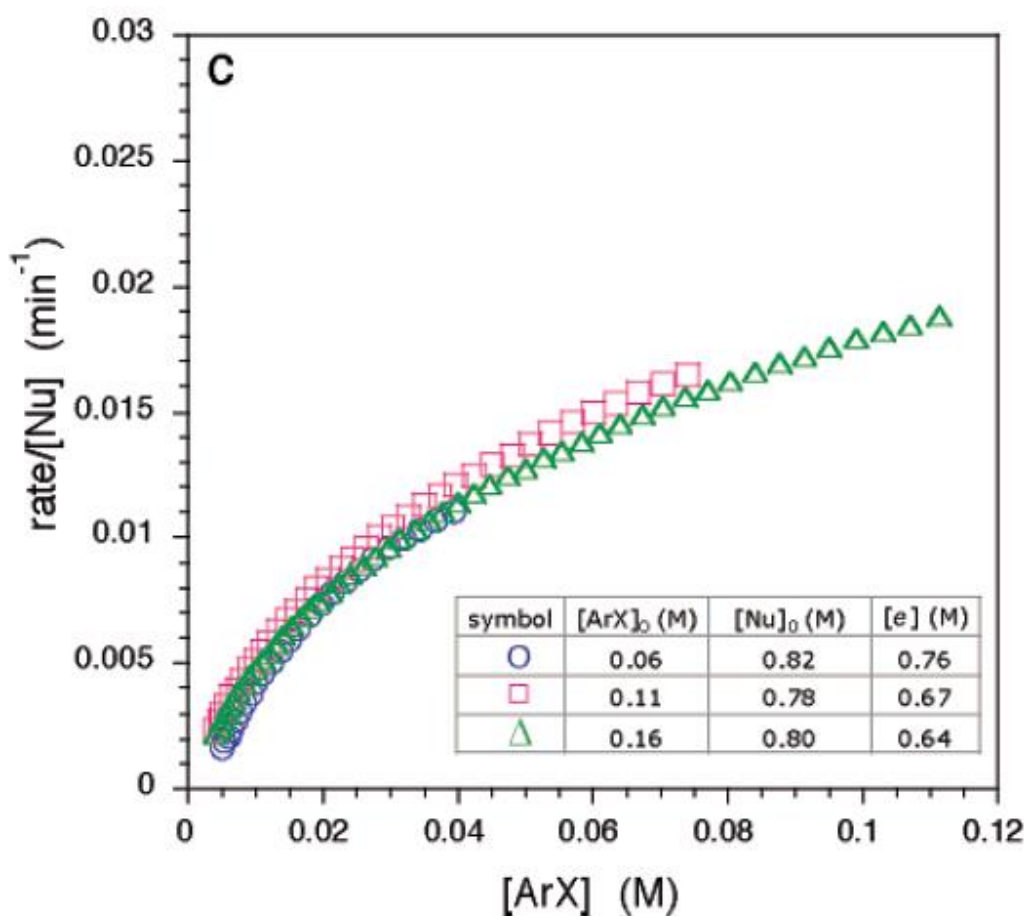


Figure 44 A published example of RPKA on Pd catalyzed Sonogashira reactions
Adapted from Ref 64 with permission. Copyright 2006 American Chemical Society.

In this example, the lines show the best overlay when assumed 1st order on the nucleophile in the normalized rate (figure 44, the y-axis values). The fact that the lines are not straight when x-axis is $[\text{ArX}]^1$ indicates there is a complex order in the electrophile, i.e., $[\text{ArX}]$ is not first order, otherwise, the lines should be straight.

3.4.3 The Alkene substrate order:

The next “different excess” experiment is to investigate the order of the alkene substrate.

In this experiment, the only variable is the [Alkene] and all other reagents are the same in the three sets of reaction conditions. The detailed conditions are shown below (Table 9).

Table 8 Reaction conditions of the "different excess" experiments to investigate the order of alkene substrate

| | [Alkene] <i>M</i> | [PinBH] <i>M</i> | “Excess” <i>M</i> |
|----------------|-------------------|------------------|-------------------|
| different xs 1 | 0.0528 | 0.2112 | 0.1584 |
| Standard | 0.1056 | 0.2112 | 0.1056 |
| different xs 2 | 0.1584 | 0.2112 | 0.0528 |

The graphical analysis is shown below.

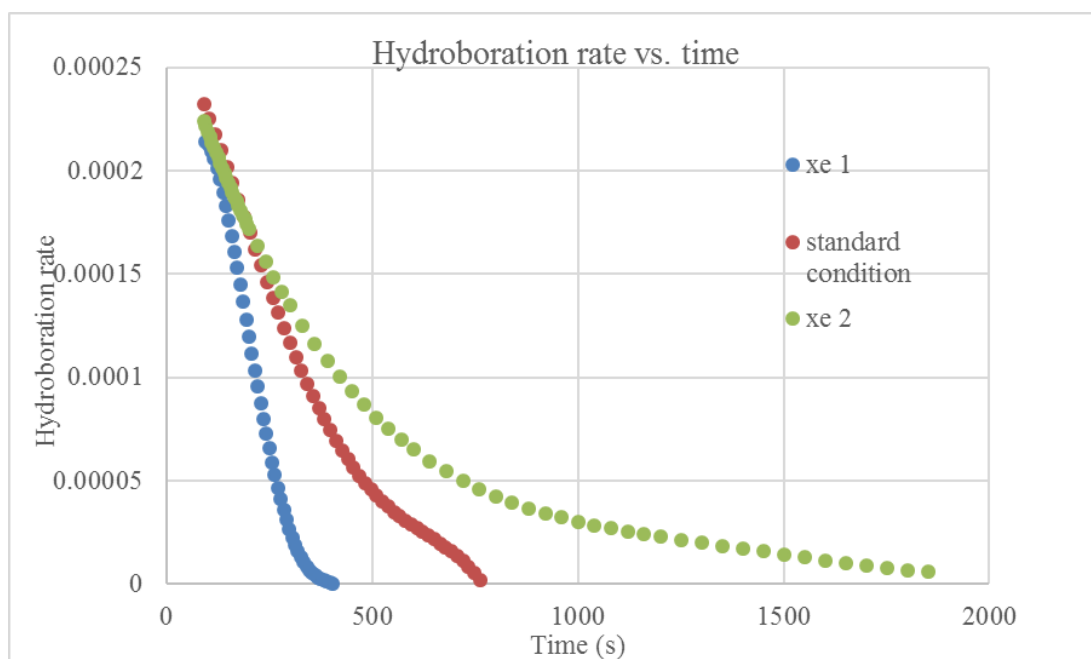


Figure 45 Substrate order by the "different excess" experiments: rate vs. time

In the hydroboration rates vs. time plot (figure 45), It's interesting to see the initial rates of the three reactions are about the same whereas the initial concentrations of alkene are rather different (table 9). This implies that the hydroboration rate has no dependence on alkene substrate.

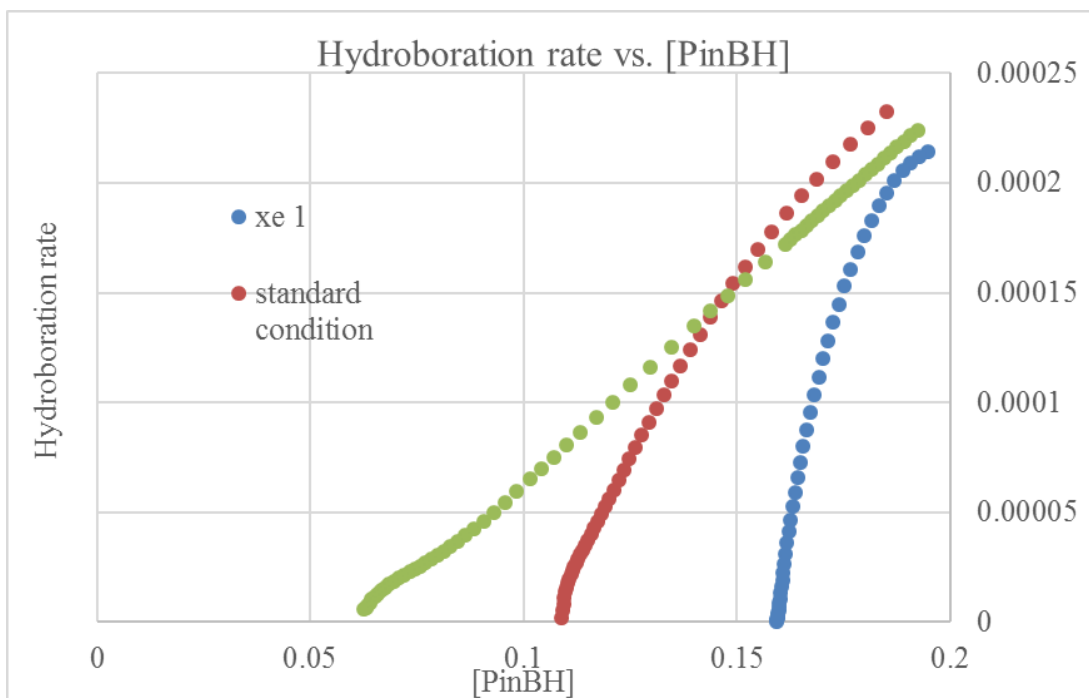
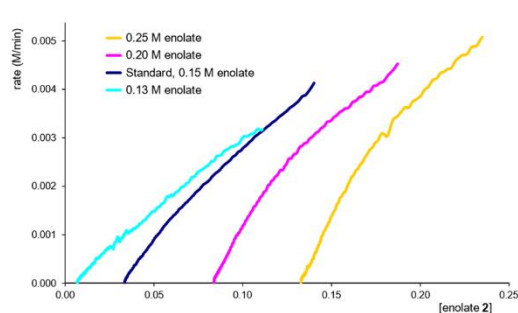
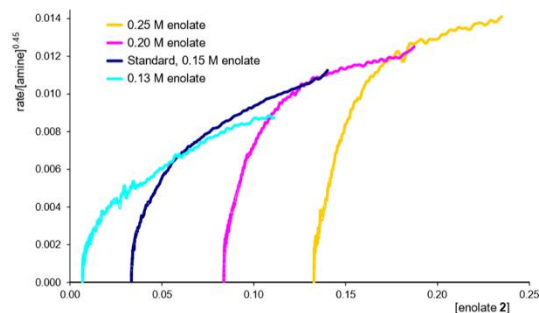


Figure 46 Substrate order by "different excess" experiments: normalized rate vs. [PinBH]

As we can see from figure 46, by assuming 0 order on alkene substrate, i.e., the y-axis is hydroboration rate/[Alkene]⁰, there is a good overlay at the beginning part of the reaction. This indicates the rate at that moment is not affected by the concentration of alkene substrate. The fact that at higher conversions (figure 46, the left part), 3 curves stopping to overlay can be explained since the x-axis is the [PinBH] and its remaining concentration at the end of each reaction would be different with the different initial [Alkene]. This kind of kinetic result can be compared with a published example below (figure 47).



Supplementary Figure S7: Graphical rate equations of oxidative coupling experiments performed at different amine concentrations, conditions as shown in Supplementary Table S3.



Supplementary Figure S8: Graphical evaluation of amine reaction order, plotting reaction rate divided by the amine concentration to the power of 0.45.

Figure 47 A published example of RPKA on the oxidative coupling reactions^[65]

Adapted from Ref 65 with permission. Copyright 2014 American Chemical Society.

Figure 47 shows the oxidative coupling reactions between the amine and the excessive enolate. The enolate is used as x-axis which is similar to our analysis that using excessive PinBH as the x-axis. In this example, the top right part of lines is overlapped the best when the arbitrary number is 0.45. Figure 48 shows the best overlay happen when “m” is 0 in the three CAHB experiments. It supports the prediction that the reaction rate is independent of [Alkene].

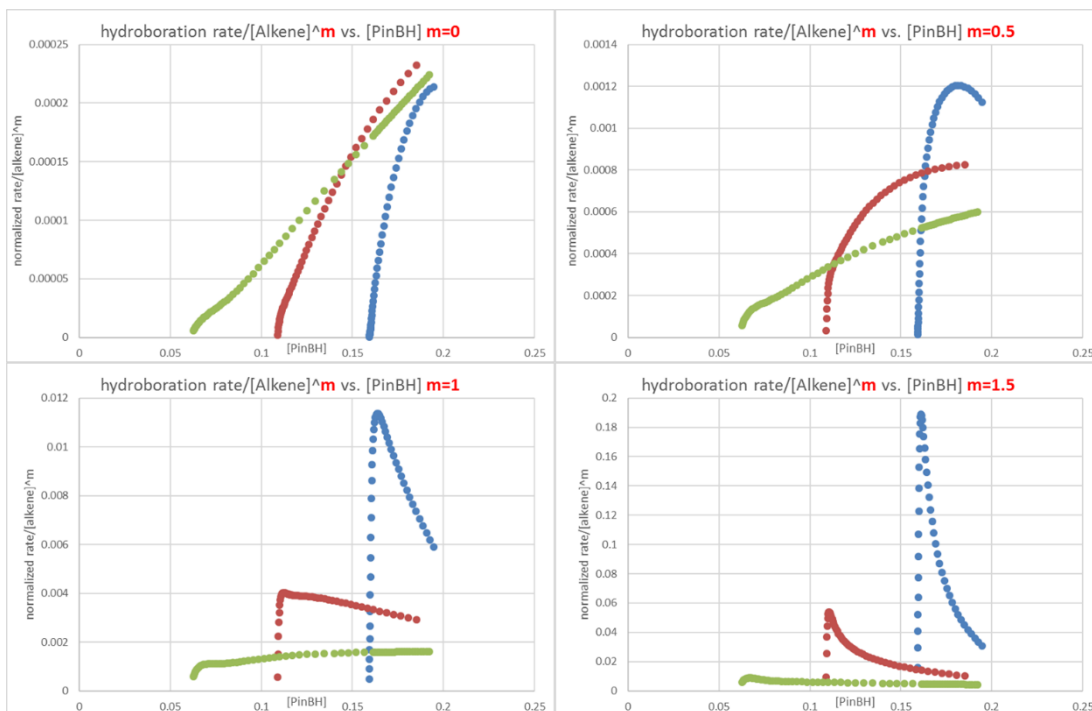


Figure 48 The adjusting on "m" in our RPKA on CAHB.

3.5 The Order of catalyst determined by “normalized time” graphical analysis.

3.5.1 Introduction:

The most common methods to determine the order of catalyst are initial rates and RPKA we just discussed above. However, some may find that these approaches require either setting up too many reactions or too much mathematical manipulation. In this section, we would apply the third choice, the normalized time graphical analysis reported by Bures^[66], to determine the reaction order of the catalyst. According to the rate equation definition, for a bimolecular elementary reaction:

$$\text{Rate} = -(d[A])/dt = f([A],[B], \text{kinetic const.}) \cdot [\text{Cat}]_t^n \quad (7)$$

After integration on both sides we can have the equation (8):

$$[A] = ([A]_0, [B]_0, v_A, v_B, \text{kinetic const. } t[\text{Cat}]_t^n) \quad (8)$$

Equation 8 reveals that the concentration of a reactant ($[A]$) is a function of the normalized time ($t[\text{Cat}]_t^n$), where “ t ” is the reaction time and $[\text{Cat}]_t$ is the total catalyst concentration and “ n ” is an arbitrary power of $[\text{Cat}]_t$. If the reactions are only different in the $[\text{Cat}]_t$ loading, then $[A]_0$, $[B]_0$, v_A , v_B and kinetic constant should be the same. Thus, we can find out the catalyst order by plotting the [**Alkene**] against a normalized time scale, “ $t[\text{Cat}]_t^n$ ”, from several different $[\text{Cat}]_t$ conditions. The value of “ n ” that provides the best curves overlay is the order of catalyst.^[66] For example, a published study by the Bures group is shown below.

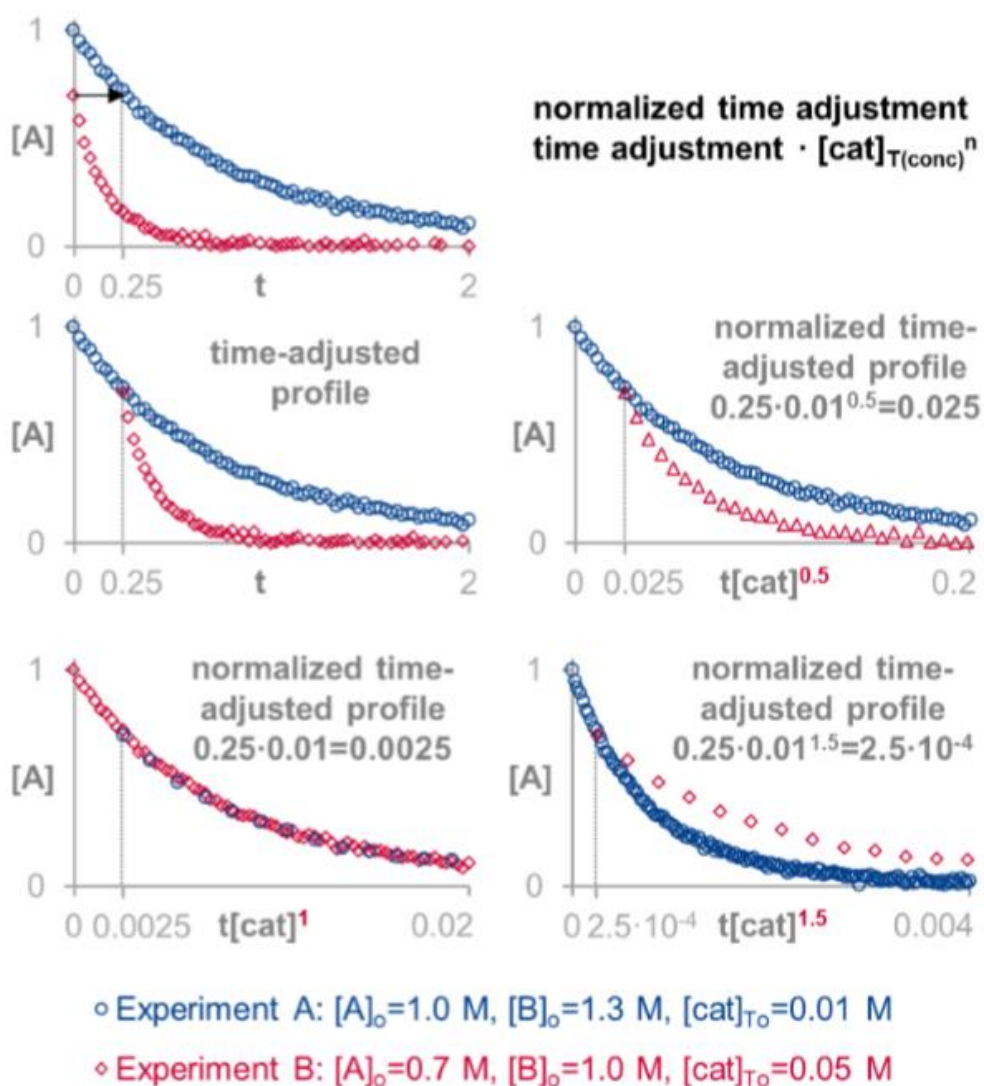
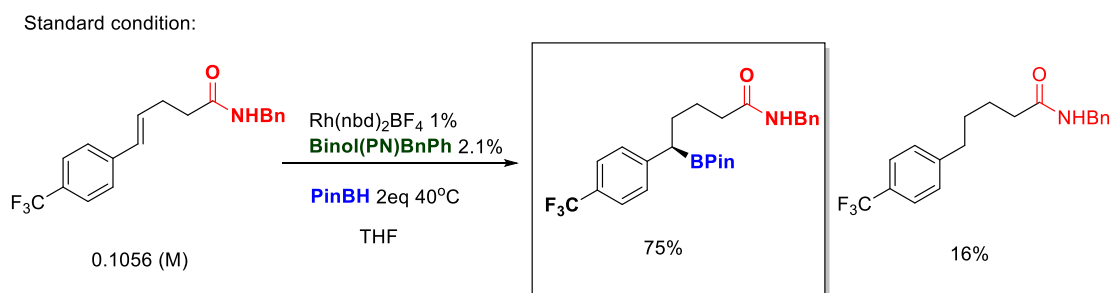


Figure 49 A published example of normalized time analysis from the Ref 66.

The permission is not required for this type of reuse.

The example is a little complicated because the experiment B is the condition of experiment A at 70 % conversion but with higher catalyst loading. That's why they adjust the time before studying the order of the catalyst. In their analysis, the two lines show the best overlap when "n" is 1, which indicates the reaction studied is first order in the catalyst.

3.5.2 Experimental conditions:



In our experimental design, to simplify the operations, the only variable is the $[\text{Cat}]_t$ which is changing from 0.5 mol% to 1.5 mol% relative to the alkene.

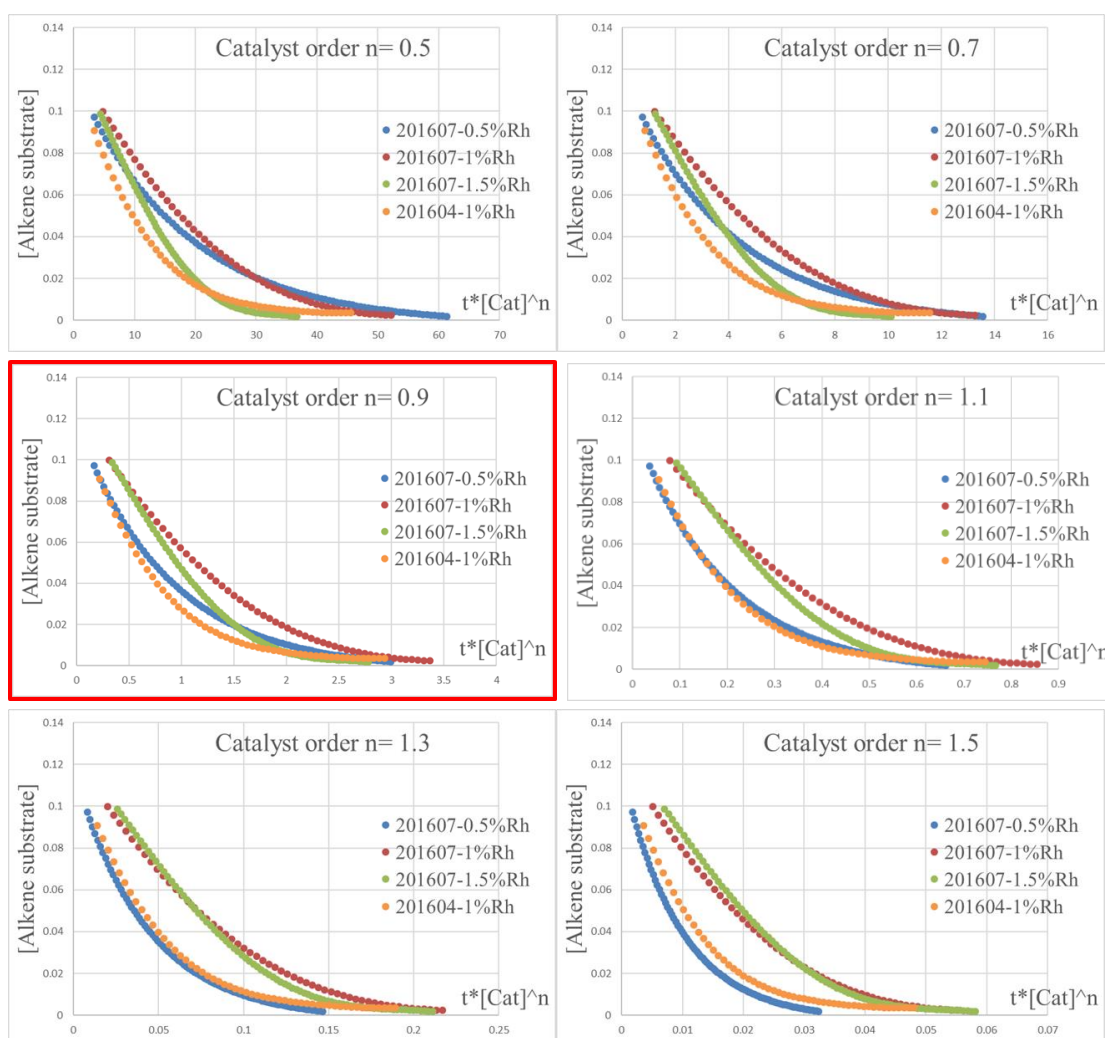


Figure 50 The adjusting of "n" in the normalized time graphical analysis.

While the data are not completely convincing, the figures show that most lines overlay best when the order of catalyst is 0.9. It suggests the Rh complex overall behaves first order in the reaction. There are some important technical problems, and further work will be required to address this random error due to inconsistency. Note that some lines are overlapped very well when “n” = 0.5 or 1.5; however, they are generally from the catalysts prepared from different batches on different days. Due to the extremely small scale of the reactions (0.1 mg of Rh complex is 0.5 mol % catalyst) as well as the issue of catalyst deactivation, the catalysts from different batches or the reactions initiated at different times may lead to results with large deviations. One should also note that there is a competing hydrogenation pathway catalyzed by the same Rh complex under the conditions of CAHB; i.e., a 16% yield of reduced product is obtained along with the hydroboration product. The non-integer order of the catalyst (i.e., $n = 0.9$) determined in the above analysis may reflect the competition of two catalyzed processes. Thus, the actual order of Rh catalyst for hydroboration pathway could be slightly different.

3.6 The mechanistic implications derived from the kinetic results.

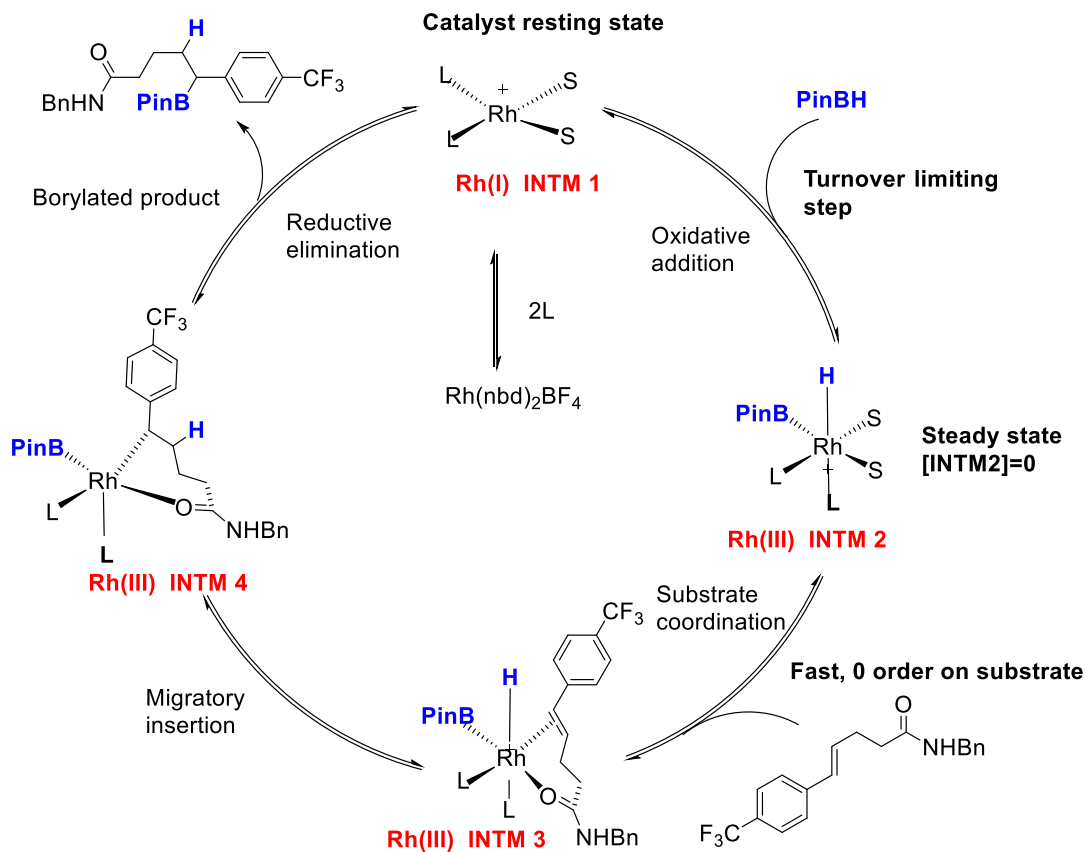


Figure 51 The mechanistic insights based on the kinetic studies

Based on the kinetic results we discussed earlier, we propose the mechanism shown in Figure 51 for the CAHB of para-CF_3 phenyl substituted γ,δ -unsaturated 1,2-amide. PinBH behaves 1st order while the substrate is 0 order in the hydroboration pathway. This suggests that oxidative addition of PinBH is the turnover limiting step, a higher concentration of PinBH leads to faster reaction rate. The resting state of Rh complex in the catalytic cycle should be the one before oxidative addition. This interpretation contradicts that in a previous computational study^[30g] in our group; it suggested that C–

B reductive elimination is the turnover limiting step of the CAHB albeit on a different substrate, a cyclic γ,δ -unsaturated amide substrate.

However, if we assume that reductive elimination is the turnover limiting step, then it means the catalyst resting state should be the **INMT 4**. We can deduce two conclusions from this assumption: (1) a higher [Alkene] should accelerate the formation of **INMT 4** thus increasing the rate, (2) **INMT 1** after **INMT 4** should be in a steady state (concentration = 0) and react very fast with PinBH. However, conclusion (1) is contradicted by the observed zero order dependence on [Alkene], and conclusion (2) is contradicted by the observed first order dependence on [PinBH]. The RPKA results obtained with the acyclic substrate are not consistent with reductive elimination being the turnover limiting step in the catalytic cycle.

When there is a large amount of alkene substrate as is the case at the beginning of the reaction, oxidative addition is the turnover limiting step. **INMT 2** is essentially at steady state concentration; i.e., once **INMT 1** is generated by oxidative addition of PinBH, it quickly reacts with the alkene substrate present in much higher concentration. **INMT 1** is therefore the limiting reagent in the following steps, and consequently, the reaction shows no dependence on [Alkene]. Thus, the alkene substrate behaves zero order until the reaction reaches high conversion and the concentration of alkene is not high enough to be considered as unchanging. Gradually the reaction rate would depend both on the substrate and the **INMT 1** which is generated by PinBH.

3.7 The Hydrogenation process:

The major side product in CHAB is from a hydrogenation pathway. For example, the reduced product in our kinetic study condition is about 15–25% varying with the loading amount of PinBH. The origin of reduction in the CAHB is explained by a working assumption that there is a sigma bond metathesis^[67] between the borylated–rhodium intermediate and H₂; the latter make arise from partial decomposition of PinBH by the adventitious moisture or other proton source.^[68]

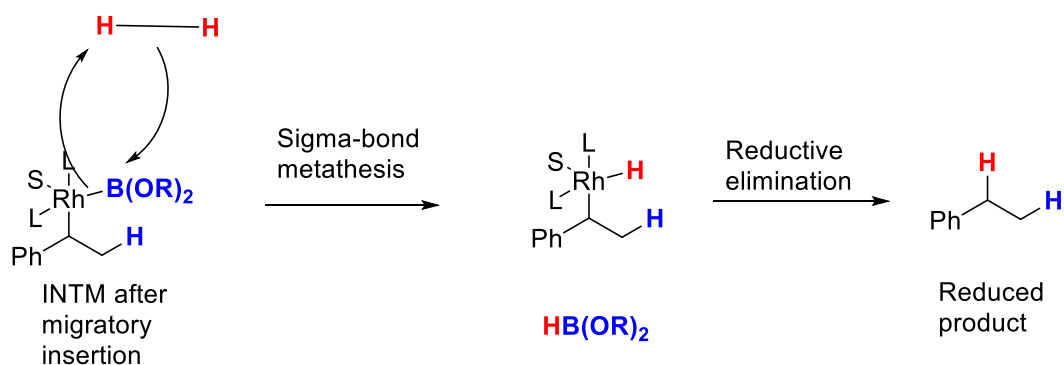


Figure 52 The assumption for a competing hydrogenation process in the CAHB condition illustrated for a simple, hypothetical alkyl-rhodium intermediate

To investigate the mechanism of the hydrogenation process, the “different excess” experiment was carried out. The data were from the same set of experiments described above as monitored by ¹⁹F NMR (Table 10).

Table 9 The reaction conditions in the “different excess” experiment to study the

hydrogenation process.

| | [Alkene] <i>M</i> | [PinBH] <i>M</i> | "Excess" <i>M</i> |
|-----------|-------------------|------------------|-------------------|
| 1.0 PinBH | 0.1056 | 0.1056 | 0 |
| 2.0 PinBH | 0.1056 | 0.2112 | 0.1056 |
| 4.0 PinBH | 0.1056 | 0.4224 | 0.3168 |

In this analysis, the [PinBH] is the only variable changing from 0.1056 *M* (1 equivalent of PinBH relative to alkene substrate) to 0.4224 *M* (4 equivalents compared to substrate); the other reagents are in the same concentration in all three experiments. The graph of normalized rate (rate of reduction/[PinBH] vs. [alkene substrate]) is shown below (figure 53).

$$\frac{\text{reduction rate}}{[\text{PinBH}]^1} = k \cdot [\text{Alkene}]^1 \quad (9)$$

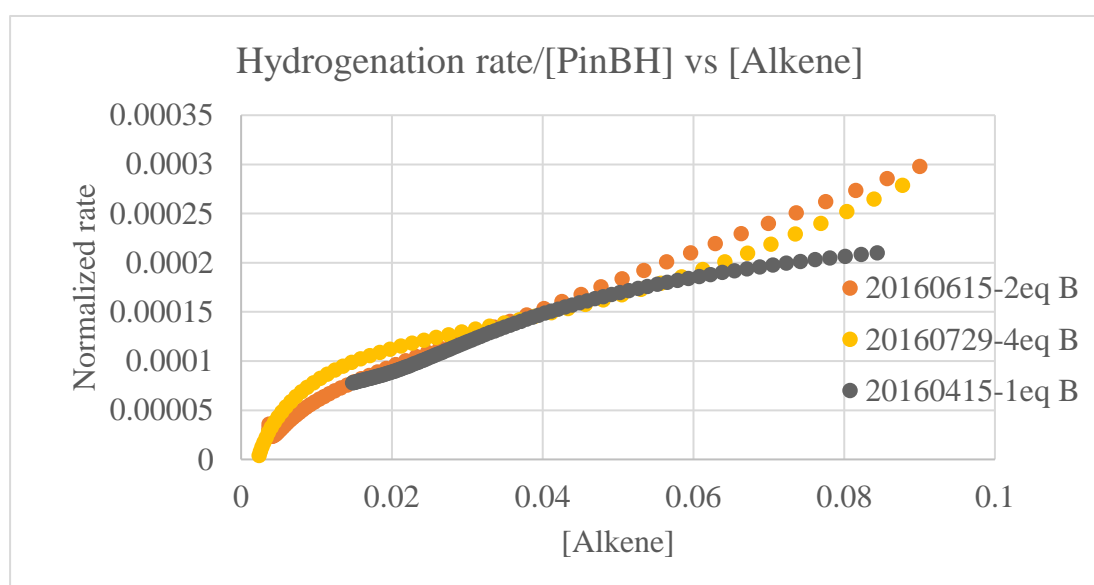


Figure 53 The "different excess" analysis on reduction pathway. The normalized rate

versus $[\text{Alkene}]^1$

The graph in Figure 53 has an x-axis describing $[\text{alkene}]^1$. The linear relationship between the normalized rate and $[\text{alkene}]^1$ indicates the alkene is 1st order in the hydrogenation process. If we assume that PinBH is 1st order as well as graphed in Figure 53), then the lines from the three different conditions overlay with each other. This suggests the function of $\frac{\text{Hydrogenation rate}}{[\text{PinBH}]^1}$ is independent of $[\text{PinBH}]$. Thus, the hydrogenation has a 1st order dependence on PinBH. Based on the kinetic profiles, we can interpret the mechanism that the 1st order dependence on PinBH means the slow oxidative addition step is the turnover limiting step, which leads to the common intermediate for both the hydroboration and the hydrogenation. The 1st order dependence on substrate in the hydrogenation process also suggests the postulated borylated–rhodium-borylated intermediate (figure 51, **INMT 4**) is a resting state species for the sigma bond metathesis. However, this intermediate is also the precursor to the hydroboration product by C–B reductive elimination. Most of **INMT 4** must undergo faster hydroboration pathway in competition with sigma-bond metathesis when H₂ is available; thus, it generates the reduced products.

The moisture in the reaction condition may affect the yield of hydrogenation. The high humidity weather in the summer and injecting PinBH solution outside the glovebox could account for the relatively high amounts of reduction product. In order to improve the hydroboration yield, the initial $[\text{PinBH}]$ should be increased so that the hydroboration is facilitated while less alkene substrate undergoes the sigma-bond

metathesis.

3.8 Discussion.

The Hammett equation $\log \frac{k'}{k} = \rho \cdot \sigma$ can be used to decipher the transition state of a reaction. We can calculate the reaction rate constant k by steady state approximation based on the results from the Reaction Progress Kinetic Analysis. However, it requires the rate constant k from a substrate without any substituents on the aromatic ring. Currently we are unable to monitor the reaction without fluorine. But if the equipment like ReactIR or calorimetry can be successfully employed in our study, it's worthy to work on this area since we have several substrates with different substituents on the phenyl group in this work and a Hammett study could yield further mechanistic understanding. As an alternative approach if ^{19}F is still the primary tool we rely on, it's possible to monitor the reaction by installing the fluorine element into the benzyl amide moiety of the substrate with different substituents at the styrene moiety.

3.9 Conclusion

The reaction progress kinetic analysis (RPKA) on catalytic asymmetric hydroboration (CAHB) by ^{19}F NMR discussed in this chapter reveals some mechanistic insights of the catalytic cycle which have two competitive reactions inside, the hydroboration and the hydrogenation. For the major hydroboration pathway, the 1st order dependence on PinBH and 0 order on alkene substrate indicates the oxidative addition should be the turnover limiting step. 1st order dependence on both PinBH and alkene substrate in the

hydrogenation suggests that sigma-bond metathesis is also a rate limiting step for hydrogenation.

To suppress the hydrogenation, we should lower the ratio of alkene: PinBH or avoid the decomposition of PinBH with the moisture.

Chapter 4: Experimental procedures

General procedures.

All the CAHB reactions were set up in a dry N₂ atmosphere. The moisture, oxygen, and peroxide free Tetrahydrofuran (THF) were freshly distilled by the benzophenone-sodium method. HPLC solvents were filtered by Mollipore filter. The borane reagents were freshly distilled by Kugelrohr apparatus immediately before use. The distillation temperature for 4,4,6-trimethyl-1,3,2-dioxaborinane(TMDBH) at 180 °C and Pinnacol borane at 150 °C in standard atmosphere. All synthesized substrates were preparing and stored under N₂ atmosphere. Flash column chromatography was applied to purify the compounds by using EMD silica GEL 60 Geduran®. The solvent was removed by

vacuum evaporation. Thin layer chromatography was performed to monitor the reaction progress using Analtech Silica Gel HLF (0.25 mm) and visualized by short wavelength UV light, vanillin stain (vanillin, conc. H₂SO₄ and 96% ethanol) or iodine stain (I₂ solid and EMD Silica Gel60 Geduran®). HPLC analysis was performed with use of an ISCO model 2360 HPLC and chiral HPLC columns (Chiralcel OD; column: 250 x 4.6 mm) protected by guard column. The Data were collected and analyzed by ChromPerfect chromatography software (version 5.1.0). NMR spectra were recorded on 300, 400 and 700 MHz Bruker Advance NMR spectrometers, calibrated with residue CHCl₃ (δ 7.26 ppm) or CDCl₃ (δ 77.0 ppm) unless otherwise specified. Peaks in spectra are expressed as m (unresolved multiplet), q (quartet), t (triplet), d (doublet) or s (singlet).

4.1 Reaction progress kinetic analysis experiments setup and data processing.

4.1.1 Setting up reactions:

All the reactions were carried out almost the same with procedures in the previous section, performing the CAHB reaction, in terms of stock solution preparation. The difference is to monitor the reaction progress, we set up reactions in the NMR tube. NMR tubes and rubber septum were stored inside the drying chamber overnight before the experiments. Once the Rh complex, substrate stock solution and borane stock solution were ready, the Rh complex and substrate solution were transferred into the

NMR tube by syringes. NMR tubes were capped with the rubber septum and sealed with parafilm. The borane solution was stored inside the syringes which were later inserted into a rubber septum sealed round bottom flask.

When NMR program was ready, the probe temperature was set up to the appropriate level, in our case, the temperature was set to 313K (40°C). the F19DCP was chosen in this study. In order to obtain better resolution, a template NMR tube was used for calibration before reaction started, which was filled with only alkene substrate solution in the same volume amount of total reaction after the injection of borane solution. The receiver gain was manually shimmed until it reach the best FID. The template NMR tube is ejected, the borane solution injected into the NMR tube with alkene substrate and Rh complex, mix it on vortex for 5 seconds then inject into the NMR spectrometer; record the scanning time for each scanning and control the total time by command “Multizg n”.

4.1.2 Integration on raw data

After the NMR scanning, the raw data were integrated by Topspin to get the relation between concentration of each species to time. because there could be 200 scanning of spectra for just one condition, this integration process could be time consuming. To save time as well as to make sure all the integration was taken under the same chemical shift range, a template integration spectrum was set up and all the rest spectra would be integrated based on parameters in the template spectrum. This would lead to a more

smoothly and consistent plot than the manual operation.

4.2 Procedures:

Chose a spectrum as template, which is at about half conversion so that both starting material and the products signals are noticeable.

4.2.1 Set up the template:

Integrate peaks of interests, right click then select “save A” regions to intrng.

Command “wrmisc” to write the current integration as template and name it.

4.2.2 Automatic integration:

Command “multicmd” then type efp, apk, abs (automatic baseline flatten).

Command “multi_integ” then type the name of the template and execute button.

After this, all the spectra were integrated at the same area as the template spectrum and the integral numbers were collected into a txt file named as “intall.txt”, which is located at the 1st spectrum folder.

4.2.3 Import the data into Excel

After importing the intall.txt file into Excel, the data are shown in group of each NMR scan in ascending scan number, that is from the beginning to the end of the reaction.

Each group contains for example 4 sets of integral number which are representative to 4 components in the reaction. They are labeled as #1 to #4.

Select the label number column, sort the number in ascending order, and chose expanding the selection to all the integrals attached to labeled. Although there are a lot (same to the number of spectra) of rows labeled by the same number, the rows with same label number will ascend in the group number (1st spectrum to last spectrum). In this way, we can get the integrals in a time order.

4.3 Data analysis

The integrals are proportional to concentration of components. Thus, the primary integrals data can be converted to concentration data by normalization to percentage then multiply with total concentration.

To construct the mathematical function of time-concentration data for further analysis, the curve fitting program Origin Pro 8 was applied to data with polynomial model to the 7th order. The fitted function described the mathematical relation between concentration of one reaction component and time. The rate vs. time function can be get by taking the 1st derivative of the fitted function. Once the rate vs. time function is obtained, the profile of rate vs. time can be generated by plugging in time to the function.

Rearrange the rate equation: $rate = k \cdot [alkene]^m \cdot [PinBH]^n$ to “normalized rate” vs. one reagent. That is rate “normalized” by one substrate’s concentration plotted against the other substrate’s concentration. For example:

$$\frac{rate}{[alkene]^m} = k \cdot [PinBH]^n$$

Or

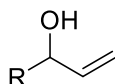
$$\frac{\text{rate}}{[\text{PinBH}]^n} = k \cdot [\text{alkene}]^m$$

The goal is to seek “n” or “m” that give the best overlay between data plots from several experiments using one of normalized rate equations above. A priori, we don’t know which of the normalized equations and what order number would give the best result. Basically, we use trial and error and change each one in turn until the best overlay exhibited. To observe better overlay between plots, our experience is that the constant reagent from several “different excess” experiments should be used as x-axis. In this way, the plots would have same scale on x-axis and easier to observe the overlay.

To study the order of substrates, typically two “different excess experiments are sufficient to determine the values. However, in our graphical analysis experience, the “overlay” of data plots standard is easier to achieve than the “straight line” standard. We typically take data from over 20%-80% conversion into consideration when plotting the data in the form of these graphical rate equations. Because there are induction periods at the outset and the end of the reactions, normalization by the limiting reagent becomes inaccurate as the concentration decreased to zero.

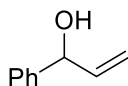
Chapter 5: Representative procedure for the preparation of substrates

5.1 procedures for preparing the γ,δ -unsaturated amide



General synthetic procedure A: secondary allylic alcohols

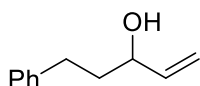
Aldehyde (1 eq.) was dissolved in dry THF at 0 °C. Vinylmagnesium bromide (1.0 M in THF, 1.0-1.2 eq.) was stirred at -78 °C. The freshly distilled aldehyde (1 eq.) was dissolved in Et₂O (1.0 M) and was added to the vinylmagnesium bromide-solution within 30 min. The reaction mixture was stirred for 1 hour at -78 °C and was then allowed to warm up to room temperature. The reaction mixture was quenched with saturated NH₄Cl solution and stirred for 15 min. The reaction mixture was acidified with an HCl solution (1 M) and the phases were separated. The aqueous phase was extracted with Et₂O (3 times). The combined organic phases were washed with brine (1 time), dried over Na₂SO₄, filtrated and concentrated *in vacuo*. The crude product was purified by flash column chromatography (EtOAc/ Hexane).



Compound 1: 1-phenylprop-2-en-1-ol

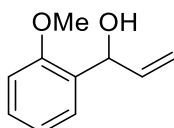
Following the general procedure, phenyl magnesium bromide (0.9 mL of 3.0 M solution

in Et₂O, 2.7 mmol) added to a solution of acrolein (150 mg, 2.78 mmol) in anhydrous THF (10 mL) at -78 °C for 12 h. The reaction was quenched with saturated NH₄Cl. After purification by column chromatography (20% EtOAc with Hexane, R_f = 0.3), the title compound 1 (308 mg, 83%) as a yellow oil. ¹H NMR (400 MHz, CDCl₃) δ H: 1.94 (1H, s), 5.23 (3H, dt, *J* = 10.3, 1.3Hz), 5.24 (1H, s), 5.39 (1H, dt, *J* = 17.2, 1.3Hz), 6.08 (1H, ddd, *J* = 17.1, 10.3, 6.1), 7.29–7.43 (5H, m). ¹³C NMR (300 MHz, Chloroform-d) δ 142.64, 140.27, 128.60, 127.83, 126.42, 115.16, 75.31



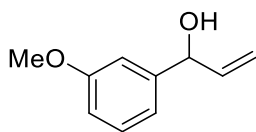
Compound 2 : 5-phenylpent-1-en-3-ol

According to general procedure A, compound 2 (5-phenyl-pent-1-en-3-ol) (3.02 g, 18.6 mmol, 93%) was obtained as colorless oil liquid from commercially available hydro cinammylaldehyde (2.76 ml, 2.68 g, 20.0 mmol) and vinyl magnesiumbromide (1.0 M, in THF, 24.0 ml, 24.0 mmol, 1.2 eq.). R_f = 0.57 (EtOAc : Hexane = 50:50). ¹H-NMR (400.130 MHz, CDCl₃): δ = 1.54 (s br, 1H,), 1.82-1.89 (m, 2H,), 2.64-2.81 (m, 2H,), 4.14 (m, 1H,), 5.14 (dd, *J* = 10.5, 1.4 Hz, 1H,), 5.25 (dd, *J* = 17.2, 1.4 Hz, 1H,), 5.91 (ddd, *J* = 17.2, 10.4, 6.2 Hz, 1H,), 7.15-7.22 (m, 3H), 7.25-7.31 (m, 2H). ¹³C- NMR (300MHz, CDCl₃): δ = 31.7, 38.6, 72.6, 115.0, 125.9, 128.5, 128.5, 141.1, 142.0. The analytical data were consistent with those reported previously.^[69]

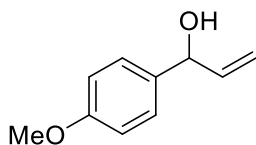


Compound 3 : 1-(2-methoxyphenyl)prop-2-en-1-ol

Following General Procedure A, vinyl magnesium bromide (10 mL of 0.7M solution in THF, 7 mmol) added to a solution of 2-methoxybenzaldehyde (600 mg, 4.40 mmol) in anhydrous THF (30 mL) at 0°C for 3 h. After purification by column chromatography (EtOAc : Hexane = 20 : 80, Rf=0.28), the title compound 3 (600 mg, 83%) as a yellow liquid with spectroscopic data in accordance with the literature. ¹H NMR (400 MHz, CDCl₃) δH: 2.76 (1H, d), 3.87 (3H, s), 5.17 (1H, dt, *J*= 10.4, 1.5 Hz.), 5.31 (1H, dt, *J* = 17.2, 1.6 Hz), 5.40 (1H, d, *J* = 5.3 Hz), 6.14 (1H, ddd, *J* = 17.2, 10.4, 5.5 Hz), 6.87–6.94 (1H, m), 6.96 (1H, td, *J* = 7.5, 1.1 Hz), 7.22–7.34 (2H, m)

**Compound 4 : 1-(3-methoxyphenyl)prop-2-en-1-ol**

Following general procedure A, vinyl magnesium bromide (15 mL of 0.7 M solution in THF, 10.5 mmol) added to a solution of 3-methoxybenzaldehyde (900 mg, 6.60 mmol) in anhydrous THF (45 mL) at 0 °C for 3 h. After purification by flash column chromatography (EtOAc : Hexane = 20 : 80, Rf=0.28), the title compound 4 (432 mg, 40%) as a colourless oil. The analytical data were consistent with those previously reported.^[70] ¹H NMR (400 MHz, CDCl₃) δ H: 1.92 (1H, s), 3.82 (3H, s), 5.18 (1H, s), 5.20 (1H, dt, *J* = 10.2, 1.3 Hz), 5.36 (1H, dt, *J*=17.0, 1.3), 6.04 (1H, ddd, *J* 17.0, 10.2, 6.1 Hz), 6.83 (2H, ddd, *J* = 8.3, 2.5, 1.1 Hz.), 6.92–6.99 (3H, m), 7.23–7.32 (2H, m).

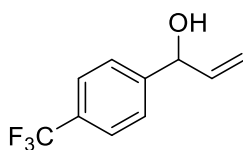


Compound 5: 1-(4-methoxyphenyl)prop-2-en-1-ol

Following general procedure A, vinyl magnesium bromide (39 mL of 0.7 M solution in THF, 28 mmol) added to a solution of anisaldehyde (2.5 g, 18.3 mmol) in anhydrous THF (50 mL) at 0 °C for 3 h. After purification by column chromatography (EtOAc : Hexane = 20 : 80, R_f = 0.33), the title compound 5 (2.5 g, 83%) was isolated as a yellow liquid. The analytical data were consistent with those reported previously. ^[71]

¹H NMR (400 MHz, CDCl₃) δ H: 1.85 (1H, d, *J* = 3.6Hz), 3.81 (3H, s,), 5.17 (1H, s), 5.19 (1H, d, *J* = 10.3Hz,), 5.34 (1H, d, *J* = 17.1Hz), 6.05 (1H, ddd, *J* = 16.8, 10.3, 5.9 Hz), 6.89 (2H, d, *J* = 8.7 Hz), 7.30 (2H, d, *J* = 8.7 Hz,).

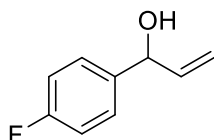
¹³C NMR (300 MHz, CDCl₃) δ 157.95, 139.50, 133.99, 126.70, 113.53, 112.79, 73.65, 54.16



Compound 6 : 1-(4-(trifluoromethyl)phenyl)prop-2-en-1-ol

Following general procedure A, vinyl magnesium bromide (8.0 mL of 0.7 M solution in THF, 5.6 mmol) added to a solution of 4-trifluoromethylbenzaldehyde (600 mg, 3.44 mmol) in anhydrous THF (20 mL) at -78 °C for 16 h and quenched with saturated

NH₄Cl. After purification by column chromatography (EtOAc : Hexane = 20 : 80, R_f = 0.33), the title compound 6 (696 mg, 100%) was isolated as a yellow oil. ¹H NMR (400 MHz, CDCl₃) δH: 2.02 (1H, br s), 5.25 (1H, dt, *J* = 10.3, 1.2 Hz), 5.28 (1H, s), 5.38 (1H, dt, *J* = 17.1, 1.3), 6.02 (1H, ddd, *J* = 17.1, 10.3, 6.3 Hz), 7.45–7.54 (2H, m), 7.62 (2H, d, *J* = 8.1 Hz). ¹³C NMR (300 MHz, CDCl₃) δ 146.3, 139.7, 129.8 (q), 126.7, 125.54, 116.1, 74.9.



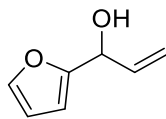
Compound 7 : 1-(4-fluorophenyl)prop-2-en-1-ol

Prepared according to general procedure A. 152.2 mg 1 mmol of corresponding aldehyde was dissolved in 5 ml of anhydrous THF solution. Vinyl magnesium bromide (2.0 mL of 0.7 M solution in THF, 1.4 mmol) was added into the reaction flask. After 2 h stirring, the reaction was quenched with saturated NH₄Cl. The title compound was purified by column chromatography (EtOAc : Hexane = 80 : 20) to yield the title compound as the colorless oil 121 mg (78%)

¹H NMR (400 MHz, CDCl₃) δ 7.26-7.32 (2H, m), 7.02 (2H, tt, *J* = 8.8, 2.1 Hz), 5.96 (1H, ddd, *J* = 17.1, 10.3, 6.0 Hz), 5.29 (1H, dt, *J* = 17.1, 1.4 Hz), 5.16 (1H, dt, *J* = 10.3, 1.3 Hz), 3.18 (1H, br), 5.09 (1H, d, *J* = 6.0 Hz)

¹³C NMR (300 MHz, CDCl₃) δ 160.9-163.5, 139.9, 138.22, 127.9, 115.3, 115.2, 115,

74.4



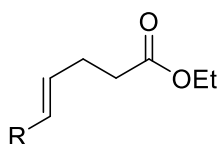
Compound 8 : 1-(furan-2-yl)prop-2-en-1-ol

Prepared according to general procedure A. 124 mg (1 mmol) of corresponding aldehyde was dissolved in 5 ml anhydrous THF. The Vinyl magnesium bromide 1.5 mmol in THF solution was slowly added into the reaction flask. The title compound was purified by column chromatography (EtOAc : Hexane = 80 : 20) to yield the title compound as an oil 96.8 mg (72 %) The analytical data were consistent with those previously reported.^[72]

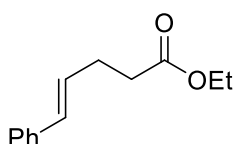
¹H NMR (400 MHz, CDCl₃) δ 7.34-7.31 (1 H, m), 6.28-6.25 (1H, m), 6.19 6.17 (1H, m), 6.05 (1H, ddd, *J* = 17.1, 10.3, 6.0 Hz), 5.35 (1H, dt, *J* = 17.1, 1.4 Hz), 5.21 (1H, dt, *J* = 10.3, 1.3 Hz), 5.16 (1H, s), 2.07 (1H, s). ¹³C NMR (300 MHz, CDCl₃) δ 155.41, 142.71, 137.0, 116.61, 110.61, 107.0, 69.0

General synthetic procedure B for the synthesis of γ,δ -unsaturated esters from secondary allylic alcohols

γ,δ -unsaturated esters were generated by the Johnson-Orthoester-Claisen rearrangement.^[73]



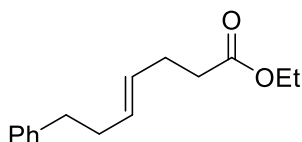
Propionic acid (0.1 eq.) and triethylorthoacetate (ToEA) (1.5-12 eq.) were added to the secondary allylic alcohol (1 eq). The sand bath was heated to 160 °C and the formed by product ethanol was distilled off. A lower temperature was used for the reaction with low boiling point allylic alcohols to prevent the loss of the starting material. After 3 h, the reaction mixture was allowed to cool to the room temperature, then it was quenched with saturated NaHCO₃ solution. To remove the excess amount of triethylorthoacetate (ToEA) the reaction mixture was dissolved in DCM to 0.2 M, an aqueous HCl-solution (1 M) (equal volume amount) was added and the mixture was stirred overnight. After phase separation, the aqueous layer was extracted with DCM (3 x equal amount) and the combined organic phases were washed with saturated NaHCO₃ solution and dried over Na₂SO₄. After filtration, the solvent was concentrated *in vacuo*. The crude product was purified by flash column chromatography (EtOAc and Hexane).



Compound 9 : ethyl (E)-5-phenylpent-4-enoate

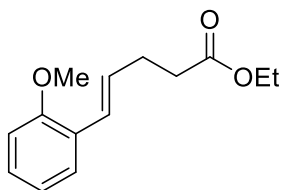
According to general procedures 2, alcohol compound 1 (10.6 g, 80 mmol) was treated with triethyl orthoacetate 3 eq and 3 drops of propionyl acid. The reaction mixture was heated to 160 °C for 3 h then quenched with saturated NH₄Cl solution. The crude product was isolated after solvent evaporation under reduced pressure. The crude was subjected to the flash column chromatography (EtOAc : Hexane = 5 : 95),

afford the ester compound 9 (9.12 g, 44.6 mmol, 57%) as a colourless oil. δ H (400 MHz, CDCl₃) 7.44-7.20 (5H, m,), 6.45 (1H, d, J = 15.9 Hz), 6.25 (1H, dt, J = 15.9, 6.5 Hz), 4.17 (2H, q, J = 7.1 Hz), 2.60–2.46 (4H, m), 1.29 (3H, t, J = 7.1 Hz); δ ¹³C NMR (300 MHz, CDCl₃) 171.8 (C=O), 137.3 (Ar), 131.1 (PhCH=CH), 128.4 (Ar & PhCH=CH), 127.2 (Ar), 125.1 (Ar), 60.3 (OCH₂), 34.1 (CH₂), 28.3 (CH₂), 14.3 (CH₃). Data are consistent with literature values.^[73]



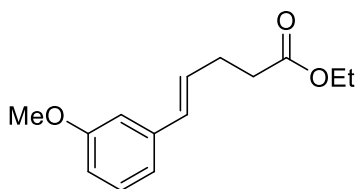
Compound 10 : ethyl (E)-7-phenylhept-4-enoate

According to general procedure B, compound 10 (trans-7-phenyl-hept-4-enoic acid ethyl ester) (12g, 50 mmol, 84%) was obtained as colorless oil from 5-phenyl-pent-1-en-3-ol (9.8 g, 60.4 mmol) and triethylorthoacetate (14.5 g, 90 mmol, 1.45 eq.). R_f = 0.46 (EtOAc : Hexane = 90:10). ¹H NMR (400 MHz, CDCl₃): δ 1.24 (t, J = 7.1 Hz, 3H), 2.25-2.38 (m, 6H), 2.62-2.68 (m, dd, J = 9.2, 6.4 Hz, 2H), 4.12 (q, J = 7.2 Hz, 2H), 5.38-5.58 (m, 2H), 7.15-7.22 (m, 3H), 7.24-7.31 (m, 2H). ¹³C-NMR (300 MHz, CDCl₃): δ = 14.4, 28.0, 34.3, 36.0, 60.2, 125.7, 128.2, 128.6, 128.8, 130.8, 142.1, 173.3.



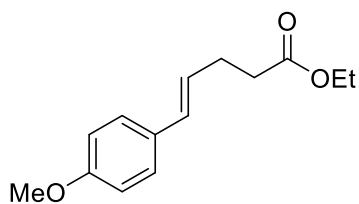
Compound 11 : ethyl (E)-5-(2-methoxyphenyl)pent-4-enoate

According to general procedures B, alcohol compound 3 (8.2 g, 50 mmol) was treated with triethyl orthoacetate 3 eq and 3 drops of propionyl acid. The reaction mixture was heated to 160 °C for 3 h then quenched with saturated NH₄Cl solution. The crude product was isolated after solvent evaporation under reduced pressure. The crude was subjected to the flash column chromatography (EtOAc : Hexane = 5 : 95), afford the ester compound 9 (7.72 g, 30 mmol, 60%) as a colourless oil.



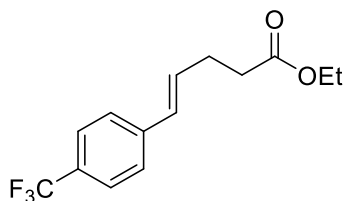
Compound 12 : ethyl (E)-5-(3-methoxyphenyl)pent-4-enoate

According to general procedure B, alcohol compound 4 (4.1g 25 mmol) was treated with triethyl orthoacetate, which after flash column chromatography (gradient elution: 10% to 15% EtOAc with Hexane mixture), afford titled ester (3.86 g, 15 mmol, 60%) as a colourless oil. R_f = 0.53 (EtOAc : Hexane = 20 : 80); δ H (400 MHz, CDCl₃) 7.28–7.19 (1H, m), 6.96–6.74 (3H, m), 6.42 (1H, d, *J* = 15.8 Hz), 6.22 (1H, dt, *J* = 15.7, 6.4 Hz), 4.17 (2H, q, *J* = 7.1 Hz), 3.81 (3H, s), 2.60–2.44 (4H, m), 1.27 (3H, t, *J* = 7.1 Hz); δ ¹³C (300 MHz, CDCl₃) 173.0 (C=O), 159.9 (Ar), 138.8 (Ar), 130.7 (ArCH=CH), 129.6 (ArCH=CH), 128.7 (Ar), 118.5 (Ar), 112.6 (Ar), 111.3 (Ar), 60.4 (COCH₂), 55.1 (OCH₃), 34.1 (CH₂), 28.2 (CH₂), 14.1 (OCH₂CH₃);



Compound 13 : ethyl (E)-5-(4-methoxyphenyl)pent-4-enoate

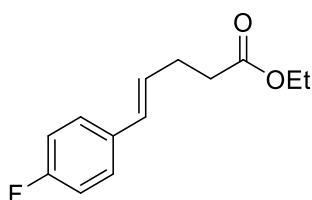
According to general procedure B, alcohol compound 5 (3.2 g, 20.0 mmol) was treated with triethyl orthoacetate 1.5 eq. The reaction mixture was heated to 160 °C for 3 h then quenched with saturated NH₄Cl solution. The crude product was isolated after solvent evaporation under reduced pressure. The crude was subjected to the flash column chromatography (EtOAc : Hexane = 5 : 95), afford the ester compound 13 (2.34 g, 10 mmol, 50%) as a colorless oil. δ ¹H (400 MHz, CDCl₃) 7.30–7.22 (2H, m), 6.84 (2H, d, *J* = 8.8 Hz), 6.38 (1H, d, *J* = 15.8 Hz), 6.08 (1H, dt, *J* = 15.8, 6.1 Hz), 4.16 (2H, q, *J* = 7.1 Hz), 3.81 (3H, s), 2.56–2.43 (4H, m), 1.27 (3H, t, *J* = 7.1 Hz); δ ¹³C (300 MHz, CDCl₃) 173.1, 158.8, 130.3, 127.8, 127.1, 126.3, 113.9, 60.3, 55.3, 34.2, 28.3, 14.3 . Data are consistent with literature values.^[74]



Compound 14 : ethyl (E)-5-(4-(trifluoromethyl)phenyl)pent-4-enoate

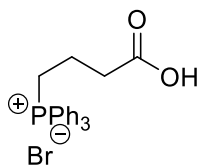
According to general procedure B, alcohol compound 6 10.1 g (50 mmol) was dissolved in ToEA 3 eq (24.3 g) and 6 drops of propionyl acid. The reaction mixture was heated

to 160 °C for 3 h. After work up, the residue was purified by column chromatography to give compound 14 in 80% (10.88 g) isolated yield. ^1H NMR (300 MHz, CDCl_3): δ = 7.51 (d, J = 8.2 Hz, 2H), 7.35 (d, J = 8.2 Hz, 2H), 6.43 (d, J = 16.0 Hz, 1H), 6.31 (dt, J = 16.0, 6.3 Hz, 1H), 4.13 (q, J = 7.2 Hz, 2H), 2.51 (m, 4H), 1.25 (t, J = 7.1 Hz, 3H). ^{13}C NMR (75 MHz, CDCl_3): δ = 172.5, 140.7, 131.2, 129.8, 128.5, 126.2, 125.3, 124.1, 60.4, 33.7, 28.2, 14.2. Data are consistent with literature values.^[74]



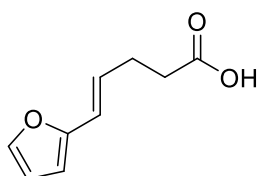
Compound 15 : ethyl (E)-5-(4-fluorophenyl)pent-4-enoate

According to general procedure B, alcohol compound 7 (15.2g, 100 mmol) was treated with triethyl orthoacetate 3 eq (48.6 g) and 10 drops of propionyl acid. The reaction mixture was heated to 160 °C for 3 h. After work up, the residue was purified by column chromatography to give compound 14 in 80%. R_f = 0.6 (EtOAc : Hexane = 10 : 90); δ ^1H (400 MHz, CDCl_3) 7.31–7.26 (2H, m), 6.98 (2H, dd, J = 8.7 Hz), 6.39 (1H, d, J = 15.9 Hz), 6.10 (1H, dt, J = 15.9, 6.4 Hz), 4.15 (2H, q, J = 7.1 Hz), 2.55–2.42 (4H, m), 1.26 (3H, t, J = 7.1 Hz); δ ^{13}C (300 MHz, CDCl_3) 172.9, 162.0, 133.5, 129.7, 128.2, 127.5, 115.3, 60.4, 34.0, 28.2, 14.2. δ ^{19}F (300 MHz, CDCl_3) 115. Data are consistent with literature values.^[74]



Compound 16 : butyric phosphonium bromide

This Ylide (phosphonium salt) derives from the 4-bromo butyric acid. A mixture of acid 136 mg, (1 mmol, 1 equiv) and triphenylphosphine (257 mg, 1 mmol, 1 equiv) in CH₃CN (10 mL) was refluxed for 24 h under N₂. The solution was cooled at room temperature and filtered and dried over Na₂SO₄, the solution was concentrated *in vacuo* to give pentanoic phosphonium bromide as a white precipitate (310 mg, 88%).

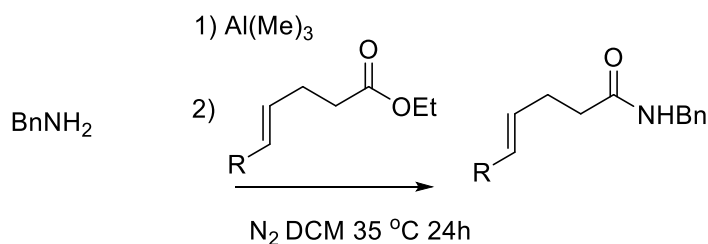


Compound 17 : (E)-5-(furan-2-yl)pent-4-enoic acid

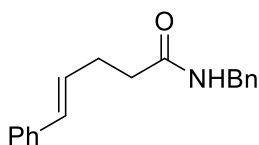
Wittig reaction

A mixture of Ylide 1 mmol (1 equiv) and furanal aldehyde (0.75 equiv) in THF (150 mL) was refluxed for 48 h in N₂. The resulting solution was allowed to cool to room temperature then evaporated under reduced pressure. The crude was purified by flash column chromatography (EtOAc : Hexane =10 : 90) to afford the corresponding unsaturated acid. 149 mg, 90% yield.

General synthetic procedure C for preparing γ,δ -unsaturated amide by transamidation.

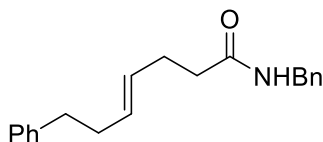


The 1eq amine reagent was dissolved in 4 M DCM solution under N_2 condition. Slowly add 1eq of $\text{Al}(\text{Me})_3$ 2M hexane solution at $0\text{ }^\circ\text{C}$. Stir 20 min then slowly add the 1eq ester substrate in neat. Raise to $35\text{ }^\circ\text{C}$ and stir for 24 h. Slowly quench the reaction with 3 M HCl solution to same volume. Extract the aqueous phase by DCM 100ml x 2 times for 2.5 mmol scale reaction. Combine the organic extracts and evaporate the solvent in reduced pressure to provide the crude product.



Compound 18: (*E*)-N-benzyl-5-phenylpent-4-enamide: Following the general procedure C. Compound 9 4.3 g (21.07 mmol) was dissolved in 50 ml DCM under N_2 atmosphere. At room temperature, the $\text{Al}(\text{Me})_3$ 38 ml 1M THF solution reagent (1.8 equiv) was inserted in to the reaction flask and stirred for 1 h. After Lewis acid activated the substrate, BnNH_2 4.5 g (42 mmol, 4.8 ml, 2 equiv) was added into the reaction mixture and stirred for overnight. Then the condition was cooled to $0\text{ }^\circ\text{C}$ and diluted with equal amount of DCM. Followed by adding 1 M HCl solution slowly to quench

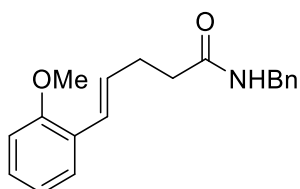
the $\text{Al}(\text{Me})_3$ and amine. After filter the aluminum gel, the liquid was extracted by DCM (3x 50 ml). Combine all the organic phase then concentrated *in vacuo*. The crude product was purified by flash chromatography with eluent (EtOAc: Hexane = 20 : 80).



Compound 18 : (E)-N-benzyl-7-phenylhept-4-enamide

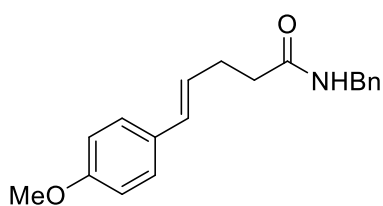
To a solution of BnNH_2 (2 equiv, 20 mmol, 1.82 mL) in DCM (40 mL) was slowly added trimethylaluminum (TMA) (1.62 equiv, 2.0 M in hexanes, 16.2 mmol, 8.1 mL) at room temperature. The reaction mixture was stirred at room temp for 1 h, and the corresponding ethyl ester ethyl (E)-7-phenylhept-4-enoate 10 mmol, 2.32 g) was added dropwise. The reaction mixture was heated overnight at 35 °C. After cooling to room temperature, the reaction mixture was quenched with aqueous HCl solution (1M) and extracted with DCM (3 x 40 mL). The combined organic extracts were dried over with anhyd. Na_2SO_4 and concentrated *in vacuo* to afford the crude product. Flash chromatography on silica gel (EtOAc: Hexane = 80:20-60:40) affords the title compound (2.08 g, 71%) as a white solid. Following GP1 with benzyl amine (2 equiv, 10 mmol, 1.1 mL) affords, after flash chromatography on silica gel (80:20- 60:40 hexanes:ethyl acetate), the title compound (1.15 g, 78%) as a white solid. TLC analysis $R_f = 0.4$ (EtOAc: Hexane = 40: 60); $^1\text{H NMR}$ (400 MHz, CDCl_3) δ 7.15–7.40 (10H, m), 5.89 (1H, br s), 5.40–5.60 (2H, m), 4.44 (2H, d, $J = 5.7$ Hz), 2.67 (2H, t, $J = 7.3$ Hz),

2.20–2.40 (6H, m); ^{13}C NMR (100 MHz, CDCl_3) δ 172.45, 142.04, 138.55, 131.03, 129.23, 128.80, 128.61, 128.38, 127.9, 127.60, 125.89, 43.66, 36.71, 35.96, 34.40, 28.73



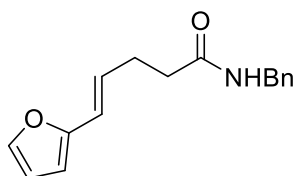
Compound 19 : (E)-N-benzyl-5-(2-methoxyphenyl)pent-4-enamide

General procedures C was followed. BnNH_2 (20 mmol, 1.82 mL) in DCM (40 mL) was slowly added trimethylaluminum (TMA) (2.0 M in hexanes, 16.2 mmol, 8.1 mL) at room temperature and stirred for 1 h. The corresponding ester 2.35 g (10 mmol) was injected dropwise then stirred overnight. After work-up the crude was purified by chromatography EtOAc: Hexane = 40: 60 $R_f=0.3$. isolated 2.07g 70% yield.



Compound 20 : E-N-(4-methoxyphenyl)-5-phenylpent-4-enamide Followed general procedure C. BnNH_2 (20 mmol, 1.82 mL) in DCM (40 mL) was slowly added trimethylaluminum (TMA) (2.0 M in hexanes, 16.2 mmol, 8.1 mL) at room temperature and stirred for 1 h. The corresponding ester 2.35 g (10 mmol) was injected dropwise then stirred overnight. After work-up the crude was purified by chromatography EtOAc:

Hexane = 40: 60 Rf=0.3. Isolated 2.07g 70% yield. ^1H NMR (300 MHz, CDCl_3) δ 7.57 – 7.34 (m, 2H), 7.31 – 7.21 (m, 2H), 7.14 – 7.10 (m, 2H), 7.08 – 7.00 (m, 1H), 6.81 – 6.71 (m, 2H), 6.33 (d, $J = 15.9$ Hz, 1H), 6.23 (s, 1H), 6.11 (dt, $J = 15.8, 6.7$ Hz, 1H), 3.26 (s, 3H), 2.56 – 2.32 (m, 2H), 1.91 (t, $J = 7.4$ Hz, 2H).; ^{13}C NMR (300 MHz, CDCl_3) δ 169.28, 156.62, 137.96, 132.10, 131.42, 129.26, 128.85, 127.41, 126.48, 121.45, 114.34, 54.96, 36.93, 29.11.; Data are consistent with literature values. [75]

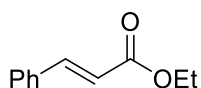


Compound 21 : (E)-N-benzyl-5-(furan-2-yl)pent-4-enamide

Dissolve the corresponding acid compound 17 166 mg (1 mmol) in dry DCM (0.5 M), cool the reaction mixture to 0 °C then slowly inject 2 equiv of Oxalyl chloride 0.17 ml and 3 drops of DMF. Stir 30 min then remove the solvent under reduced pressure. After that, add 1.5 eq of BnNH_2 0.164 ml in 20 ml DCM and 2 equiv of Et_3N . Stir another 2h then quenched with 1 M bicarbonate solution. The crude product was subjected to flash chromatography on silica gel (EtOAc: Hexane= 40: 60, Rf = 0.4) to afford the title compound (184 mg, 73%) as a light yellow oil; ^1H NMR (400 MHz, CDCl_3) δ 7.15–7.41 (10H, m), 6.02 (1H, br s), 5.44–5.55 (1H, m), 5.34–5.45 (1H, m), 4.42 (2H, d, $J = 5.7$ Hz), 2.68 (2H, t, $J = 7.8$ Hz), 2.43 (2H, q, $J = 7.4$ Hz), 2.32 (2H, q, $J = 7.4$ Hz), 2.07 (2H, t, $J = 8.6$ Hz); ^{13}C NMR (100 MHz, CDCl_3) δ 172.52, 142.1, 138.56, 130.29, 128.81,

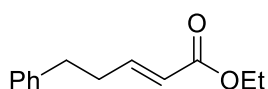
128.77, 128.43, 127.91, 127.55, 125.91, 43.66, 36.52, 35.92, 29.28, 23.62.

5.2 Procedures for preparing pre-chiral installed γ,δ -unsaturated amide



Compound 22 : ethyl cinnamate

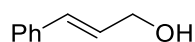
Horner emmons reaction. Followed the procedure in compound 23. LiCl anhydrous (0.9 g, 21.0 mmol) in dry CH₃CN (25 mL), ethyl diethylphosphonoacetate (3.9 mL, 19.5 mmol) and DBU (2.7 mL, 18.0 mmol) at 0 °C. 30 min later add phenyl aldehyde 1.95 g (15 mmol) into the reaction mixture. After workup and purification, the product was isolated 2.4 g for 90% yield as colorless yield. ¹H NMR (400 MHz, CDCl₃) δ 7.70 (d, J = 16.0 Hz, 1H), 7.55-7.53 (m, 2H), 7.43-7.37 (m, 3H), 6.47 (d, J = 16.0 Hz, 1H), 4.28 (q, J = 6.8 Hz, 2H), 1.38 (t, J = 6.8 Hz, 3H). ¹³C NMR (300 MHz, CDCl₃) δ 166.91, 144.6, 134.5, 130.2, 128.9, 128.1, 118.1, 60.3, 14.4.



Compound 23: ethyl (E)-5-phenylpent-2-enoate

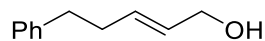
To a solution of LiCl anhydrous (0.9 g, 21.0 mmol) in dry CH₃CN (25 mL) were added ethyl diethylphosphonoacetate (3.9 mL, 19.5 mmol) and DBU (2.7 mL, 18.0 mmol) at 0 °C and the mixture was stirred for 30 min at that temperature until the LiCl was

completely dissolved. Hydrocinnamaldehyde (2.0 mL, 15.0 mmol) was slowly added into reaction mixture then allowed to warm to room temperature and stirred for 2 h. The reaction was quenched with saturated aqueous NaHCO₃, and the aqueous phase was extracted with EtOAc (3 x 25 ml). The combined organic phase was washed with brine, dried over anhydrous Na₂SO₄ and evaporated in reduced pressure. The crude was purified by silica gel column chromatography (EtOAc : Hexane = 5:95, R_f= 0.8) to afford title compound (2.7 g, 13.5 mmol, 88%) as a colorless oil. ¹H NMR (400 MHz, CDCl₃) 7.37-7.16 (m, 5H), 7.02 (dt, *J* = 15.6, 6.8 Hz, 1H), 5.89 (dt, *J* = 15.7, 1.6 Hz, 1H), 4.20 (q, *J* = 7.1 Hz, 2H), 2.85-2.77 (m, 2H), 2.58-2.51 (m, 2H), 1.30 (t, *J* = 7.1 Hz, 3H). Data are consistent with literature values.^[76]



Compound 24: (E)-3-phenylprop-2-en-1-ol

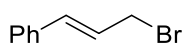
The product was prepared according to general procedure compound 25, 862 mg (4.9 mmol) ester was used. After column chromatography, the title product was isolate as colorless oil 510 mg 81% yield.



Compound 25: (E)-5-phenylpent-2-en-1-ol

To a solution of compound 23 (1.00 g, 4.90 mmol) in DCM (40 mL), DIBAL (8.2 mL, 1.5 M in toluene) was added dropwise at -78 °C and the resultant solution was stirred for 4 h. The reaction was quenched with MeOH (20 mL) and the mixture poured onto

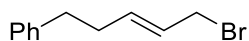
Rochelle salt (Potassium sodium tartrate tetrahydrate) or 1 M NaOH aqueous solution (75 mL). The phases were separated and the aqueous phase was extracted with DCM (3 x 50 mL). The combined organic phases were washed with H₂O (2 x 100 mL), dried (Na₂SO₄) and concentrated *in vacuo*. Flash chromatography (EtOAc: Hexane= 20: 80, R_f= 0.4) of the residue afford compound 25 (665 mg, 86%) as a colorless oil. ¹H NMR (400 MHz, CDCl₃) 7.35-7.27 (m, 3H), 7.24-7.20 (m, 2H), 5.80-5.65 (m, 2H), 4.10 (t, *J*= 5.5 Hz, 2H), 2.80-2.71 (m, 2H), 2.40 (dd, *J* = 14.5, 6.7 Hz, 2H), 1.23 (t, *J* = 5.8 Hz, 1H). Data are consistent with literature values.^[77]



Compound 26: (E)-(3-bromoprop-1-en-1-yl)benzene

Cinnamyl bromide. To an oven dried RBF was added cinnamyl alcohol (6.0 g, 0.045 mol) and PBr₃ 0.8 equiv at 0 °C and the reaction mixture was warmed to room temperature and stirred for 3 hours. The reaction was quenched with saturated NaHCO₃ and extracted with EtOAc (2 x 50 mL). The organic phase was separated, dried over NaSO₄ and the solvent was evaporated *in vacuo* to obtain the brown solid (8.5 g, 96%)

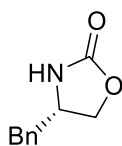
¹H NMR (400 MHz, CDCl₃) 7.34-7.23 (m, 5H), 6.59 (d, 1H), 6.34 (m, 1H), 4.11 (d, 2H)



Compound 27: (E)-(5-bromopent-3-en-1-yl)benzene

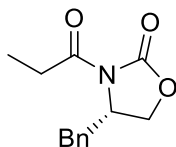
Preparation of (E)-(5-bromopent-3-en-1-yl)benzene. Same procedure as previous

molecule. To a cooled (0 °C) solution of allylic alcohol compound 25 (2.5 g, 15.4 mmol) in Et₂O (25 mL) was added phosphorous tribromide (0.73 mL, 0.5 equiv, 7.7 mmol). The resultant mixture was stirred at 0 °C for 1 h and quenched with saturated brine solution. The layers were separated and the aqueous layer was extracted with Et₂O (3 x 20 mL). The combined organic layers were dried over anhydrous Na₂SO₄ and concentrated *in vacuo* to afford the title compound (3.3 g, 95%) as yellow liquid: ¹H NMR (300 MHz, CDCl₃) δ 7.41–7.30 (2H, m), 7.31–7.20 (3H, m), 5.91–5.70 (2H, m), 3.98 (2H, d, *J* = 6.8 Hz), 2.74 (2H, t, *J* = 7.3 Hz), 2.51–2.40 (2H, m); ¹³C NMR (300 MHz, CDCl₃) δ 141.35, 135.48, 128.45, 128.41, 127.02, 126.02, 35.23, 33.81, 33.35



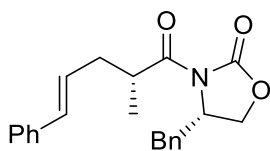
Compound 28: 2-Phenyl-oxazolidinone

To a 50ml RBF, a mixture of L-phenyl alanine 3.17g (21 mmol) and diethyl carbonate 5.1ml, anhydrous KCO₃ 100mg was added. The mixture was stirred at 120°C for 3h. After cooling to r.t, the reaction was quenched by 2 times volume amount of 1M HCl aqueous solution. Extracted by EA 50ml, 3 times. The organic layers were combined and washed by brine. After solvent evaporation under reduced pressure, the product was formed as white solid. ¹H NMR (CDCl₃): δ 7.33 (t, 3H), 7.26(t, 1H), 7.15(d,2H), 5.38(broad, 1H) 4.43(t, 1H), 4.14 (dd, 1H), 4.06 (m, 1H), 2.86 (d, 2H);



Compound 29: (S)-4-benzyl-3-propionyloxazolidin-2-one

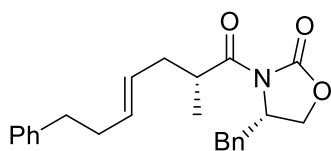
To a solution of compound 29 (S)-4-benzyloxazolidin-2-one (2.1 g, 11.8 mmol) in THF (20 mL) was added dropwise a solution of 2.0 M n-BuLi (6.6 mL, 13.2 mmol) at -78 °C under N₂ over 10 min. After 10 min of stirring, propionyl chloride (1.63 g, 17.05 mmol) was added. The reaction was stirred for 30 min at -78 °C and then allowed to warm to room temperature. After 30 min, the reaction was quenched with saturated aqueous NH₄Cl, and the mixture was extracted with DCM (3 x 25 ml). The organic extract was washed with aq. 1M NaOH solution, dried over Na₂SO₄ and concentrated *in vacuo*. The residue was purified by column chromatography (EtOAc : Hexane= 20: 80) to afford product as a white solid (2.74 g, 99%): ¹H NMR (400 MHz, CDCl₃) δ 7.35-7.20 (m, 5H), 4.70-4.63 (m, 1H), 4.22-4.30 (m, 2H), 3.29 (dd, *J* = 13.4, 3.0 Hz, 1H), 3.04-2.86 (m, 2H), 2.76 (dd, *J* = 13.3, 9.6 Hz, 1H), 1.21 (t, *J* = 7.3 Hz, 3H); ¹³C NMR (300 MHz, CDCl₃) δ 174.1, 153.3, 135.3, 129.4, 128.9, 127.1, 66.1, 55.2, 37.8, 29.2, 8.2.



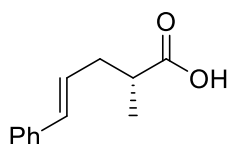
Compound 30: (S)-4-benzyl-3-((R,E)-2-methyl-5-phenylpent-4-enoyl)oxazolidin-2-one

The Evans auxiliary group (compound 29) (2g, 8.56 mmol) is dissolved in THF (200

ml) and cooled to -78°C . NaHMDS (2 M in THF, 12.84mmol, 6.42 ml) is added over a period of 15 min and the solution is stirred for 1 h. The bromide (compound 26) 2 equiv 3.36 g (17.12 mmol) is added slowly and the solution is stirred for 16 hours. After addition of saturated NaHCO_3 solution, the aqueous layer is extracted by DCM (3 x 50 ml). Washed with saturated NaHCO_3 , brine, dried over Na_2SO_4 . Filtered and the organic solvents are removed under the reduced pressure. The crude is purified by column chromatography to afford α -Me product.



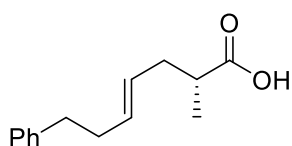
Compound 31: (S)-4-benzyl-3-((R,E)-2-methyl-7-phenylhept-4-enoyl)oxazolidin-2-one Same procedure was used above. The Evans auxiliary group (compound 29) (1g, 4.28 mmol) is dissolved in THF (100 ml) and cooled to -78°C . NaHMDS (2 M in THF, 6.42mmol, 3.21 ml) is added over a period of 15 min and the solution is stirred for 1 h. The bromide (compound 27) 2 equiv 1.92 g (8.56 mmol) is added slowly and the solution is stirred for 16 hours.



Compound 32: (R,E)-2-methyl-5-phenylpent-4-enoic acid

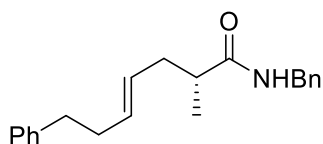
Compound 30 (663 mg, 1.9 mmol), in THF (27 mL) and water (9 mL), was stirred with

aqueous H₂O₂ (30%, 1.4 mL) and lithium hydroxide hydrate (150 mg, 3.8 mmol) at r.t. for 3 h. The reaction was quenched by addition of aqueous sodium sulfite (1.5 M, 13 mL, 20 mmol). The mixture was acidified with aqueous HCl (1.0 M) to pH 1 and extracted thrice with dichloromethane. Drying, evaporation and chromatography (EtOAc: Hexane = 45:55 R_f=0.3) gave title compound 32 (320 mg, 91%) as a colorless oil



Compound 33: (R,E)-2-methyl-7-phenylhept-4-enoic acid

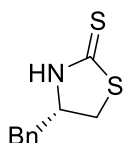
Same procedures. Compound 31 (763 mg, 1.9 mmol), in THF (27 mL) and water (9 mL), was stirred with aqueous H₂O₂ (30%, 1.4 mL) and lithium hydroxide hydrate (150 mg, 3.8 mmol) at r.t. for 3 h. After workup, the titled compound was isolated 352 mg 85% yield.



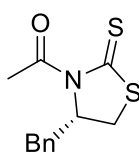
Compound 34: (R,E)-N-benzyl-2-methyl-5-phenylpent-4-enamide

Dissolve the corresponding acid compound 33, 218 mg (1 mmol) in dry DCM (0.5 M), cool the reaction mixture to 0 °C then slowly inject 2 equiv of Oxalyl chloride 0.17 ml

and 3 drops of DMF. Stir 30 min then remove the solvent under reduced pressure. After that, add 1.5 eq of BnNH₂ 0.164 ml in 20 ml DCM and 2 equiv of Et₃N. Stir another 2h then quenched with 1 M bicarbonate solution. The crude product was subjected to flash chromatography on silica gel (EtOAc: Hexane= 40: 60, R_f = 0.4) to afford the title compound (260 mg, 85%) as a white solid.

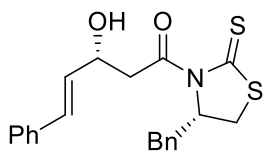


Compound 35: (S)-4-benzylthiazolidine-2-thione. L-phenyl alanine 6 g (0.04 mol) was suspended in aqueous KOH (2M, 100 ml). Carbon disulfide (7.6 ml, 0.2 mol) was added to the suspension then heat the mixture to reflux for 14 h. The suspension turned into bright orange and was allowed to cool to room temperature. The reaction mixture was extracted with DCM 100 ml x 3. The organic layers were combined and dried over Na₂SO₄ then concentrated by rotavapor to afford the crude as white solid. Recrystallization by EtOH afforded 5.8g of the title compound as white crystal. ¹H NMR (300 MHz, CDCl₃) δ 7.38-7.19 (m, 5H), 4.50-4.42 (m, 1H), 3.59 (dd, J=11.2, 7.7 Hz, 1H), 3.31 (dd, J = 11.2, 6.8 Hz, 1H) 3.05 (dd, J =13.5, 7.6 Hz, 1H), 2.97 (dd, J = 13.5, 6.6 Hz, 1H); ¹³C NMR δ 200.7, 135.7, 129.1, 128.8, 127.4, 65.0, 40.0, 38.2.



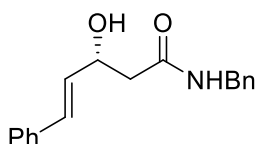
Compound 36: (S)-1-(4-benzyl-2-thioxothiazolidin-3-yl) ethan-1-one

Compound (S)-4-benzylthiazolidine-2-thione 3g (14 mmol), DMAP (0.176 g) and Et₃N 1eq 14 mmol (2 ml) were dissolved in DCM 40ml. N₂ condition. The mixture was stirred and cooled to 0 °C. Acetyl chloride was added dropwise to the cooled stirred solution and the resulting yellow solution was allowed to reach the r.t. The mixture was allowed to stir at r.t for 14 h, then quenched with saturated aqueous NH₄Cl 10 ml and diluted with Et₂O (100ml). The organic layers were combined and washed with saturated CuSO₄ aqueous solution (35 ml x 3), water 35 ml and brine 35 ml. Then dried over Na₂SO₄ and concentrated *in vacuo* to afford the crude product as brown solid. The Crude product was recrystallized from EtOH to afford the yellow needles crystal. For column chromatography, use 5% - 10% EA with hexane. 30% EA with hexane for developing solvent. R_f = 0.6. ¹H NMR (700 MHz, CDCl₃) δ 7.38-7.25 (m, 5H), 5.37 (dddd, *J* = 10.6, 6.7, 3.9, 0.4 Hz, 1H), 3.39 (ddd, *J* = 11.5, 7.2, 1.2 Hz, 1H), 3.22 (dd, *J* = 13.2, 3.8 Hz, 1H), 3.04 (dd, *J* = 13.3, 10.5 Hz, 1H), 2.89 (dd, *J* = 11.5, 0.4 Hz, 1H), 2.80 (s, 3H); ¹³C NMR (300 MHz, CDCl₃) δ 201.6, 170.6, 136.4, 129.4, 128.9, 127.1, 68.2, 35.6, 31.7, 27.0.



Compound 37: (R,E)-1-((S)-4-benzyl-2-thioxothiazolidin-3-yl)-3-hydroxy-5-phenylpent-4-en-1-one

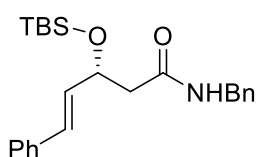
To a dry 25 ml RBF under N₂ atmosphere, add (S)-1-(4-benzyl-2-thioxothiazolidin-3-yl) ethan-1-one 380 mg (1.52 mmol), dissolved in dry DCM 3 ml. the solution was cooled to 0 °C and TiCl₄ was added dropwise (0.199 ml, 1.82 mmol). The thick suspension was stirred for 10 min at 0 °C, then the DIPEA (diisopropylethyl amine) 0.311 ml, 1.82 mmol was added dropwise. Then the solution was stirred at same temperature for another 10 min. Cool the solution to -78 °C, then add the freshly distilled cinnamaldehyde 0.2 g in dry DMC 1.5 ml. The reaction was stirred at this temperature for 1 h then allow it to reach the room temperature. The reaction mixture was quenched with saturated ammonium chloride. Separate the layers, the aqueous layer was extracted by DCM (5 ml x 3). Combine all the organic layers and dry over with anhydrous Na₂SO₄ for 30 min. Then filter the DCM solution and concentrated *in vacuo* to afford the orange color oil crude product. Based on ¹H NMR spectrum, the d.r. in the crude is 85: 15. The crude was purified by column chromatography. TLC developing solvent EtOAc: Hexane = 3:7. Starting material R_f= 0.6. Minor diastereomer R_f= 0.5, major diastereomer R_f= 0.4. Use 5% EtOAc hexane mixture as an eluent to flash starting material. Slowly added to 10% of EtOAc hexane mixture as eluent to provide the minor and major diastereomers product. The products are yellow liquid. ¹H NMR (300 MHz, CDCl₃) : δ 7.40- 7.17 (m, 10H), 6.67 (d, *J*=16.0 Hz, 1H), 6.25 (dd, *j*=16.0, 5.8 Hz, 1H) 5.43-5.34 (m, 1H,) 4.88-4.80 (m, 1H), 3.72 (dd, *J*=3.0, 17.6 Hz, 1H), 3.41 (dd, *J*= 17.5, 8.4 Hz, 1H) 3.38 (d, *J*= 10.9 Hz, 1H).



Compound 38: (R,E)-N-benzyl-3-hydroxy-5-phenylpent-4-enamide

The transamidation procedure was based on a similar reaction published in 1981.^[78]

The substrate that contained thiazolidinone 500 mg (1.31 mmol) was dissolved in 2.6 ml THF to form a 0.5 M solution. The amine 1eq was added to the solution and stirred at 15 °C for 10 min then poured into 1% sodium bicarbonate solution 50 ml. All precipitations were collected after 30 min stirring. Dry the crude to afford the yellow solid. The crude can be purified by flash chromatography. EtOAc: Hexane = 50% : 50%. The top spot on TLC was replaced thiazolidinone and the polar product was washed out later. Isolated 222 mg, 60% yield. HPLC condition: IC column, iPr : Hexane = 40 : 60. Pressure : 300 Psi. Retention time: minor diastereomer 22 min, major diastereomer 27 min.



Compound 39 : (R,E)-N-benzyl-3-((tert-butyldimethylsilyl)oxy)-5-phenylpent-4-enamide

The β -OH γ,δ -unsaturated amide 222 mg (0.79 mmol) was dissolved in DCM to 0.25 M. TBSCl 238 mg (1.58 mmol) and 162 mg imidazole (2.37 mmol) were slowly added in to solution at room temperature under N₂ atmosphere followed with DMAP 5 mg.

The reaction mixture was stirred overnight and quenched by saturated NH_4Cl . The crude was extracted by DCM 3 x 20 ml. combine the organic phase and concentrate *in vacuo*. A flash column chromatography was performed to purify the crude with 15% to 30% of EtOAc and Hexane mixture. TLC analysis developing solvent is 50% EtOAc and Hexane. The product isolated is white solid.

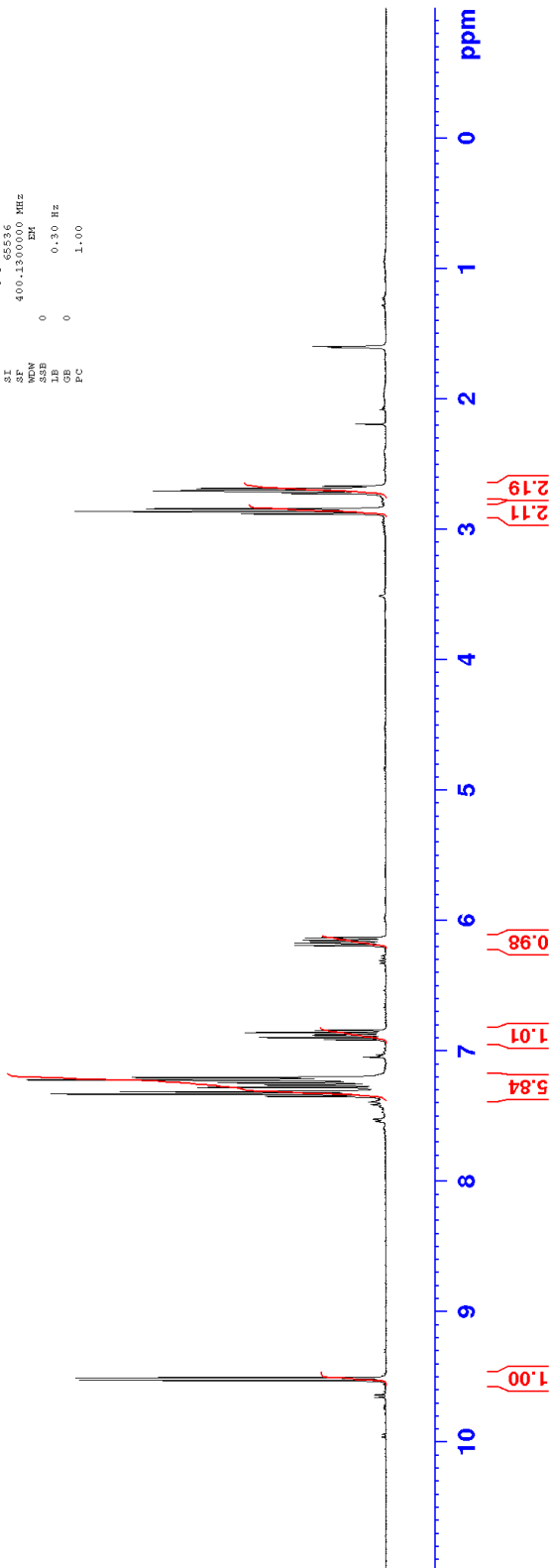
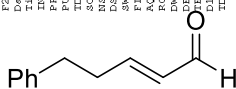


2.883
2.865
2.845
2.727
2.726
2.708
2.691
2.689
2.672

7.335
7.316
7.228
7.225
7.208
6.918
6.901
6.885
6.879
6.862
6.846
6.195
6.175
6.156
6.136

9.530
9.511

Current Data Parameters
 NAME s2-20160221-phenethyl-a,b,aldehyde
 EXPNO 3
 PROCNO 1
 F2 - Acquisition Parameters
 Date_ 20160221
 Time 17:09
 INSTRUM spect
 PROBHD 5 mm PABBO BE/
 PULPROG zg30
 TD 65536
 SFO1 400.1324710 MHz
 CH1 1H
 DS 2
 SSF 8012.820 Hz
 AQ 4.0829485 sec
 RG 103.57
 DM 62.400 usec
 DE 288.2 K
 FE 1.00000000 sec
 TD0 1
 ===== CHANNEL f1 =====
 SFO1 400.1324710 MHz
 NUC1 1H
 P1 12.00 usec
 P1M1 16.00000000 W
 F2 - Processing Parameters
 SI 32768
 SF 400.1300000 MHz
 WEN 0 EX
 SSB 0
 GB 0
 PC 0 1.00



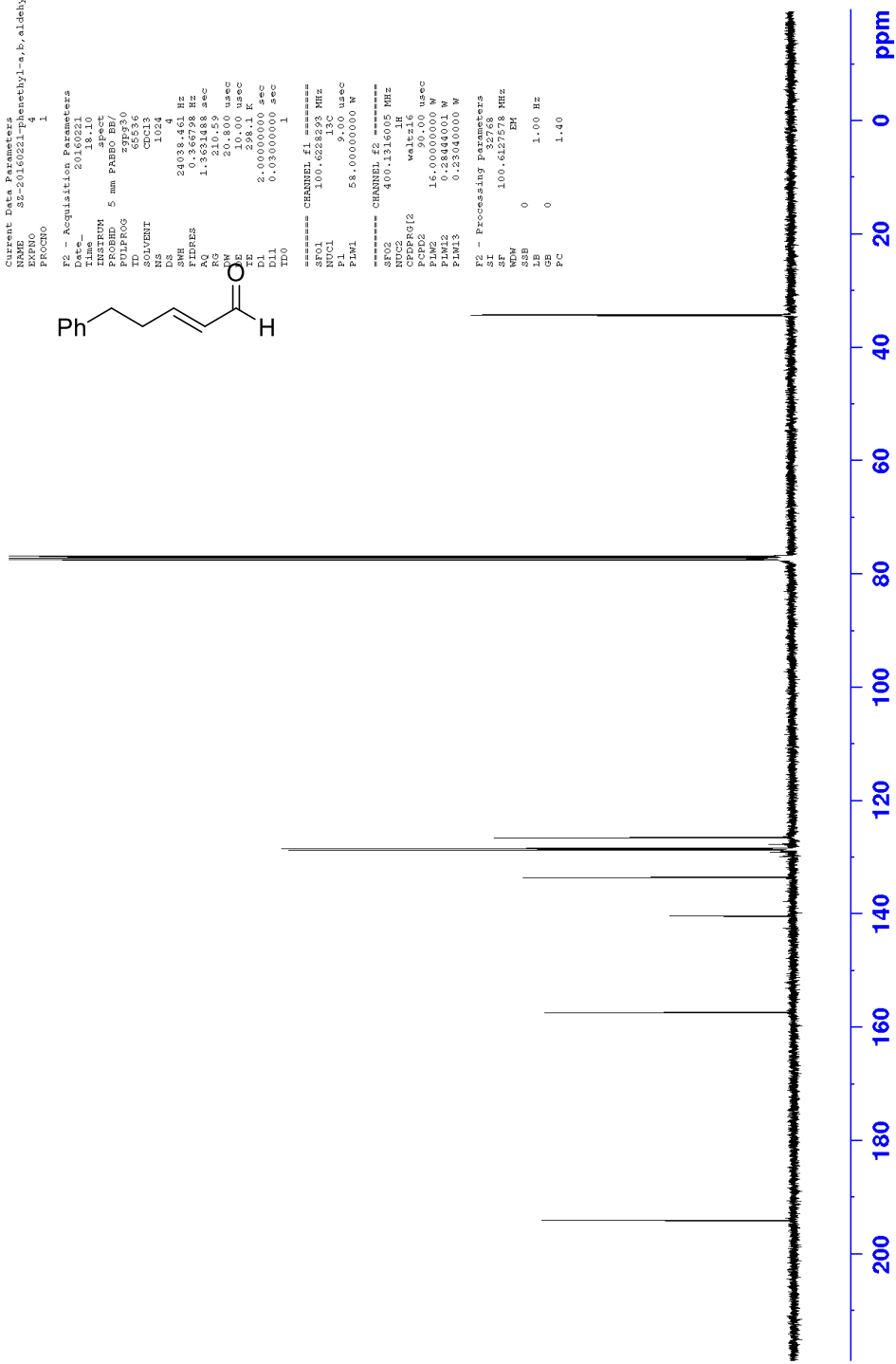
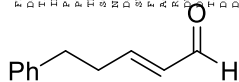


Current Data Parameters
 NAME: 32-20160221-phenethyl-a,b,aldehyde
 PROCNO: 1

F2 - Acquisition Parameters
 Date_ 20161110
 Time_ 10:10
 INSTRUM spect
 PROBRD 5 mm PABBO BE/
 PULPROG zgpg30
 SOLVENT CDCl3
 NS 1024
 DS 4
 SS 24038.41 Hz
 FIDRES 0.386738 Hz
 AQA 1.363148 sec
 RG 210.59
 EQ 10.00 usec
 DE 10.00 usec
 TE 298.1 K
 D1 2.00000000 sec
 D11 0.05000000 sec
 D10 1.1

===== CHANNEL f1 =====
 SFO1 100.626183 MHz
 NUC1 13C
 P1 5.00 usec
 PLW1 58.00000000 W
 ===== CHANNEL f2 =====
 SFO2 400.1316005 MHz
 NUC2 1H
 P2 16.00000000 usec
 PLW2 16.00000000 W
 PLM12 0.2844001 W
 PLM13 0.23040000 W
 F2 - Processing Parameters
 SI 32768
 SF 100.6127578 MHz
 WH 2048
 SSB 0
 LB 1.00 Hz
 GB 0
 PC 1.40

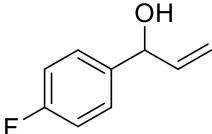
194.06
 157.39
 140.38
 133.52
 126.50
 34.20
 34.35



200 180 160 140 120 100 80 60 40 20 0 ppm

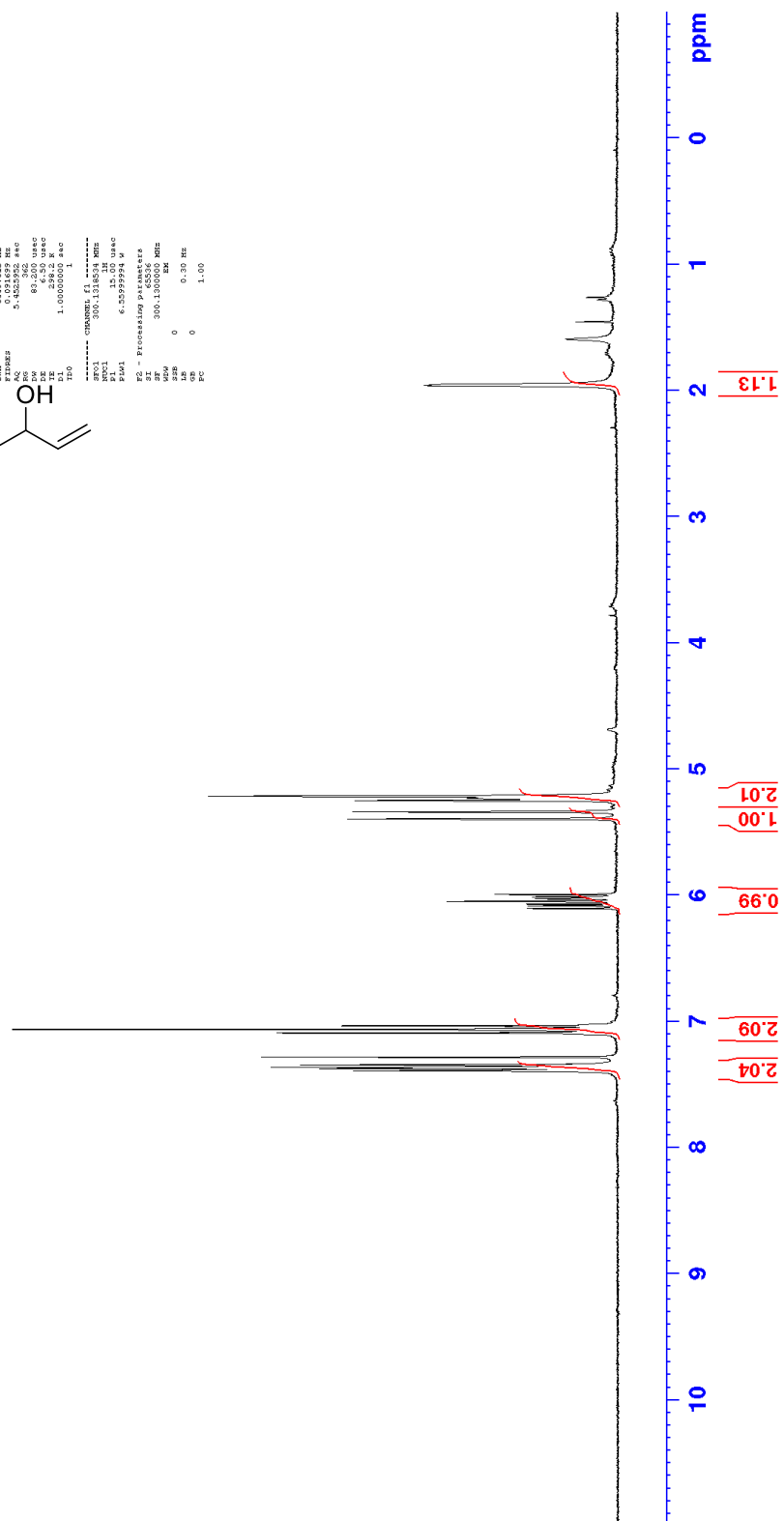


NAME: 4-Fluorobenzyl alcohol
 EXPNO: 1
 PROCNO: 1
 F2 - Acquisition Parameters
 Date_UTC: 20140608
 Time: 11:54:33
 INSTRUM: spect
 PROBRD: 3 mm PASPO 500
 TD: 65536
 ID: 45526
 NS: 2048
 DS: 4
 SWH: 6000.432 MHz
 FIDRES: 0.0014699 MHz
 AQ: 0.14366440 sec
 SFO: 500.1300000 MHz
 P1: 12.00
 PL1: 0.00
 PC: 1.00000000 sec
 TD0: 1



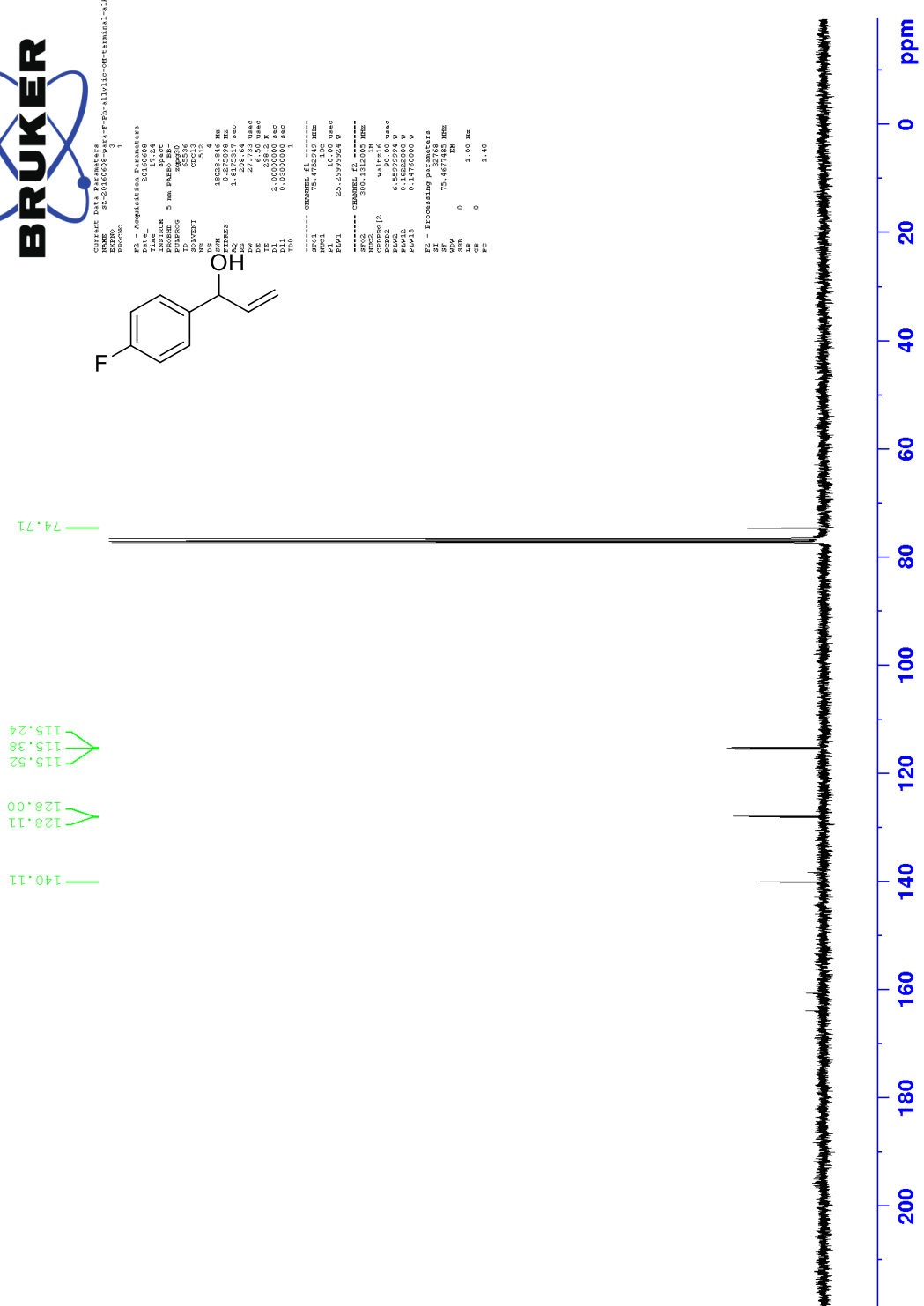
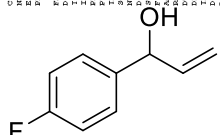
7.395
7.376
7.366
7.347
7.284
7.094
7.036
6.106
6.086
6.073
6.051
6.030
6.015
5.995
5.397
5.340
5.252

===== CHANNEL f1 =====
 NUCL1: 13C
 PULPROG: zgpg30
 FREQ1: 101.325131 MHz
 P1: 12.00
 PL1: 0.00
 PC: 1.00000000 sec
 =====
 F2 - Processing parameters
 SI: 65536
 SF: 500.1300000 MHz
 DS: 4
 SWH: 6000.432 MHz
 FIDRES: 0.0014699 MHz
 AQ: 0.14366440 sec
 SFO: 500.1300000 MHz
 P1: 12.00
 PL1: 0.00
 PC: 1.00



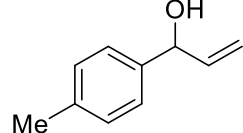


CURRENT DATA PARAMETERS
 NAME: 25-20160009-9147-99-4131-001-001-011-001
 PROCNO: 1
 F2 - Acquisition Parameters
 Date_ 20160804
 Time_ 17:04
 INSTRUM spect
 PROBRW 5 mm WBH500
 PULPROG zgpg30
 PROCNO 1
 SOLVENT CDCl3
 NS 512
 DS 4
 SWH 18028.846 MHz
 FIDRES 0.000100000 Hz
 AQ 1.9175217 sec
 RG 327.500
 DM 27.733 uMm
 DE 6.50 uMm
 E1 2.000000000 sec
 E2 0.100000000 sec
 TD 1
 ----- CHANNEL f1 -----
 RF01 75.4752849 MHz
 P1 10.00 uMm
 PL1 25.2979764 W
 FREQ1 75.4752849 MHz
 ----- CHANNEL f2 -----
 RF02 400.146303 MHz
 P2 0.50 uMm
 PL2 0.1822200 W
 FREQ2 400.146303 MHz
 ----- Processing parameters -----
 SI 0
 SF 75.477482 MHz
 GB 0
 LB 0 1.00 Hz
 GB 0 1.40





Current Data Parameters
 Name: 08-20180814 F1 Me-Pt-tert-allylic-OH
 EXPNO: 1
 PROCNO: 1



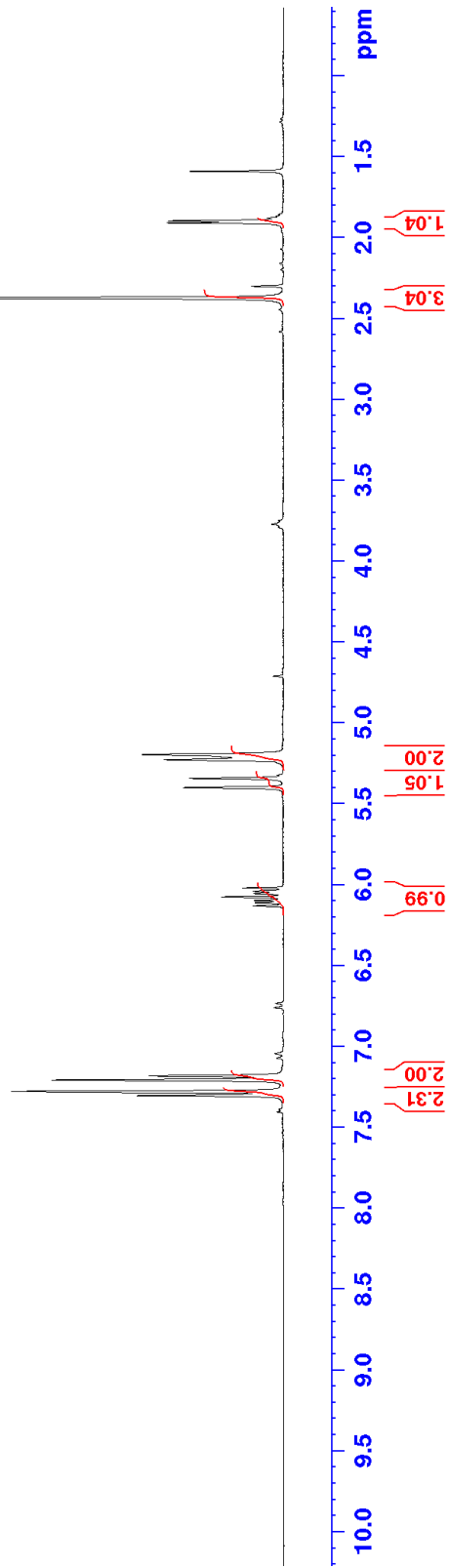
F2 - Acquisition Parameters
 Date_ 01060614
 Time 17:02
 Processor 64
 PROBNM 5 mm HAMB3
 PULPROG zgpg30
 ID 65536
 SOLVENT CDCl3
 NS 2
 DS 2
 SMH 500.615 Hz
 AQ 0.050000 sec
 FIDRES 51422592 Hz
 RG 406
 SFO1 83.200 usec
 SF 300.135000 MHz
 T1 298.0 usec
 D1 1.10000000 sec
 TD0 1

===== CHANNEL f1 =====
 SFO1 300.1318534 MHz
 NUC1 1H
 P1 15.00 usec
 PL1 6.45599994 W

F2 - Processing Parameters
 SI 32768
 SF 300.1300000 MHz
 MDW 0 EM
 SSB 0
 GB 0
 PC 1.00

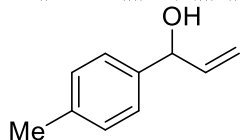
6.132
6.112
6.098
6.076
6.055
6.041
6.021
5.401
5.343
5.228
5.196

7.305
7.182





Current Data Parameters
 RMBO_032-20160614 P-Me-Ph-term-allylic-OH
 PROCNO 1



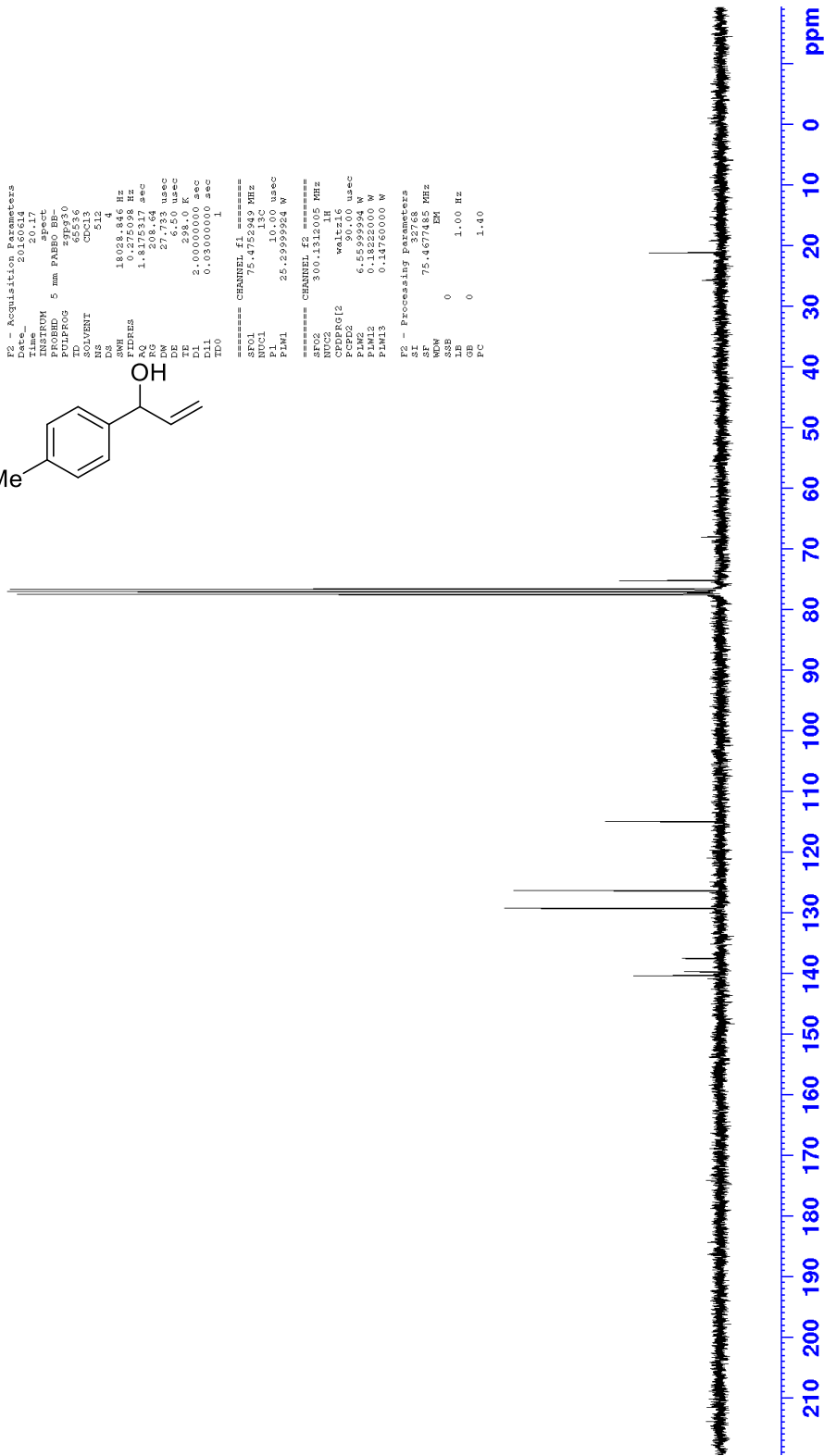
F2 - Acquisition Parameters
 Exp 20.17
 Time 20.17
 INSTRUM spect
 PROBED 5 mm PABBO EB-
 PULPROG zgpg30
 TD 65536
 SOLVENT CDCl3
 NS 512
 DS 4
 SWH 18038.846 Hz
 FIDRES 0.275098 Hz
 AQ 1.8178754 sec
 RG 327.733
 DW 27.733 usec
 DE 6.50 usec
 DI 2.0000000 K
 D1 0.0300000 sec
 D11 0.0300000 sec
 TD0 1

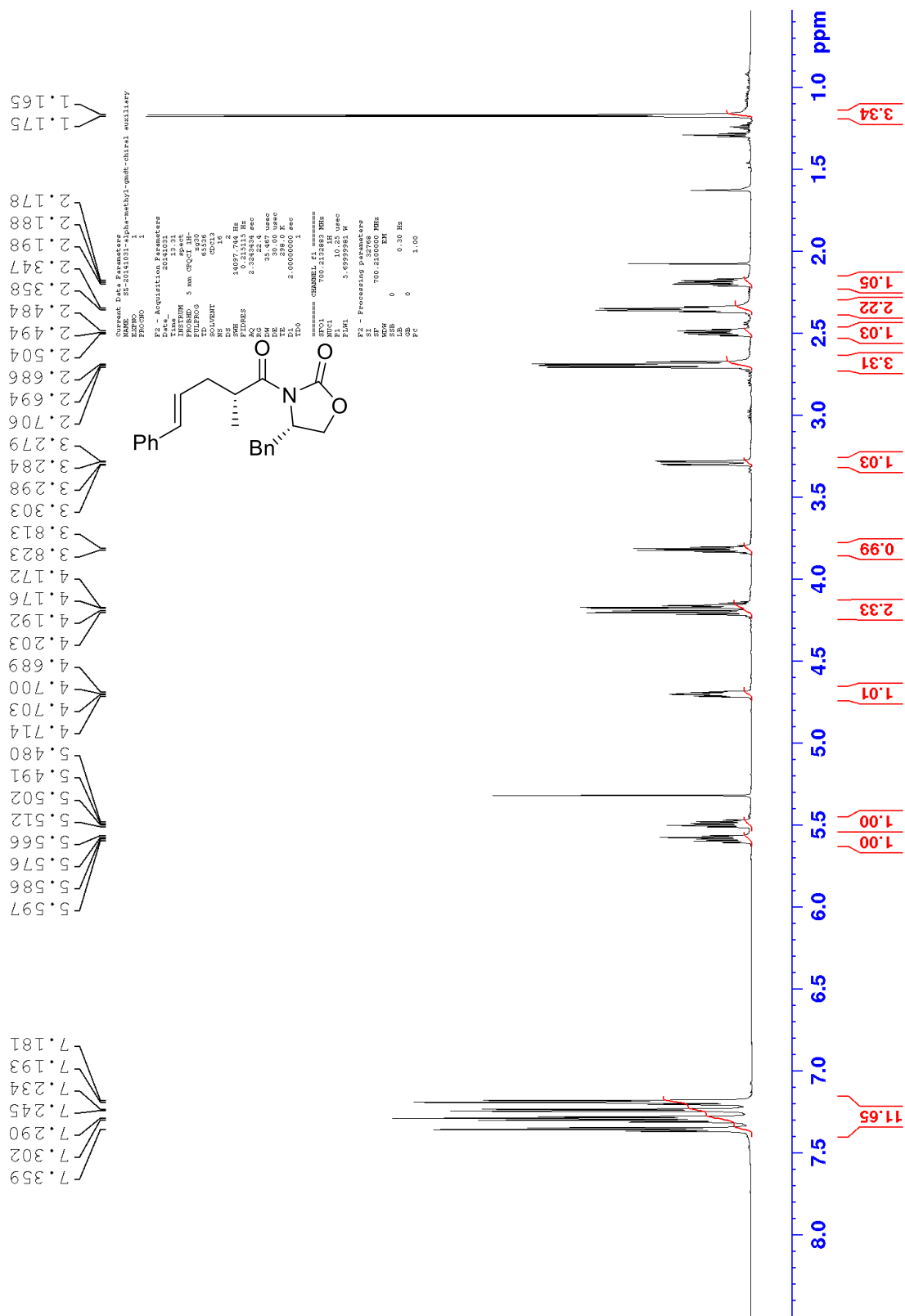
***** CHANNEL f1 *****
 SF01 75.4752849 MHz
 NUCL1 13C
 P1M1 25.2395924 W

***** CHANNEL f2 *****
 SF02 300.1320000 MHz
 NUCL2 1H
 P1M2 0.0000000 W
 P1M3 0.14760000 W

F2 - Processing Parameters
 SI 32768
 SF 75.4677485 MHz
 WDW EM
 LB 0 1.00 Hz
 GB 0 1.40
 PC

140.35
 139.71
 137.53
 129.27
 126.30
 114.90
 75.22





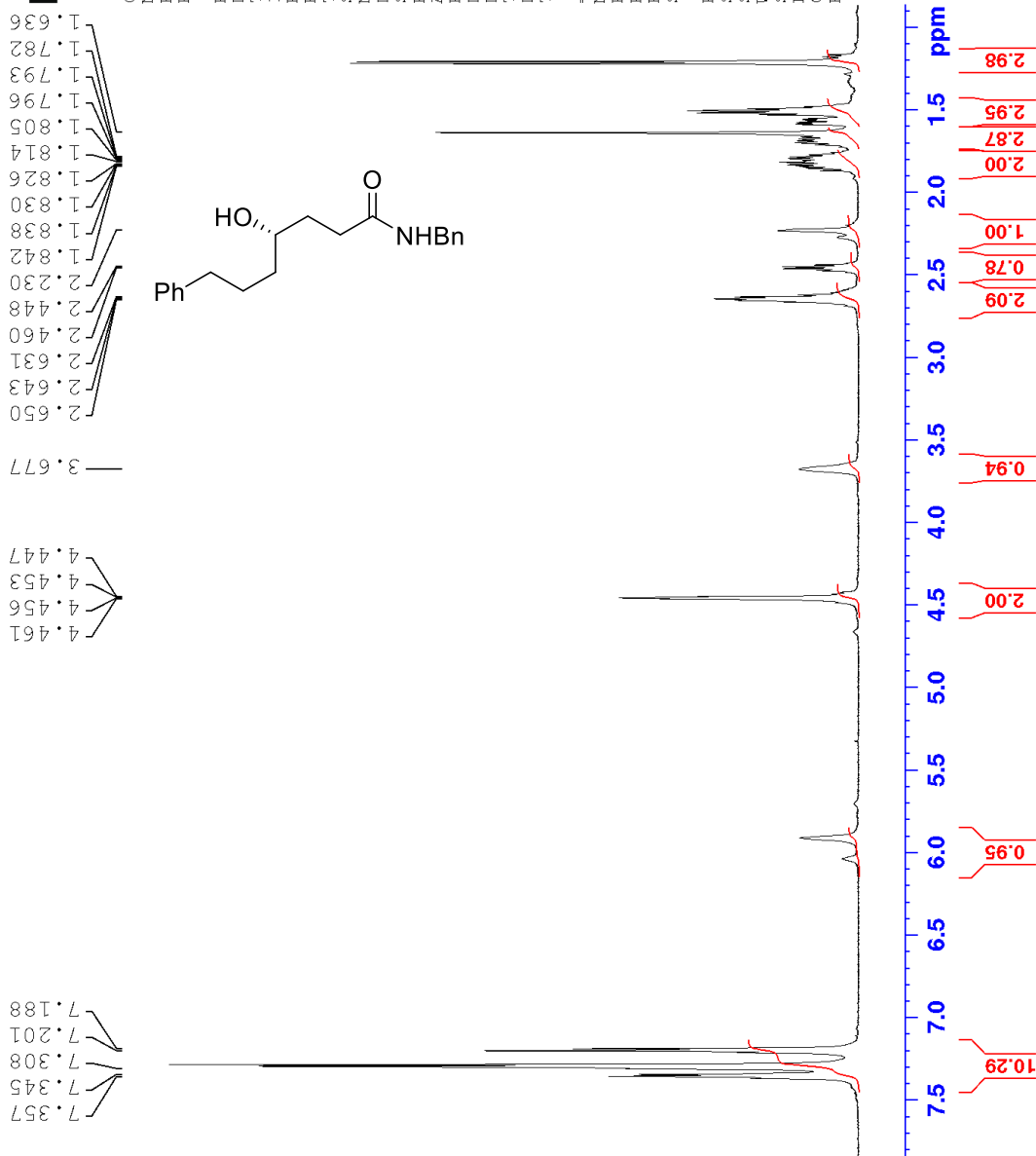
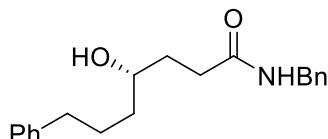


Current Data Parameters
 NAME SZ-20150701-Phe-OH
 EXPNO 2
 PROCNO 1

F2 - Acquisition Parameters
 Date_ 20150701
 Time 18.26
 INSTRUM spect
 PROBD 5 mm Multinucl
 PULPROG zg30
 TD 65536
 SOLVENT CDCl3
 NS 16
 DS 2
 SWH 12376.237 Hz
 FIDRES 0.188846 Hz
 AQ 2.6476543 sec
 RG 645.1
 DW 40.400 usec
 DE 6.50 usec
 TE 296.7 K
 D1 1.00000000 sec
 TDO 1

===== CHANNEL f1 =====
 NUC1 1H
 P1 11.20 usec
 PL1 -2.00 dB
 PLLW 59.71607590 W
 SFO1 600.1637062 MHz
 F2 - Processing parameters
 SI 32768
 SF 600.1600000 MHz
 WDW EM
 SSB 0
 LB 0.30 Hz
 GB 0
 PC 1.00

7.357
7.345
7.308
7.201
7.188
 4.461
4.456
4.453
4.447
 3.677
 2.650
2.643
2.631
2.460
2.448
2.230
 1.830
1.838
1.842
1.830
1.826
1.814
1.805
1.796
1.793
1.782
1.636



7.5 7.0 6.5 6.0 5.5 5.0 4.5 4.0 3.5 3.0 2.5 2.0 1.5 1.0 0.5 ppm

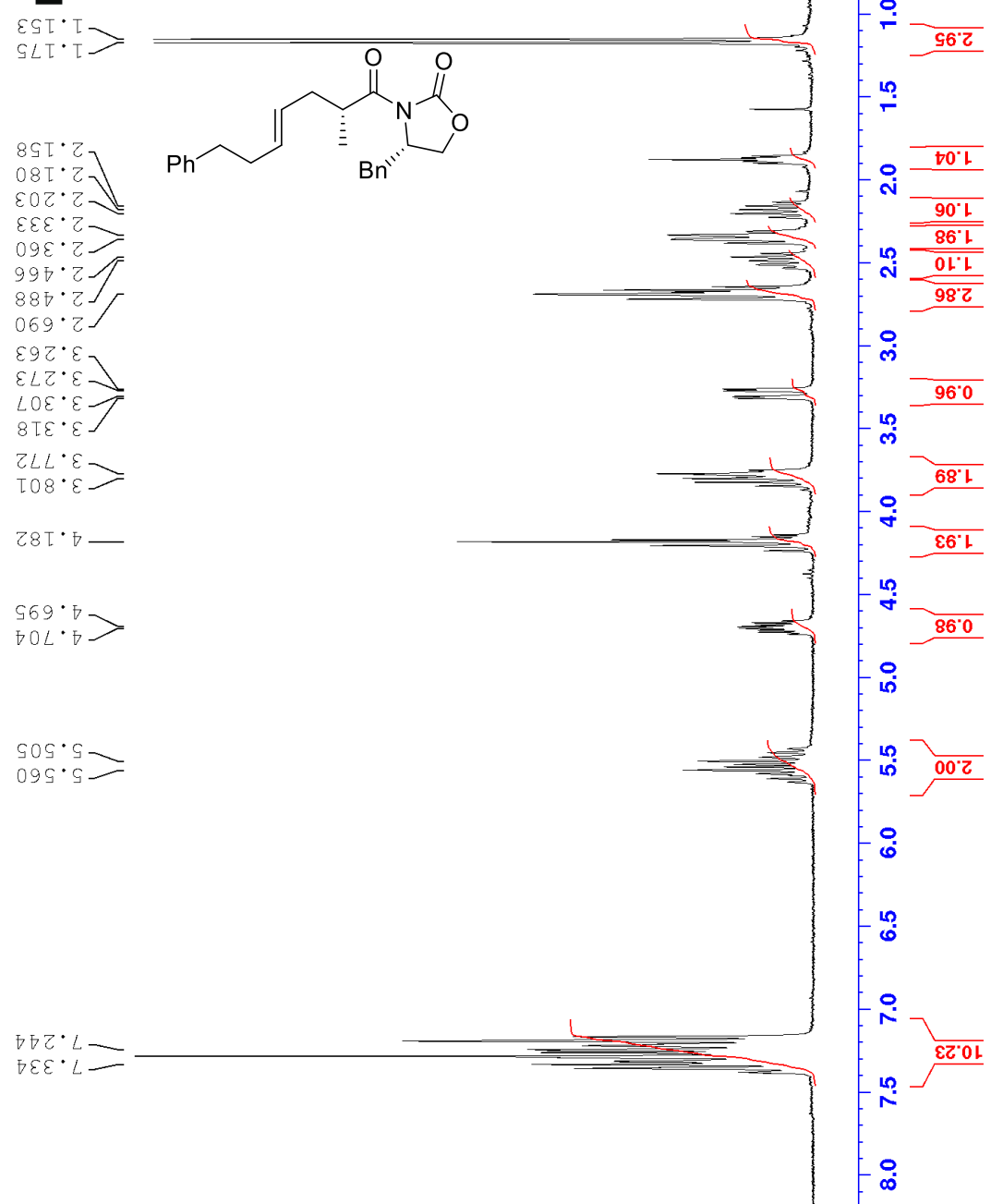
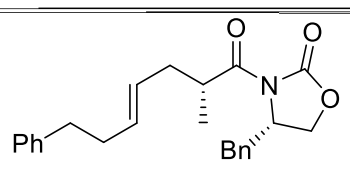
10.29
0.94
2.00
0.78
2.09
2.00
2.87
2.95
2.98



NAME 82-20160121-Phenethyl-Chiral-Aux
 EXPNO 1
 PROCNO 1

F2 - Acquisition Parameters
 Date_ 20160121
 Time 11.28
 INSTRUM spect
 PROBHD 5 mm PABBO BE-
 PULPROG zgpg30
 TD 65536
 SOLVENT CDCl3
 NS 4
 DS 2
 SWH 6009.612
 FIDRES 0.091699 Hz
 AQ 5.4525952 sec
 RG 362
 DW 83.200 usec
 DE 8.700 usec
 TE 298.1 K
 D1 1.00000000 sec
 ID0 1

===== CHANNEL f1 =====
 SF01 300.1318534 MHz
 NUC1 1H
 P1 15.00 usec
 PLW1 6.5599994 W
 SI 65536
 SF 300.1300000 MHz
 WDR 0
 SSB 0
 GB 0
 PC 1.00





Current Data Parameters
 NAME SZ-20160210-SUB-Phenethyl-ester
 EXENO 2
 PROCNO 1

F2 - Acquisition Parameters
 Date_ 20160210
 Time 11.47
 INSTRUM spect
 PULPROG zgpg30
 EDUSERG 65536
 TD 65536
 SOLVENT CDCl3
 NS 5
 DS 2
 SWH 14097.744 Hz
 FIDRES 0.215115 Hz
 AQ 2.3243434 sec
 RG 34.85
 DW 35.467 usec
 DE 1.00 usec
 TE 298.1 K
 D1 2.00000000 sec
 TDO 1

===== CHANNEL f1 =====
 SFO1 700.213283 MHz
 NUC1 1H
 P1 10.25 usec
 PLW1 5.6959581 W
 F2 - Processing Parameters
 SI 32768
 SE 700.2100000 MHz
 WDW EM
 SSB 0
 GB 0
 BR 0
 PC 1.00

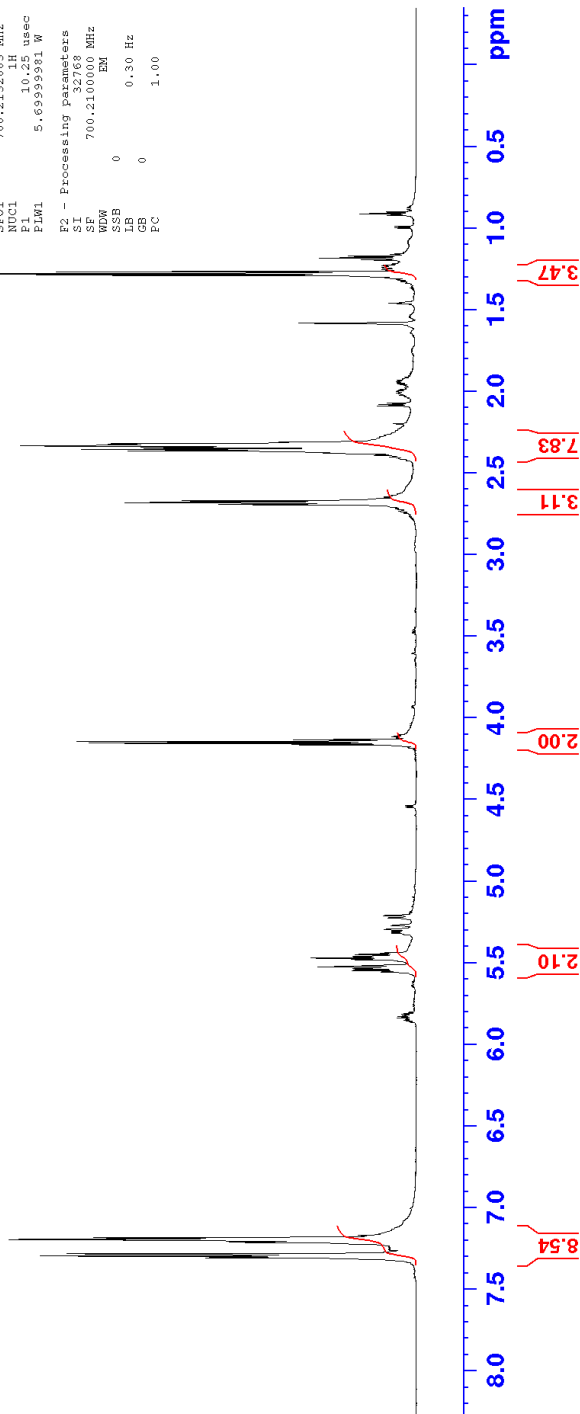
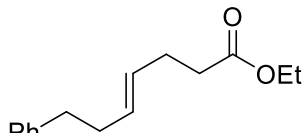
1.276

2.320
 2.341
 2.363
 2.669
 2.681

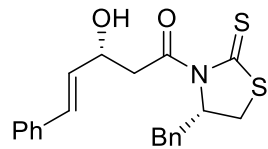
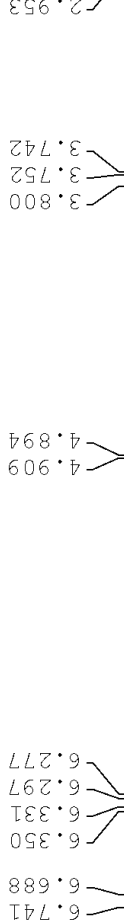
4.144
 4.154

5.471
 5.526

7.197
 7.283
 7.297

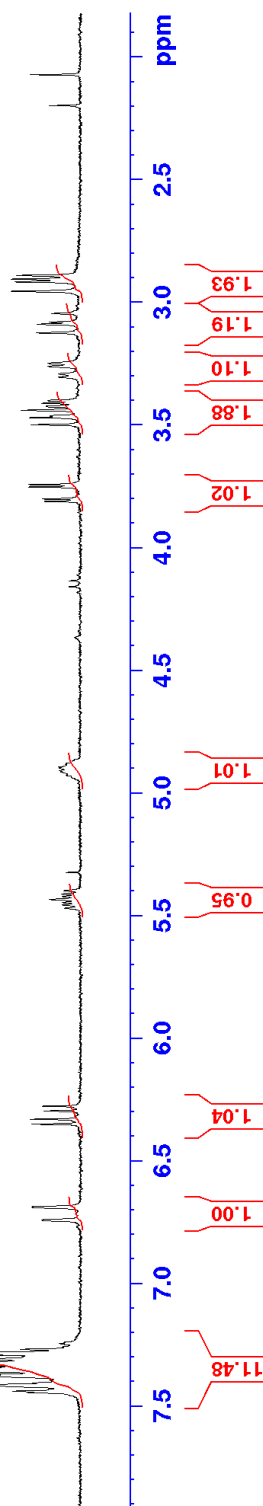


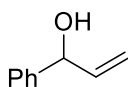
8.0 7.5 7.0 6.5 6.0 5.5 5.0 4.5 4.0 3.5 3.0 2.5 2.0 1.5 1.0 0.5 1.00 ppm



```

Current Data Parameters
=====
NAME          SS-20150218-01-01-chiral-But-01h-2Thio-C-
EXPNO         1
PROCNO        1
P2 - Acquisition Parameters
=====
Date_         20150218
Time          12.50
INSTRUM      spect
PROBHD      5 mm F401P
PULPROG      zgpg30
RG           655.56
AQ           0.02000000
SFO400       400.1362994
NS           4
DS           4
SWH           6009.415 Hz
FIDRES       0.001459 Hz
AQRES       5.4525522 sec
RG           655.56
DM           83.200 usec
DE           0.00000000
TE           298.2 K
TD           1.00000000 sec
=====
NAME          CHIRAL-01
PROCNO        1
PROBHD      5 mm F401P
PULPROG      zgpg30
RG           655.56
AQ           0.02000000
SFO400       400.1362994
NS           4
DS           4
SWH           6009.415 Hz
FIDRES       0.001459 Hz
AQRES       5.4525522 sec
RG           655.56
DM           83.200 usec
DE           0.00000000
TE           298.2 K
TD           1.00000000 sec
=====
P2 - Processing parameters
=====
SI           32768
SF           300.1300000 MHz
WDW          EM
SSB          0
GB           0
PC           1.00
    
```

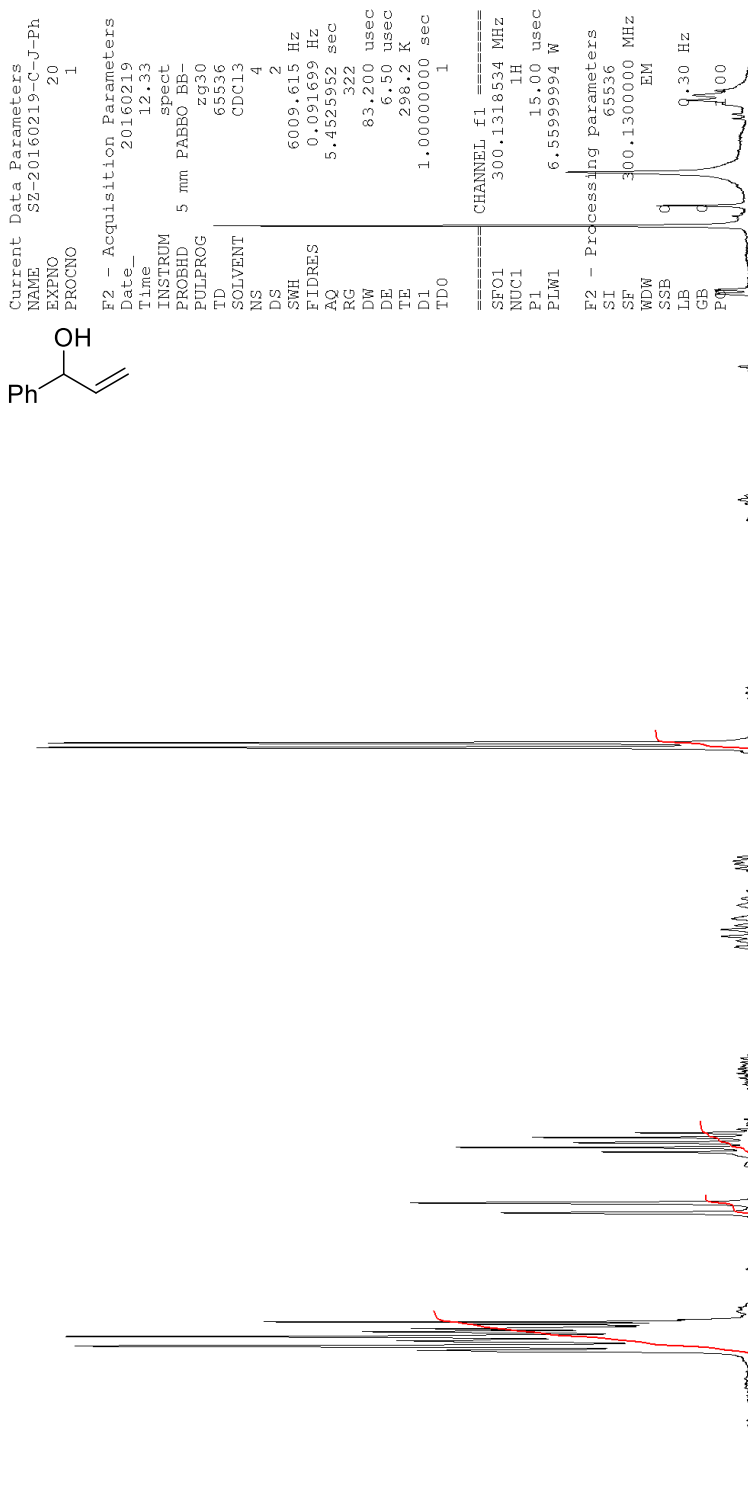




4.289
4.286
4.265
4.262

6.716
6.664
6.398
6.374
6.350
6.322

7.411
7.284



8.0 7.5 7.0 6.5 6.0 5.5 5.0 4.5 4.0 3.5 3.0 2.5 2.0 1.5 1.0 0.0 ppm

Current Data Parameters
 NAME SZ-20160219-C-J-Ph
 EXPNO 20
 PROCNO 1
 F2 - Acquisition Parameters
 Date_ 20160219
 Time 12.33
 INSTRUM spect
 PROBD 5 mm PABBO BB-
 PULPROG zg30
 TD 65536
 SOLVENT CDCl3
 NS 4
 DS 2
 SWH 6009.615 Hz
 FIDRES 0.091699 Hz
 AQ 5.4525952 sec
 RG 322
 DW 83.200 usec
 DE 6.50 usec
 TE 298.2 K
 D1 1.00000000 sec
 TD0 1

CHANNEL f1 =====
 SF01 300.1318534 MHz
 NUC1 1H
 P1 15.00 usec
 PLW1 6.55999994 W

F2 - Processing parameters
 SI 65536
 SF 300.1300000 MHz
 WDW EM
 LB 0.30 Hz
 GB 0.00

2.00

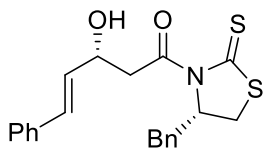
1.10

0.99

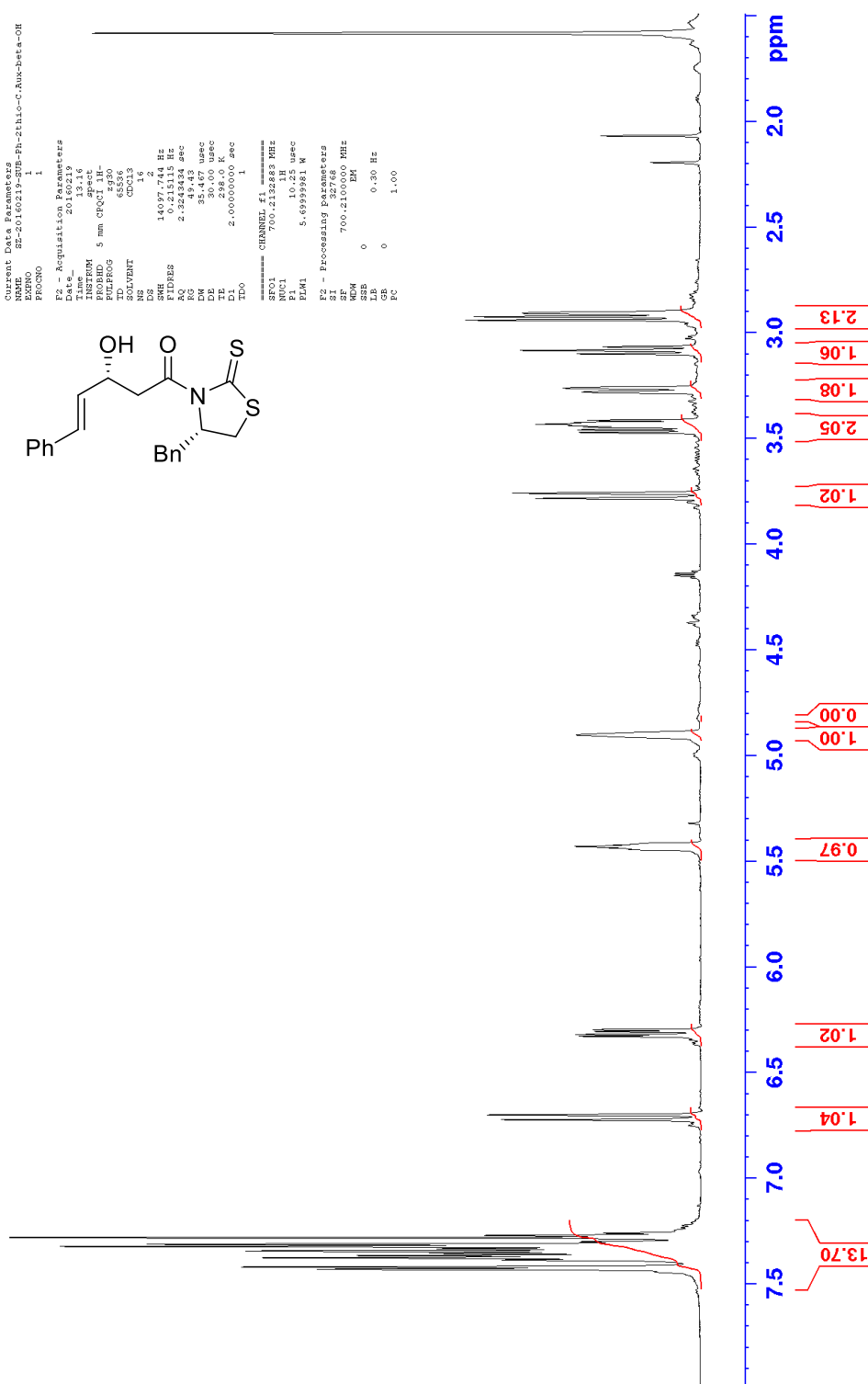
6.48



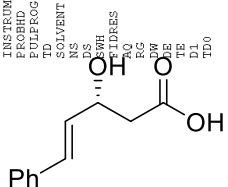
Current Data Parameters
 NAME SP-20160219-gmp-ph-zbilo-c-amin-beta-oh
 PROBHD 1
 PFGPCO 1
 F2 - Acquisition Parameters
 Date_ 20160219
 Time 13:16
 RunDir 1300000000
 PROBHD 5 mm CPQCI 1H-
 PULPROG zgpg30
 SOLVENT CDCl3
 NS 16
 DS 2
 SWH 14097.71 Hz
 FIDRES 0.215115 Hz
 AQ 2.3248434 sec
 SFO1 700.2132683 MHz
 NUC1 1H
 ELM1 5.6959961 W
 F2 - Processing Parameters
 SI 32768
 SF 700.2100000 MHz
 DM 0
 LB 0 0.30 Hz
 GB 0
 PC 1.00



7.421
7.378
7.345
7.324
7.282
6.724
6.701
6.329
6.321
6.306
6.298
4.903
4.827
3.784
3.759
3.472
3.459
3.446
3.438
3.433
3.424
3.414
3.281
3.262
3.252



7.5
7.0
6.5
6.0
5.5
5.0
4.5
4.0
3.5
3.0
2.5
2.0
ppm



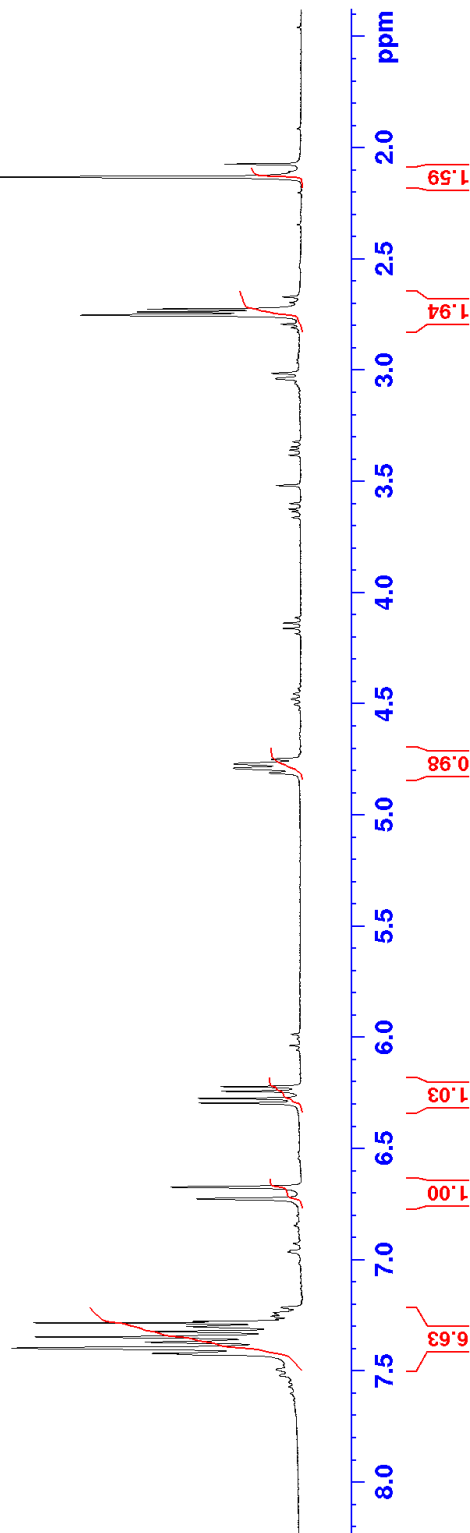
4.789
4.771

6.221
6.242
6.275
6.295
6.674
6.727

7.284
7.347
7.398

```

===== Acquisition Parameters =====
Date_      20160227
Time       12.07
INSTRUM    spect
PROBHD     5 mm F4BBO BB-
PULPROG    zgpg30
TD         65536
SOLVENT    CDCl3
NS         16
DS         2
AQ         6009.615 Hz
RG         0.091699 Hz
RG2        5.4525952 sec
RG3        83.200 usec
RG4        6.50 usec
RG5        6.50 usec
RG6        298.0 K
TE         1.10000000 sec
D1         1
TD0        1
===== CHANNEL f1 =====
SFO1       304.1318634 MHz
NUC1       1H
P1         15.00 usec
PL1        6.45899954 W
PLM1
F2 - Processing Parameters
SI         65536
SF         304.1300000 MHz
WDW        EM
SSB        0
RB         0
GB         0
PC         1.00
    
```



Chapter 6: Reference

- [1] aE. Hupe, M. I. Calaza, P. Knochel, *Tetrahedron Letters* **2001**, *42*, 8829–8831; bE. Hupe, M. I. Calaza, P. Knochel, *Journal of Organometallic Chemistry* **2003**, *680*, 136–142; cE. Hupe, M. I. Calaza, P. Knochel, *Chemistry - A European Journal* **2003**, *9*, 2789–2796.
- [2] T. Hayashi, Y. Matsumoto, Y. Ito, *Tetrahedron: Asymmetry* **1991**, *2*, 601–612.
- [3] S. M. Smith, M. Uteuliyev, J. M. Takacs, *Chemical Communications* **2011**, *47*, 7812–7814.
- [4] D. Imao, B. W. Glasspoole, V. S. Laberge, C. M. Crudden, *Journal of the American Chemical Society* **2009**, *131*, 5024–5025.
- [5] E. Fernandez, M. W. Hooper, F. I. Knight, J. M. Brown, *Chemical Communications* **1997**, 173–174.
- [6] E. Fernandez, K. Maeda, M. W. Hooper, J. M. Brown, *Chemistry - A European Journal* **2000**, *6*, 1840–1846.
- [7] A. C. Chen, L. Ren, C. M. Crudden, *Chemical Communications* **1999**, 611–612.
- [8] A. Chen, L. Ren, C. M. Crudden, *The Journal of Organic Chemistry* **1999**, *64*, 9704–9710.
- [9] R. Larouche-Gauthier, T. G. Elford, V. K. Aggarwal, *Journal of the American Chemical Society* **2011**, *133*, 16794–16797.
- [10] aA. Ros, V. K. Aggarwal, *Angewandte Chemie International Edition* **2009**, *48*, 6289–6292; bR. P. Sonawane, V. Jheengut, C. Rabalakos, R. Larouche-Gauthier, H. K. Scott, V. K. Aggarwal, *Angewandte Chemie International Edition* **2011**, *50*, 3760–3763.
- [11] S. Nave, R. P. Sonawane, T. G. Elford, V. K. Aggarwal, *Journal of the American Chemical Society* **2010**, *132*, 17096–17098.
- [12] aH. C. Brown, P. Veeraraghavan Ramachandran, *Journal of Organometallic Chemistry* **1995**, *500*, 1–19; bH. C. Brown, G. Zweifel, *Journal of the American Chemical Society* **1961**, *83*, 486–487.
- [13] aS. Masamune, B. M. Kim, J. S. Petersen, T. Sato, S. J. Veenstra, T.

- Imai, *Journal of the American Chemical Society* **1985**, *107*, 4549–4551; bA. Z. Gonzalez, J. G. Román, E. Gonzalez, J. Martinez, J. R. Medina, K. Matos, J. A. Soderquist, *Journal of the American Chemical Society* **2008**, *130*, 9218–9219.
- [14] T. Katsuki, K. B. Sharpless, *Journal of the American Chemical Society* **1980**, *102*, 5974–5976.
- [15] R. Noyori, *Advanced Synthesis & Catalysis* **2003**, *345*, 15–32.
- [16] D. Astruc, *New Journal of Chemistry* **2005**, *29*, 42–56.
- [17] C. C. C. JohanssonSeechurn, M. O. Kitching, T. J. Colacot, V. Snieckus, *Angewandte Chemie International Edition* **2012**, *51*, 5062–5085.
- [18] D. Männig, H. Nöth, *Angewandte Chemie International Edition in English* **1985**, *24*, 878–879.
- [19] K. Burgess, M. J. Ohlmeyer, *The Journal of Organic Chemistry* **1988**, *53*, 5178–5179.
- [20] C. Widauer, H. Grützmacher, T. Ziegler, *Organometallics* **2000**, *19*, 2097–2107.
- [21] S. Demay, F. Volant, P. Knochel, *Angewandte Chemie International Edition* **2001**, *40*, 1235–1238.
- [22] A. P. Luna, M. Bonin, L. Micouin, H. -P. Husson, *Journal of the American Chemical Society* **2002**, *124*, 12098–12099.
- [23] L. Zhang, Z. Zuo, X. Wan, Z. Huang, *Journal of the American Chemical Society* **2014**, *136*, 15501–15504.
- [24] J. Chen, T. Xi, Z. Lu, *Organic Letters* **2014**, *16*, 6452–6455.
- [25] Y. Xi, J. F. Hartwig, *Journal of the American Chemical Society* **2016**, *138*, 6703–6706.
- [26] Y. Lee, A. H. Hoveyda, *Journal of the American Chemical Society* **2009**, *131*, 3160–3161.
- [27] D. A. Evans, G. C. Fu, *Journal of the American Chemical Society* **1991**, *113*, 4042–4043.
- [28] C. E. Garrett, G. C. Fu, *The Journal of Organic Chemistry* **1998**, *63*, 1370–1371.
- [29] M. Rubina, M. Rubin, V. Gevorgyan, *Journal of the American Chemical Society* **2003**, *125*, 7198–7199.
- [30] aG. L. Hoang, Z. -D. Yang, S. M. Smith, R. Pal, J. L. Miska, D. E. Pérez, L. S. W. Pelter, X. C. Zeng, J. M. Takacs, *Organic Letters* **2015**, *17*, 940–943; bV. M. Shoba, N. C. Thacker, A. J. Bochat, J. M. Takacs, *Angewandte Chemie International Edition* **2016**, *55*, 1465–1469; cS. M. Smith, G. L. Hoang, R. Pal, M. O. B. Khaled, L. S. W. Pelter, X. C. Zeng, J. M.

- Takacs, *Chemical Communications* **2012**, *48*, 12180–12182; dS. M. Smith, J. M. Takacs, *Organic Letters* **2010**, *12*, 4612–4615; eS. M. Smith, J. M. Takacs, *Journal of the American Chemical Society* **2010**, *132*, 1740–1741; fS. M. Smith, N. C. Thacker, J. M. Takacs, *Journal of the American Chemical Society* **2008**, *130*, 3734–3735; gZ. -D. Yang, R. Pal, G. L. Hoang, X. C. Zeng, J. M. Takacs, *ACS Catalysis* **2014**, *4*, 763–773.
- [31] D. A. Evans, G. C. Fu, B. A. Anderson, *Journal of the American Chemical Society* **1992**, *114*, 6679–6685.
- [32] D. G. Musaev, A. M. Mebel, K. Morokuma, *Journal of the American Chemical Society* **1994**, *116*, 10693–10702.
- [33] A. E. Dorigo, P. von Ragué Schleyer, *Angewandte Chemie International Edition in English* **1995**, *34*, 115–118.
- [34] I. D. Gridnev, T. Imamoto, *Accounts of Chemical Research* **2004**, *37*, 633–644.
- [35] aZ. -T. He, Y. -S. Zhao, P. Tian, C. -C. Wang, H. -Q. Dong, G. -Q. Lin, *Organic Letters* **2014**, *16*, 1426–1429; bX. Feng, H. Jeon, J. Yun, *Angewandte Chemie International Edition* **2013**, *52*, 3989–3992; cD. Noh, H. Chea, J. Ju, J. Yun, *Angewandte Chemie International Edition* **2009**, *48*, 6062–6064; dF. Y. Kwong, Q. Yang, T. C. W. Mak, A. S. C. Chan, K. S. Chan, *The Journal of Organic Chemistry* **2002**, *67*, 2769–2777; eA. Schnyder, L. Hintermann, A. Togni, *Angewandte Chemie International Edition in English* **1995**, *34*, 931–933.
- [36] aD. Noh, H. Chea, J. Ju, J. Yun, *Angewandte Chemie International Edition* **2009**, *48*, 6938–6938; bAdvanced Synthesis & Catalysis **2005**, *347*, 601–604.
- [37] D. A. Evans, G. C. Fu, A. H. Hoveyda, *Journal of the American Chemical Society* **1992**, *114*, 6671–6679.
- [38] A. Bauzá, A. Frontera, *Angewandte Chemie International Edition* **2015**, *54*, 7340–7343.
- [39] L. Hie, E. L. Baker, S. M. Anthony, J. -N. Desrosiers, C. Senanayake, N. K. Garg, *Angewandte Chemie International Edition* **2016**, *55*, 15129–15132.
- [40] E. L. Baker, M. M. Yamano, Y. Zhou, S. M. Anthony, N. K. Garg, *Nature Communications* **2016**, *7*, 11554.
- [41] P. von Matt, O. Loiseleur, G. Koch, A. Pfaltz, C. Lefebvre, T. Feucht, G. Helmchen, *Tetrahedron: Asymmetry* **1994**, *5*, 573–584.
- [42] B. Wiese, G. Helmchen, *Tetrahedron Letters* **1998**, *39*, 5727–5730.
- [43] H. Eichelmann, H. -J. Gais, *Tetrahedron: Asymmetry* **1995**, *6*, 643–646.
- [44] S. J. Roseblade, A. Pfaltz, *Accounts of Chemical Research* **2007**, *40*,

1402-1411.

- [45] C. Clarke, C. A. Incerti-Pradillos, H. W. Lam, *Journal of the American Chemical Society* **2016**, *138*, 8068-8071.
- [46] H. Shimizu, I. Nagasaki, K. Matsumura, N. Sayo, T. Saito, *Accounts of Chemical Research* **2007**, *40*, 1385-1393.
- [47] G. Desimoni, G. Faita, K. A. Jørgensen, *Chemical Reviews* **2011**, *111*, PR284-PR437.
- [48] S. A. Moteki, K. Toyama, Z. Liu, J. Ma, A. E. Holmes, J. M. Takacs, *Chemical Communications* **2012**, *48*, 263-265.
- [49] aF. Y. Zhou, C. F. Lu, Z. X. Chen, G. C. Yang, *Chemistry of Natural Compounds* **2010**, *46*, 83-85; bJ. M. Concellón, H. Rodríguez-Solla, P. Díaz, *The Journal of Organic Chemistry* **2007**, *72*, 7974-7979; cK.-W. Lin, C.-H. Tsai, I. L. Hsieh, T.-H. Yan, *Organic Letters* **2008**, *10*, 1927-1930; dM. Badioli, R. Ballini, M. Bartolacci, G. Bosica, E. Torregiani, E. Marcantoni, *The Journal of Organic Chemistry* **2002**, *67*, 8938-8942.
- [50] D. J. Hardee, T. H. Lambert, *Journal of the American Chemical Society* **2009**, *131*, 7536-7537.
- [51] S. P. Thomas, V. K. Aggarwal, *Angewandte Chemie International Edition* **2009**, *48*, 1896-1898.
- [52] A. H. Hoveyda, D. A. Evans, G. C. Fu, *Chemical Reviews* **1993**, *93*, 1307-1370.
- [53] F. Maier, O. Trapp, *Angewandte Chemie International Edition* **2014**, *53*, 8756-8760.
- [54] K. Aikawa, K. Mikami, *Chemical Communications* **2012**, *48*, 11050-11069.
- [55] D. G. Blackmond, *Journal of the American Chemical Society* **2015**, *137*, 10852-10866.
- [56] D. G. Blackmond, *Angewandte Chemie International Edition* **2005**, *44*, 4302-4320.
- [57] J. E. Hein, A. Armstrong, D. G. Blackmond, *Organic Letters* **2011**, *13*, 4300-4303.
- [58] A. C. Ferretti, J. S. Mathew, I. Ashworth, M. Purdy, C. Brennan, D. G. Blackmond, *Advanced Synthesis & Catalysis* **2008**, *350*, 1007-1012.
- [59] S. P. Mathew, H. Iwamura, D. G. Blackmond, *Angewandte Chemie International Edition* **2004**, *43*, 3317-3321.
- [60] R. D. Baxter, D. Sale, K. M. Engle, J.-Q. Yu, D. G. Blackmond, *Journal of the American Chemical Society* **2012**, *134*, 4600-4606.
- [61] S. J. Zuend, E. N. Jacobsen, *Journal of the American Chemical Society* **2009**, *131*, 15358-15374.

- [62] C. LeBlond, J. Wang, R. D. Larsen, C. J. Orella, A. L. Forman, R. N. Landau, J. Laquidara, J. R. Sowa, D. G. Blackmond, Y. K. Sun, *Thermochimica Acta* **1996**, *289*, 189–207.
- [63] R. N. Landau, U. Singh, F. Gortsema, Y. K. Sun, S. C. Gomolka, T. Lam, M. Futran, D. G. Blackmond, *Journal of Catalysis* **1995**, *157*, 201–208.
- [64] J. S. Mathew, M. Klussmann, H. Iwamura, F. Valera, A. Futran, E. A. C. Emanuelsson, D. G. Blackmond, *The Journal of Organic Chemistry* **2006**, *71*, 4711–4722.
- [65] M. Scott, A. Sud, E. Boess, M. Klussmann, *The Journal of Organic Chemistry* **2014**, *79*, 12033–12040.
- [66] J. Burés, *Angewandte Chemie International Edition* **2016**, *55*, 2028–2031.
- [67] V. M. Shoba, J. M. Takacs, *Journal of the American Chemical Society* **2017**.
- [68] aE. A. Romero, J. L. Peltier, R. Jazzar, G. Bertrand, *Chemical Communications* **2016**, *52*, 10563–10565; bT. Bolaño, M. A. Esteruelas, M. P. Gay, E. Oñate, I. M. Pastor, M. Yus, *Organometallics* **2015**, *34*, 3902–3908.
- [69] B. M. Trost, R. J. Kulawiec, *Journal of the American Chemical Society* **1993**, *115*, 2027–2036.
- [70] B. Schmidt, *The Journal of Organic Chemistry* **2004**, *69*, 7672–7687.
- [71] F. Wu, H. Li, R. Hong, L. Deng, *Angewandte Chemie International Edition* **2006**, *45*, 1498–1498.
- [72] V. J. Garza, M. J. Krische, *Journal of the American Chemical Society* **2016**, *138*, 3655–3658.
- [73] W. S. Johnson, L. Werthemann, W. R. Bartlett, T. J. Brocksom, T. -T. Li, D. J. Faulkner, M. R. Petersen, *Journal of the American Chemical Society* **1970**, *92*, 741–743.
- [74] M. Lemhadri, A. Battace, T. Zair, H. Doucet, M. Santelli, *Journal of Organometallic Chemistry* **2007**, *692*, 2270–2281.
- [75] A. J. Musacchio, L. Q. Nguyen, G. H. Beard, R. R. Knowles, *Journal of the American Chemical Society* **2014**, *136*, 12217–12220.
- [76] H. Kakei, R. Tsuji, T. Ohshima, M. Shibasaki, *Journal of the American Chemical Society* **2005**, *127*, 8962–8963.
- [77] R. A. Barrow, T. Hemscheidt, J. Liang, S. Paik, R. E. Moore, M. A. Tius, *Journal of the American Chemical Society* **1995**, *117*, 2479–2490.
- [78] M. Ueda, K. Seki, Y. Imai, *Synthesis* **1981**, *12*, 991–993.

